Issue 2 2017 | Volume 13

The Journal on Advanced Studies in Theoretical and Experimental Physics, including Related Themes from Mathematics

PROGRESS IN PHYSICS

"All scientists shall have the right to present their scientific research results, in whole or in part, at relevant scientific conferences, and to publish the same in printed scientific journals, electronic archives, and any other media." — Declaration of Academic Freedom, Article 8

ISSN 1555-5534

The Journal on Advanced Studies in Theoretical and Experimental Physics, including Related Themes from Mathematics

PROGRESS IN PHYSICS

A quarterly issue scientific journal, registered with the Library of Congress (DC, USA). This journal is peer reviewed and included in the abstracting and indexing coverage of: Mathematical Reviews and MathSciNet (AMS, USA), DOAJ of Lund University (Sweden), Scientific Commons of the University of St. Gallen (Switzerland), Open-J-Gate (India), Referativnyi Zhurnal VINITI (Russia), etc.

Electronic version of this journal:
http://www.ptep-online.com

Postal Address

Department of Mathematics and Science,
University of New Mexico,
705 Gurley Ave., Gallup, NM 87301, USA

ISSN: 1555-5534 (print)
ISSN: 1555-5615 (online)

Standard Address Number: 297-5092
Printed in the United States of America

April 2017 **Vol. 13, Issue 2**

CONTENTS

Information for Authors

Progress in Physics has been created for rapid publications on advanced studies in theoretical and experimental physics, including related themes from mathematics and astronomy. All submitted papers should be professional, in good English, containing a brief review of a problem and obtained results.

All submissions should be designed in LaTeX format using *Progress in Physics* template. This template can be downloaded from *Progress in Physics* home page http://www.ptep-online.com

Preliminary, authors may submit papers in PDF format. If the paper is accepted, authors can manage LaTeXtyping. Do not send MS Word documents, please: we do not use this software, so unable to read this file format. Incorrectly formatted papers (i.e. not LaTeXwith the template) will not be accepted for publication. Those authors who are unable to prepare their submissions in LaTeXformat can apply to a third-party payable service for LaTeX typing. Our personnel work voluntarily. Authors must assist by conforming to this policy, to make the publication process as easy and fast as possible.

Abstract and the necessary information about author(s) should be included into the papers. To submit a paper, mail the file(s) to the Editor-in-Chief.

All submitted papers should be as brief as possible. Short articles are preferable. Large papers can also be considered. Letters related to the publications in the journal or to the events among the science community can be applied to the section *Letters to Progress in Physics*.

All that has been accepted for the online issue of *Progress in Physics* is printed in the paper version of the journal. To order printed issues, contact the Editors.

Consideration and review process does not require any payment from the side of the submitters. Nevertheless the authors of accepted papers are requested to pay the page charges. *Progress in Physics* is a non-profit/academic journal: money collected from the authors cover the cost of printing and distribution of the annual volumes of the journal along the major academic/university libraries of the world. (Look for the current author fee in the online version of *Progress in Physics*.)

A Telemetric Multispace Formulation of Riemannian Geometry, General Relativity, and Cosmology: Implications for Relativistic Cosmology and the True Reality of Time

Larissa Borissova
E-mail: borissova@ptep-online.com

This thesis reveals an extended world-picture of Riemannian geometry as a telemetric multispace model of real space on the cosmological scale: certain new aspects of General Relativity are presented in terms of a fundamental membrane-transition picture of the deeper reality of time. We refer to this as "telemetric multispace formulation of General Relativity", a world-system with heavy emphasis on Riemannian geometry "per se" (in light of a particular set of extensive, purely geometric techniques), without all the usual historical-artificial restrictions imposed on it. This seminal model gives the purely geometric realization of instantaneous long-range action in the whole space-time of General Relativity whose sub-structure is extended to include an intrinsic, degenerate gravitational-rotational zero-space hosting zero-particles. The mathematical basis of modern cosmology is the four-dimensional pseudo-Riemannian space which is the curved space-time of General Relativity. The additional restrictions pre-imposed on space-time due to so-called "physical reasons" are, regularly: the signature conditions, the prohibition of super-luminal velocities, and the strictly uni-directional flow of time. We here study the peculiar conditions by which the observable time 1) is stopped; 2) flows from the future to the past. Our world and the world wherein time flows oppositely to us are considered as spaces such that they are "mirror images" of each other. The space wherein time stops (the present) is the "mirror" reflecting the future and the past. Then we consider the interaction between a sphere of incompressible liquid (the Schwarzschild bubble) and the de Sitter bubble filled with physical vacuum: this is an example of the interaction between the future and the past through the state of the present.

1 Riemannian geometry as a mathematical model of the real world

A brief historical background is at hand, followed by a critical mathematical repraisal. As known, the mathematical basis of modern cosmology is the four-dimensional pseudo-Riemannian space — the curved space-time of General Relativity. It belongs to the whole spectrum of Riemannian spaces obtained by Bernhard Riemann as a generalization of Carl Gauss' work on curved surfaces. Riemannian spaces possess any number dimension n. The numerical value of n is determined by a maximal number of independent basis vectors (general basis, in the collective sense) of the Riemannian space V_n [1]. The basis of the V_n is introduced at every point of the flat space E_n which is tangent to the V_n at this point. If the basis vectors are linearly dependent, the dimension of the V_n is less than that of the space wherein the basis vectors are independent of each other. There exist two types of basis vectors possessing: 1) the positive square of the length (a real vector); 2) the negative square of the length (an imaginary vector). As familiar, if all the basis vectors of the space are real or imaginary, it is known as the *Riemannian space*. If some of the basis vectors are real while other ones are imaginary, the space is known as the *pseudo-Riemannian space*. Flat Riemannian spaces, where all the basis vectors possess unit or imaginary unit lengths, are known as the *Euclidean spaces* E_n. For example, the E_3 is the ordinary flat three-dimensional space where the unitary system of Cartesian coordinates can be introduced. Flat Riemannian spaces where some basis vectors are real and other ones are imaginary, are known as the *pseudo-Euclidean spaces*. The four-dimensional pseudo-Euclidean space E_4, which possesses one imaginary basis vector along with three real ones, is known as the *Minkowski space* (German Minkowski introduced time as the fourth coordinate $x^0 = ct$, where t is the coordinate time while c is the light velocity). The pseudo-Euclidean space E_4 is of course the basic space (space-time) of Special Relativity. The pseudo-Riemannian (curved) four-dimensional space V_4 with the same set of the basis vectors is the basic space (space-time) of General Relativity. The idea of applying the four-dimensional pseudo-Riemannian space to the description of the real world was suggested Marcel Grossman, a close mathematician friend of Albert Einstein. Einstein agreed with him, because the metrical properties of Riemannian spaces are simplest in comparison to the properties of other metric spaces. The point is that Riemannian metrics are invariant relative to transformations of coordinates. It implies that the square of the elementary

infinitesimal vector dx^α conserves its length:

$$ds^2 = g_{\alpha\beta}dx^\alpha dx^\beta, \quad \alpha,\beta = 0,1,2,3, \tag{1}$$

where the contraction by indices α,β denotes the summation.

Metrics of Riemannian spaces are symmetric ($g_{\alpha\beta} = g_{\beta\alpha}$) and non-degenerate ($g = \det\|g_{\alpha\beta}\| \neq 0$), while the elementary four-dimensional interval is invariant relative to any reference system ($ds^2 = const$). The invariance of the ds^2 is a very important argument on behalf of Riemannian geometry as the mathematical basis of General Relativity.

The metric coefficients are of course the cosines of the angles between the basis vectors in the locally flat tangent space. This is because ds^2 is the scalar product of dx^α with itself. The dimension of the flat tangent space and the correlation between the imaginary and real basis vectors are the same as in the corresponding Riemannian space. A system of basis vectors $\mathbf{e}_\alpha$ can be introduced at any point of the locally tangent space. The $\mathbf{e}_\alpha$ are tangent to the coordinate lines x^α. The fundamental metric tensor can be expressed through the basis vectors $\mathbf{e}_\alpha$ as [2]:

$$g_{\alpha\beta} = e_\alpha e_\beta \cos\left(\widehat{x^\alpha, x^\beta}\right), \tag{2}$$

where e_α is the length of the $\mathbf{e}_\alpha$. Assume here the temporal basis vector $\mathbf{e}_0$ to be real, while, correspondingly, the basis spatial vectors $\mathbf{e}_i$ ($i = 1,2,3$) are imaginary.

We recall that the interval ds^2 can be positive, negative, or null. The value ds is used as the parameter along trajectories of particles (world-lines of particles). These lines can be: 1) real by $ds^2 > 0$, 2) imaginary by $ds^2 < 0$, 3) zero by $ds^2 = 0$. The value ds is used as the global parameter along world-lines. Real mass-bearing particles (the rest-mass $m_0 \neq 0$, the relativistic mass $m = \frac{m_0}{\sqrt{1-V^2/c^2}}$ is real) move along the non-isotropic lines ($ds \neq 0$) at sub-luminal velocities $V < c$; imaginary mass-bearing particles or hypothetical *tachyons* (the rest-mass $m_0 \neq 0$, the relativistic mass $m = \frac{im_0}{\sqrt{1-V^2/c^2}}$ is imaginary) move along non-isotropic lines ($ds \neq 0$) at super-luminal velocities $V > c$; massless particles (the rest-mass $m_0 = 0$, the relativistic mass $m \neq 0$) move along isotropic lines ($ds = 0$) at light velocity $V = c$. Thus, for example, photons are actual light-like particles.

The description of the world is to be linked with the real reference frame of a real observer who actually defines both geometrical and mechanical properties of the space of reference he inhabits. The reference frame is a reference body where coordinate nets are spanned and clocks are installed at the every point of the reference's body. The profound problem of the introduction of physically observable quantities in the whole inhomogeneous, anisotropic curved space of General Relativity is to determine which components of the every four-dimensional quantity are the physically observable quantities. This problem was solved decisively and comprehensively by A. Zelmanov [2]. He introduced chronometric invariants (chr.-inv.) as physically observable geometric quantities in General Relativity. These fundamental quantities are linked to the reference body which can, in general, gravitate, rotate, and deform. The three-dimensional observable space (the reference space) can be both curved and flat. The reference body is considered as a set of real coordinate systems, to which the observer compares all results of his measurements. Therefore the physically observable quantities are constructed as the result of fundamentally (in a unified, simultaneous geometrical-mechanical fashion) projecting four-dimensional quantities on the lines of time and on the three-dimensional space.

The chr.-inv. form of the four-dimensional interval ds^2 is [2]

$$\begin{aligned} &ds^2 = c^2d\tau^2 - d\sigma^2, \quad d\tau = \left(1 - \frac{\mathrm{w}}{c^2}\right)dt - \frac{v_i dx^i}{c^2}, \\ &d\sigma^2 = h_{ik}dx^i dx^k, \quad h_{ik} = -g_{ik} + \frac{v_i v_k}{c^2}, \quad i,k = 1,2,3, \end{aligned} \tag{3}$$

where $d\tau$ is the interval of the observable time, $d\sigma^2$ is the observable spatial interval, $\mathrm{w} = c^2(1 - \sqrt{g_{00}})$ is the three-dimensional gravitational potential, $v_i = -\frac{cg_{0i}}{\sqrt{g_{00}}}$ is the linear velocity of the space rotation, h_{ik} is the three-dimensional fundamental metric tensor. The expression (3) may be rewritten in the form

$$ds^2 = c^2d\tau^2\left(1 - \frac{V^2}{c^2}\right), \quad V^i = \frac{dx^i}{d\tau}, \quad V^2 = h_{ik}V^iV^k, \tag{4}$$

where V^i is the observable three-dimensional velocity.

It follows from (4) that ds is: 1) real if $V < c$, 2) imaginary if $V > c$, 3) zero if $V = c$. The condition $ds = 0$ has the form

$$cd\tau = \pm d\sigma, \tag{5}$$

which is of course the equation of the elementary light cone. The term *elementary* means that this cone can be introduced only at every point of the space-time, but not into the whole space. The elements of the cone are trajectories of massless particles moving along null geodesic lines.

As follows from (4, 5), photons are at rest within the space-time ($ds = 0$) itself, but they move at light velocity ($V = c$) along three-dimensional trajectories ($cd\tau = d\sigma$) within the three-dimensional observable space. The light cone is known as the "light barrier" which "prohibits" motions at super-luminal velocities. Really, this restriction means that mass-bearing particles, both real ones and tachyons, cannot move at light velocity. The zero-particles penetrating the light cone are considered in detail in [3]. These particles are essentially thinner structures than light, because their relativistic masses m are zeroes. Zero-particles possess non-zero gravitational-rotational masses $M = \frac{m}{1-(\mathrm{w}+v_iu^i)/c^2}$, where $u^i = \frac{dx^i}{dt}$. Zero-particles transfer instantly ($d\tau = 0$) along three-dimensional null trajectories ($d\sigma = 0$). The light cone is therefore transparent for zero-particles and non-transparent for mass-bearing real particles

and tachyons. As such, we may call it a "membrane". Thus the apparatus of General Relativity allows the existence of long-range action as truly instantaneous-transfer zero-particles. Moreover, this fundamental transfer unifies the worlds of both real particles and tachyons. As for the other new aspects of General Relativity, we shall introduce them in the next sections.

2 The past and the future as the mirror reflections each other

Most contemporary scientists presuppose that time flows only in a single direction — from the past to the future. The mathematical apparatus of General Relativity does not prohibit the reverse flow of time, i.e. from the future to the past. Nevertheless, the reverse flow of time is not introduced in contemporary physics and cosmology, partly because modern scientists refer to Hans Reichenbach's "arrow of time", which is directed always to the future. However, upon further analysis, Reichenbach, speaking about a unidirectional flow of time, implied a rather limited world-process of evolution (transfer mechanism of energy). He wrote: "Super-time has not a direction, but only an order. Super-time itself, however, contains local sections, each of whom has a direction, while the directions change from one section to another" [4]. Contemporary scientists consider the light cone of Minkowski space as a mathematical illustration of the time arrow: the lower half of the cone means the *past*, while the upper half — the *future*. The past automatically turns into the future at the point $t = 0$, meaning the *present*. But such an automatic transfer is due to the fact that the Minkowski space of Special Relativity is de facto empty. Besides, it does not at all include both gravitation and rotation (in addition to deformation and the whole curvature), therefore the ideal, uniformly flowing time of Special Relativity does not (and can not) depend on gravitation and rotation. In other words, this transfer does not require fundamental transformations of matter. In fact, in this picture, photons flow continuously from the lower half of the cone to the upper one. However the "real space" perceived by us as the "present" is ultimately penetrated by gravitation. Besides, the objects of the said space, ranging from electrons to galaxies and their clusters, do rotate around their centers of gravitational attraction. The problem is therefore to describe, in the framework of General Relativity, the fundamental interaction between the future and the past as a proper energetic transfer through the present state. Such description of the future-past transfer is a more exact approximation, than in the self-limited Minkowski space, because the observable time τ essentially depends on both gravitation and rotation: see (3, 5). The expressions $d\tau = 0$, $d\sigma = 0$ describe the *membrane*, which is situated between the past and the future. These expressions can be rewritten in the form [3]:

$$\mathrm{w} + v_i u^i = c^2, \quad h_{ik} dx^i dx^k = 0, \quad u^i = \frac{dx^i}{dt}. \qquad (6)$$

As the metric form $d\sigma^2$ is positively determined, the condition $d\sigma^2 = 0$ means that it is degenerated: $h = \det \|h_{ik}\| = 0$. The determinants of the matrices $g = \det \|g_{\alpha\beta}\|$ and h are linked by the relation $\sqrt{-g} = \sqrt{g_{00} h}$ [2], therefore the four-dimensional matrix $\|g_{\alpha\beta}\|$ is degenerated: $g = \det \|g_{\alpha\beta}\| = 0$. The condition of the membrane transition can be written in the form [3]:

$$\mathrm{w} + v_i u^i = c^2, \quad d\mu^2 = g_{ik} dx^i dx^k = \left(1 - \frac{\mathrm{w}}{c^2}\right)^2 c^2 dt^2, \qquad (7)$$

where the first expression characterizes the condition of the *stopped time*, the second expression describes the geometry of the hyper-surface, where events of the present are realized.

The conditions (7) describe the zero-space, where, from a viewpoint of a real observer, zero-particles extend instantly ($d\tau = 0$) along three-dimensional null lines ($d\sigma = 0$) [3]. The instant transfer of zero-particles means the **long-range-action**. We conclude that the **future-past transfer is realized instantaneously**, i.e. it is the long-range-action. Note, the coordinate length $d\mu = \left(1 - \frac{\mathrm{w}}{c^2}\right) cdt$ depends, in part, on the gravitational potential w, wherein $d\mu = 0$ by the collapse condition: $\mathrm{w} = c^2$. Thus the metric on the hyper-surface is, in general, not a Riemannian one, because its interval $d\mu$ is not invariant (yet it is invariant by the collapse, as in this case $d\mu^2 = 0$). The region of space-time, which is located between the spaces of the past and the future, is perceptible by a real observer as the present. It is the hyper-surface where all events are realized at the same moment of observable time $\tau_0 = const$, i. e. such events are *synchronized*. The momentary interaction (the long-range-action) is transferred by particles of a special kind — *zero-particles*. They possess zero rest-mass m_0, zero relativistic mass m, and non-zero gravitational-rotational mass M. This quantity is determined in the generalized space-time where the condition $g = 0$ is satisfied. The mass M in the generalized space has the form [3]

$$M = \frac{mc^2}{c^2 - (\mathrm{w} + v_i u^i)}.$$

Thus the elements of the elementary curved light cone (the so-called "light barrier") are indeed penetrable for zero-particles. As follows from (5), trajectories of photons belong to both the space and time, because they extend along null four-dimensional trajectories $ds = 0$. The three-dimensional body of the real observer can thus move at pre-light velocity in the three-dimensional space, but it is always rigidly attached to the moment of time, which is perceptible as the present.

A brief philosophical digression: transfers both in the past and in the future are possible, so far, only mentally. The typical human mind does remember the past (not always clearly) and does predict the future (not always exactly). It is possible to say that the past and the future are virtual, because only the human consciousness moves in these virtual spaces, but the

physical body is strictly in the present ("reality"). Studying the past of the Earth and remembering our own past, we see a recurrence of some events, both planetary and individual. We know what happened with the Earth in the past due to mainly the tales of our ancestors, if not historians. Events (three-dimensional points, as well as threads extended in time) are ordered in a determined sequence in time. Comparing similar events from different intervals of time, we can say that the past and the future are similar, being mirror reflections of one other. The object of the three-dimensional space and its mirror reflection differ only by the notions of "left" and "right" possessing the opposite sense for every one of them. The intervals of both coordinate time and observable time are linked by the formula [3]

$$\frac{dt}{d\tau} = \frac{\frac{v_i V^i}{c^2} \pm 1}{\sqrt{g_{00}}}. \tag{8}$$

The expression (8) was studied in [3] by the condition $\sqrt{g_{00}} > 0$. It means that we did not consider in [3] the reverse of time while simultaneously taking into account the state of collapse $g_{00} = 0$. As follows from (8), the coordinate time t: 1) is stopped ($dt = 0$) if $v_i V^i = \mp c^2$; 2) possesses direct flow ($dt > 0$) if $v_i V^i > \mp c^2$; 3) possesses reverse flow ($dt < 0$) if $v_i V^i < \mp c^2$. Thus the spaces with direct and the reverse flows of coordinate time t are divided by a fundamental surface of rotation, where the vectors v_i and V^i are linked by the relation, see (2, 3):

$$v_i V^i = \mp c^2 |v_i||V^i| \cos\left(\widehat{v_i, V^i}\right) = \mp c^2 |e_i||V^i| \cos\left(\widehat{e_i V^i}\right),$$

where e_i is the spatial basis vector in the tangent Minkowski space. It is evident that this relation is realized for two cases:

1) the vectors v_i and V^i are co-directed, $|v_i| = |V^i| = c$;

2) the vectors v_i and V^i are anti-directed, $|v_i| = |V^i| = c$.

Since the vector v_i means the linear velocity of space rotation, we conclude that the very surface dividing the spaces with direct and reverse flow of coordinate time rotates at light velocity. The rotation is either left or right.

A real observer measures that the time τ coincides completely with the coordinate time t only in the case wherein the reference space does not rotate ($v_i = 0$) nor gravitate ($w = 0$): see (3). If $w \neq 0$ or $v_i \neq 0$, the τ, in contrast to t, depends essentially on gravitation and rotation. Because we live in the real world, where gravitation and rotation do exist, we will further consider the *observable time*.

The observable Universe, which is a part of the Infinite Whole, can belong to one of the aforementioned spaces (either possessing positive or negative flow of coordinate time). Let the flow of coordinate time in the region, where the observer is situated, be positive: $dt > 0$. The observable time is divided by the consciousness of a real observer into the "past", the "present" and the "future": time flows from the past to the future through the present. The problem stated in the beginning of this paper is to study the future-past transfer from the point of view of a real observer, who is located in the world of positive flow of coordinate time $dt > 0$. This problem is essentially simplified in the case where the reference space does not rotate. Then the expression (8) can be rewritten in the form

$$d\tau = \pm\sqrt{g_{00}}\, dt = \pm\left(1 - \frac{w}{c^2}\right) dt. \tag{9}$$

Taking into account the collapse condition $\sqrt{g_{00}}$, we shall study the direction of observable time flow in the gravitational field. It follows from (9) that the observable time τ: 1) possesses positive direction if $\sqrt{g_{00}} > 0$, 2) possesses negative direction if $\sqrt{g_{00}} < 0$, 3) stops if $\sqrt{g_{00}} = 0$. Because the condition $g_{00} = 0$ is the collapse condition, the **surface of the collapsar is the mirror separating the spaces with both positive and negative flow of the observable time**. The observable time is perceptible by human consciousness as flowing from the past to the future, therefore we call the space of such direct flow of time the "space of the past". Then the space of reverse flow of observable time is necessarily the "space of the future". The present space is situated between these spaces. The concrete spaces reflecting from the surface of the collapsar, as from the mirror, will be studied in detail in the next section.

3 The interaction between the Schwarzschild and de Sitter bubbles as instantaneous transfer

All objects in the Universe consist of the same fluid substance being at different stages of cosmic evolution. Many cosmic bodies (planets, stars, ...) are spheroids, namely spinning, deforming spheres. Probably the physical body of the Universe has the same form. The problem is to introduce the space-time (gravitational field) created by a liquid incompressible sphere. A similar model was introduced earlier by the German astronomer Karl Schwarzschild [5]. He solved the field equations (Einstein equations) for the sphere by the assumption that the solution must be everywhere regular. In other words, Schwarzschild ruled out the existence of singularities. Meanwhile the problem of singularities is very actual for astrophysics and cosmology. The more general, allowing singularities, solution of the Einstein equations for the sphere filled by ideal incompressible liquid was obtained in [6]. The substance filling the sphere is described by the energy-impulse tensor

$$T^{\alpha\beta} = \left(\rho + \frac{p}{c^2}\right) b^\alpha b^\beta - \frac{p}{c^2} g^{\alpha\beta}, \tag{10}$$

where $\rho = const$ is the density of substance, p is the pressure, $b^\alpha = \frac{dx^\alpha}{ds}$ is the four-dimensional unit velocity vector: $g_{\alpha\beta} b^\alpha b^\beta = 1$.

The solution allowing singulary states of the space-time has the form [6]

$$ds^2 = \frac{1}{4}\left(3\sqrt{1-\frac{\varkappa\rho a^2}{3}} - \sqrt{1-\frac{\varkappa\rho r^2}{3}}\right)^2 c^2dt^2 - \frac{dr^2}{1-\frac{\varkappa\rho r^2}{3}} - r^2(d\theta^2+\sin^2\theta d\varphi^2), \quad (11)$$

where $\varkappa = \frac{8\pi G}{c^2}$ is the Einstein gravitational constant, G is the Newton gravitational constant, a is its radius, r, θ, φ are the spherical coordinates.

The gravitational field described by (11) has two singularities [6]:

1) it collapses if

$$3\sqrt{1-\frac{\varkappa\rho a^2}{3}} = \sqrt{1-\frac{\varkappa\rho r^2}{3}};$$

2) it breaks the space if

$$\frac{\varkappa\rho r^2}{3} = 1.$$

The radius of the collapsar r_c and the radius of the breaking space r_{br} have the forms, respectively:

$$r_c = \sqrt{9a^2 - \frac{24}{\varkappa\rho}} = \sqrt{9a^2 - 8r_{br}{}^2}, \quad (12)$$

where the breaking radius $r_{br} = \sqrt{\frac{3}{\varkappa\rho}} = \frac{4\times10^{13}}{\sqrt{\rho}}$ cm.

It follows from (12) that the incompressible liquid sphere collapses if $a > \sqrt{\frac{8}{9}}\, r_{br} = 0.94\, r_{br}$. (Because by $a = \sqrt{\frac{8}{9}r_{br}}$ the collapsing object transforms into the point $r_c = 0$, we do not consider this case non-sense in the physical meaning). If $\rho = 10^{-29}$ g/cm^3 (the assumed value of the density of matter in the observable Universe), then the sphere collapses by $a > 1.2\times10^{28}$ cm and breaks the surrounding space by $a = 1.3\times10^{28}$ cm. If the density of matter inside the sphere is $\rho = 10^{14}$ g/cm^3 (as inside the atomic nucleus), then $a > 3.8\times10^6$ cm and $r_{br} = 4\times10^6$ cm. The density of matter inside a typical neutron star is regularly assumed to be the same as the nuclear density, while its radius is about a dozen kilometers. With these, larger-sized neutron stars may be non-observable, because they are gravitational collapsars. Estimate now the minimal value of the mass of the neutron star by the assumption that it collapses. If $a = 3.8\times10^6$ cm, then the mass $M = \frac{4\pi a^3\rho}{3} = 23\times10^{33}$ g $= 11.5M_\odot$, where $M_\odot$ is the mass of the Sun. Assuming $\rho = 1$ g/cm^3 (the density of hydrodynamical fluid), we find $r_{br} = 4\times10^{13}$ cm. It means, such a fluid sphere collapses if its radius is $a > 4\times10^{13}$ cm.

A sphere of incompressible liquid with a constant volume and a constant density, which is situated in the state of weightlessness, is a kind of *condensed matter*. The planets, rotating around the Sun, as well as the stars, rotating around the center of the Galaxy, are in the state of weightlessness [6]. Assume that stationary stars consist of condensed matter. For example, consider the Sun as an actual sphere of condensed matter. The density of the Sun is $\rho_\odot = 1.4$ g/cm^3, and its radius is $a = 7\times10^7$ cm. We find $r_{br} = 3.4\times10^{13}$ cm. It follows from (12) that the collapse of the Sun is impossible in this state of matter, because r_c has an imaginary value. It is interesting to note that the surface of breaking of the Sun is at the distance r_{br}=2.3 AU, where the *Astronomical Unit* (AU) is the average distance between the the Sun and the Earth: 1 AU = 1.49×10^{13} cm. So we obtain that the surface of breaking (curvature discontinuity), created by the Sun, is actually situated inside the asteroid strip region, very close to the orbit of the maximal concentration of asteroids: 2.5 AU from the Sun [6]. (As known, the asteroid strip's distance from the Sun is within the limit of 2.1 to 4.3 AU).

Let's now study the simultaneous mechanical and geometrical properties of the metric (11). As shown in [2], the three-dimensional observable space (the reference space) is characterized by the three mechanical characteristics and one geometrical. The mechanical characteristics are: the vector of the gravitational inertial force F_i, the tensor of the angular velocity of rotation A_{ik}, and the tensor of the rate of deformation D_{ik}:

$$F_i = \frac{c^2}{c^2-\mathrm{w}}\left(\frac{\partial \mathrm{w}}{\partial x^i} - \frac{\partial v_i}{\partial t}\right), \quad D_{ik} = \frac{1}{2}\frac{{}^*\partial h_{ik}}{\partial t},$$

$$A_{ik} = \frac{1}{2}\left(\frac{\partial v_k}{\partial x^i} - \frac{\partial v_i}{\partial v_k}\right) + \frac{1}{c^2}(F_i v_k - F_k v_i),$$

where $\frac{{}^*\partial}{\partial t} = \frac{1}{\sqrt{g_{00}}}\frac{\partial}{\partial t}$ is the chr.-inv. operator of differentiation along the temporal coordinate.

We find that the reference space of the metric (11) does not rotate ($A_{ik} = 0$) and deform ($D_{ik} = 0$), but it gravitates. The gravitational inertial force F_i has the only non-zero component [6]

$$F_1 = -\frac{\varkappa\rho c^2}{3}\frac{r}{\left(3\sqrt{1-\frac{\varkappa\rho a^2}{3}} - \sqrt{1-\frac{\varkappa\rho r^2}{3}}\right)\sqrt{1-\frac{\varkappa\rho r^2}{3}}} \quad (13)$$

$F_1 < 0$.

Thus the quantity F_i is the non-Newtonian force of attraction. Then $F_1 \to \infty$ both by the collapse and the breaking of space [6].

The pressure of the ideal liquid p is determined from the conservation law [6]. It has the form

$$p = \rho c^2 \frac{\sqrt{1-\frac{\varkappa\rho r^2}{3}} - \sqrt{1-\frac{\varkappa\rho a^2}{3}}}{3\sqrt{1-\frac{\varkappa\rho a^2}{3}} - \sqrt{1-\frac{\varkappa\rho r^2}{3}}} > 0. \quad (14)$$

It follows from (14) that $p \to \infty$ by the collapse and $p = -\frac{\rho c^2}{3}$ at the surface of break.

The geometric characteristic of the reference space is the chr.-inv. three-dimensional tensor of curvature C_{ijkl} [2] possessing all the algebraic properties of the Riemann-Christoffel four-dimensional tensor of curvature $R_{\alpha\beta\gamma\delta}$. The C_{ijkl} has the form [2]:

$$C_{ijkl} = \frac{1}{4}(H_{ijkl} + H_{ljki} - H_{jilk} + H_{kilj}), \tag{15}$$

where H_{ijkl} is the chr.-inv. close analog of the Schouten tensor in the theory of non-holonomic manifolds

$$H^{\cdots l}_{ijk\cdot} = \frac{{}^*\partial\Delta^l_{ik}}{\partial x^j} - \frac{{}^*\partial\Delta^l_{ij}}{\partial x^k} + \Delta^m_{ik}\Delta^l_{jm} - \Delta^m_{ij}\Delta^l_{km}, \tag{16}$$

where

$$\Delta^k_{ij} = h^{km}\Delta_{ij,m}, \quad \Delta_{ij,m} = \frac{1}{2}\left(\frac{{}^*\partial h_{im}}{\partial x^j} + \frac{{}^*\partial h_{jm}}{\partial x^i} - \frac{{}^*\partial h_{ij}}{\partial x^m}\right) \tag{17}$$

are the chr.-inv. Christoffel symbols of the second and first kind, respectively, $\frac{{}^*\partial}{\partial x^i} = \frac{\partial}{\partial x^i} + \frac{v_i}{c^2}\frac{{}^*\partial}{\partial t}$ is the chr.-inv.operator of differentiation along spatial coordinates [2].

The tensors H_{ijkl} and C_{iklj} are linked by the relation [2]

$$H_{ijkl} = C_{ijkl} + \frac{1}{c^2}\Big(2A_{jk}D_{li} + A_{ik}D_{jl} + A_{lj}D_{ik} + A_{il}D_{jk} + A_{lj}D_{ki}\Big). \tag{18}$$

It is evident, therefore, that $C_{lkij} = H_{lkij}$ if $A_{ik} = 0$ or $D_{ik} = 0$. Calculating the Christoffel symbols of the second kind, we obtain for the non-zero components:

$$\begin{aligned}
&\Delta^1_{11} = \frac{\varkappa\rho r}{3}\frac{1}{1-\frac{\varkappa\rho r^2}{3}},\\
&\Delta^1_{22} = \frac{\Delta^1_{33}}{\sin^2\theta} = -r\left(1-\frac{\varkappa\rho r^2}{3}\right),\\
&\Delta^2_{12} = \Delta^3_{13} = \frac{1}{r}, \quad \Delta^2_{33} = -\sin\theta\cos\theta,\\
&\Delta^3_{23} = \cot\theta.
\end{aligned} \tag{19}$$

Substituting (19) into (16) and lowering the upper indices, we find the non-zero components C_{iklj} for the space-time described by the metric (11)

$$\begin{aligned}
&C_{1212} = \frac{C_{1313}}{\sin^2\theta} = \frac{\varkappa\rho r^2}{3}\frac{1}{1-\frac{\varkappa\rho r^2}{3}},\\
&C_{2323} = \frac{\varkappa\rho r^4}{3}\sin^2\theta.
\end{aligned} \tag{20}$$

The components $C_{ik} = h^{mn}C_{imkn}$ and the three-dimensional scalar $C = h^{ik}C_{ik}$ have the form [7]

$$\begin{aligned}
&C_{11} = \frac{2\varkappa\rho}{3}\frac{1}{1-\frac{\varkappa\rho r^2}{3}}, \quad C_{22} = \frac{C_{33}}{\sin^2\theta} = \frac{2\varkappa\rho r^2}{3},\\
&C = 2\varkappa\rho > 0.
\end{aligned} \tag{21}$$

The three-dimensional reference space satisfies the condition

$$C_{ijkl} = q(h_{ik}h_{jl} - h_{jk}h_{il}), \quad q = \frac{\varkappa\rho}{3} = const, \tag{22}$$

therefore it is the space of constant positive curvature, where q is the Gaussian curvature of the three-dimensional reference space. It follows from (12) that the radius of curvature is $\frac{1}{q} = r_{br} = \sqrt{\frac{3}{\varkappa\rho}}$. It is necessary to note that the *Gaussian curvature and, consequently, the radius of space breaking depend on the density of incompressible liquid*.

Thus we have found that the three-dimensional reference space of the space-time (11) is the space of constant positive curvature. Study now the geometric properties of the four-dimensional space (11). As is well-known, the geometric properties of every curved (Riemannian) space are described by the Riemann tensor

$$\begin{aligned}
R_{\alpha\beta\gamma\delta} = &\frac{1}{2}(\partial_{\beta\gamma}g_{\alpha\delta} + \partial_{\alpha\delta}g_{\beta\gamma} - \partial_{\alpha\gamma}g_{\beta\delta} - \partial_{\beta\delta}g_{\alpha\gamma}) +\\
&+g^{\sigma\tau}(\Gamma_{\alpha\delta,\sigma}\Gamma_{\beta\gamma,\tau} - \Gamma_{\beta\delta,\sigma}\Gamma_{\alpha\gamma,\tau}),
\end{aligned} \tag{23}$$

where $\Gamma_{\alpha\beta,\sigma}$ are the Christoffel symbols of the first kind

$$\Gamma_{\alpha\beta,\sigma} = \frac{1}{2}(\partial_\alpha g_{\beta\sigma} + \partial_\beta g_{\alpha\sigma} - \partial_\sigma g_{\alpha\beta}). \tag{24}$$

Calculating the values $\Gamma_{\alpha\beta,\sigma}$ for the metric (11) we obtain

$$\begin{aligned}
&\Gamma_{01,0} = -\Gamma_{00,1} = \frac{\varkappa\rho r}{12}\frac{3\sqrt{1-\frac{\varkappa\rho a^2}{3}} - \sqrt{1-\frac{\varkappa\rho r^2}{3}}}{\sqrt{1-\frac{\varkappa\rho r^2}{3}}},\\
&\Gamma_{11,1} = -\frac{\varkappa\rho r}{3}\frac{1}{\left(1-\frac{\varkappa\rho r^2}{3}\right)^2},\\
&\Gamma_{22,1} = -\Gamma_{12,2} = r,\\
&\Gamma_{33,1} = -\Gamma_{13,3} = r\sin^2\theta,\\
&\Gamma_{33,2} = -\Gamma_{23,3} = r^2\sin\theta\,\cos\theta.
\end{aligned} \tag{25}$$

Calculating the components of Riemann tensor (23) for the metric (11) we find

$$\begin{aligned}
&R_{0101} = -\frac{1}{4r^2_{br}}\frac{3\sqrt{1-\frac{a^2}{r^2_{br}}} - \sqrt{1-\frac{r^2}{r^2_{br}}}}{\sqrt{1-\frac{r^2}{r^2_{br}}}},\\
&R_{0202} = -\frac{r^2}{4r^2_{br}}\left(3\sqrt{1-\frac{a^2}{r^2_{br}}} - \sqrt{1-\frac{r^2}{r^2_{br}}}\right)\sqrt{1-\frac{r^2}{r^2_{br}}},\\
&R_{1212} = -\frac{r^2}{r^2_{br}}\frac{1}{1-\frac{r^2}{r^2_{br}}}, \quad R_{2323} = -\frac{r^4}{r^2_{br}}\sin^2\theta,\\
&R_{0303} = R_{0202}\sin^2\theta, \quad R_{1313} = R_{1212}\sin^2\theta,
\end{aligned} \tag{26}$$

where $r_{br}^2 = \frac{1}{q} = \frac{3}{\varkappa\rho}$.

The space-time is therefore not a constant-curvature space, because the components R_{0i0k} of the Riemann tensor do not satisfy the condition

$$R_{\alpha\beta\gamma\delta} = K(g_{\alpha\gamma}g_{\beta\delta} - g_{\beta\gamma}g_{\alpha\delta}), \quad K = const, \tag{27}$$

which is a necessary and sufficient condition that the space-time possesses constant curvature. Note that the spatial components R_{ijkl} satisfy (27), while the mixed components R_{oijk} are zeroes. It means, due the structure of the components R_{0i0k}, the space-time (11) does not possess constant curvature.

So forth, study the geometric properties of the space-time (11) in terms of Zelmanov's theory of physically observable quantities. Zelmanov selected three groups of all independent curvature components $R_{\alpha\beta\gamma\delta}$ — the projections on time, the projections on space, and the mixed projections [2]:

$$X^{ik} = -c^2\frac{R^{\cdot i\cdot k}_{0\cdot 0\cdot}}{g_{00}}, \quad Y^{ijk} = c\frac{R^{\cdot ijk}_{0\cdot\cdot\cdot}}{\sqrt{g_{00}}}, \quad Z^{iklj} = c^2R^{iklj}.$$

Here we have only interest in the components X^{ik}. Calculating these components, we obtain

$$\begin{aligned} X_{11} &= \frac{c^2}{r_{br}^2}\frac{1}{\left(3\sqrt{1-\frac{a^2}{r_{br}^2}} - \sqrt{1-\frac{r^2}{r_{br}^2}}\right)\sqrt{1-\frac{r^2}{r_{br}^2}}} > 0, \\ X_{22} &= \frac{X_{33}}{\sin^2\theta} = \frac{c^2r^2}{r_{br}^2}\frac{\sqrt{1-\frac{r^2}{r_{br}^2}}}{3\sqrt{1-\frac{a^2}{r_{br}^2}} - \sqrt{1-\frac{r^2}{r_{br}^2}}} > 0. \end{aligned} \tag{28}$$

All components $X_{ik} \to \infty$ in the state of collapse. Besides, if the breaking of space takes place, the $X_{11} \to \infty$ and $X_{22} = X_{33}$ are zeroes. Comparing (13) and (28), we find that the gravitational inertial force F_1 and the radial projection of the Riemann tensor on time X_{11} are linked by the relation

$$F_1 = -rX_{11}. \tag{29}$$

It means that the sign of the r-directed force is opposite to the sign of the temporal projection of the Riemannian tensor (the "curvature of the time") in this direction: the **negative non-Newtonian force of attraction is due to the positive curvature of time.**

The partial case of the collapse of the incompressible liquid sphere $r_c = r_{br} = a$ is studied in detail in [7]. As follows from (12), in this case the surface of the sphere is simultaneously both the surface of the collapsar and the surface of the breaking of the space. Remember that $a = \frac{1}{\sqrt{q}}$ is also the radius of curvature of the sphere of condensed matter, where q is the Gaussian curvature of the reference space. Assuming $a = r_{br} = \sqrt{\frac{3}{\varkappa\rho}}$ and substituting this expression in (11), we obtain the de Sitter metric

$$ds^2 = \frac{1}{4}\left(1 - \frac{r^2}{a^2}\right)c^2dt^2 - \frac{dr^2}{1-\frac{r^2}{a^2}} - r^2(d\theta^2 + \sin^2\theta d\varphi^2). \tag{30}$$

The space-time described by the metric (30) satisfies the Einstein equations

$$R_{\alpha\beta} - \frac{1}{2}g_{\alpha\beta}R = \lambda g_{\alpha\beta}, \tag{31}$$

where the cosmological constant $\lambda = \frac{3}{a^2}$.

The term $\lambda g_{\alpha\beta}$ can be expressed in the form [7]

$$\lambda g_{\alpha\beta} = \varkappa\widetilde{T}_{\alpha\beta}. \tag{32}$$

Thus the λ-field generating the de Sitter space (30) is equivalent to the substance described by the energy-impulse tensor

$$\widetilde{T}_{\alpha\beta} = \frac{\lambda}{\varkappa}g_{\alpha\beta}. \tag{33}$$

Calculating the physically observable components of the energy-impulse tensor (33) [2], we find

$$\begin{aligned} \rho_0 &= \frac{\widetilde{T}_{00}}{g_{00}} = \frac{\lambda}{\varkappa}, \quad J_0^i = \frac{c\widetilde{T}_0^i}{\sqrt{g_{00}}} = 0, \\ U_0^{ik} &= c^2\widetilde{T}^{ik} = -\frac{\lambda c^2}{\varkappa}, \end{aligned} \tag{34}$$

where ρ_0, J_0^i and U_0^{ik} are the chr.-inv. density of matter, the (vector) density of impulse, and the tensor of stress, respectively.

As seen, the expression (10) transforms into (33) if the condition is

$$p = -\rho_0c^2 = -\frac{\lambda c^2}{\varkappa}, \tag{35}$$

i.e. it describes matter in the state of inflation.

Thus the energy-impulse tensor (33) describes substance with positive constant density $\rho_0 = \frac{\lambda}{\varkappa}$ and negative constant pressure $p_0 = -\rho_0c^2$. The flow of energy is given as $q_0 = J_0c^2 = 0$. This substance is called *physical vacuum*. We conclude that *the collapsing sphere of ideal incompressible liquid transforms into a de Sitter vacuum bubble by the special case of collapse, when the radius of the sphere a equals the breaking radius* r_{br}

$$a = r_{br} = \sqrt{\frac{3}{\varkappa\rho}} = r_c, \tag{36}$$

where the radius of the collapsar r_c coincides with the radius of the sphere and the breaking radius.

The physical vacuum is an actual substance, possessing positive density and negative pressure. Because the bubble is stationary, the negative pressure, which inflates the bubble, must be balanced by attraction, thereby compressing it. To solve the problem of stability of inflation collapsar, it is necessary to find this compressing factor. Study the physical and geometrical characteristics of the de Sitter bubble and compare them with the corresponding characteristics of the liquid bubble. This comparison allows us to consider the process of transformation of the gravitational collapsar ("black hole") into the inflational collapsar ("white hole").

The physical and geometrical properties of the de Sitter bubble, described by the metric (30), are studied in detail in [7]. The local reference space does not rotate and deform. The gravitational inertial force has the form

$$F_1 = \frac{c^2 r}{a^2 - r^2} > 0, \quad F^1 = \frac{c^2 r}{a^2} > 0, \tag{37}$$

i.e. is the force of repulsion. As seen, the formula (13) transforms into (37) by the condition (36). Thus the gravitational inertial force of attraction (13), acting inside the liquid bubble, transforms into a force of repulsion, acting inside the vacuum bubble. Using the collapse condition (36), rewrite (37) in the form

$$F^1 = \frac{\varkappa \rho_0 c^2 r}{3} = -\frac{\varkappa p r}{3} > 0. \tag{38}$$

It is easy to see that **both the positive density and the negative pressure both inflate the vacuum bubble**. As known, the generally accepted viewpoint consists in that the stability of the de Sitter vacuum bubble is due to the action of two opposite factors: 1) compression due to the positive density; 2) inflation due to the negative pressure. As follows from (38), the positive density and negative pressure effects are identical, consequently it is necessary to find the factor, which causes the compression of the bubble.

Studying the physical and geometrical characteristics of the Schwarzschild liquid bubble, we have found that the force of attraction (13) is balanced by the value $-rX_{11}$, which possesses the dimension of acceleration: see (29). The quantity $X_{11} > 0$ is the observable projection of the Riemann tensor component R_{0101} on time — the "curvature of time in the radial direction". Thus the non-Newtonian force of attraction, which is proportional to the radial distance r, is balanced by the action of the "positive curvature of the time" (the term rX_{11}).

Consider the problem of the stability of the vacuum bubble. Calculating the Riemann tensor (23) for the metric (30), we find

$$\begin{aligned} &R_{0101} = \frac{1}{4a^2}, \quad R_{0202} = \frac{R_{0303}}{\sin^2\theta} = \frac{r^2(a^2 - r^2)}{4a^4}, \\ &R_{1212} = \frac{R_{1313}}{\sin^2\theta} = -\frac{r^2}{a^2 - r^2}, \quad R_{2323} = -\frac{r^4 \sin^2\theta}{a^2}. \end{aligned} \tag{39}$$

It is easy to see that the components (26) transform into (39) by the condition $a = r_{br}$. The components (39) satisfy the condition (27), where the four-dimensional constant curvature is negative: $K = -\frac{1}{a^2}$.

The quantities C_{ijkl}, C_{ik} and C (20–21) of the reference space (30) then take the form

$$\begin{aligned} &C_{1212} = \frac{C_{1313}}{\sin^2\theta} = \frac{r^2}{a^2 - r^2}, \quad C_{2323} = \frac{r^4 \sin^2\theta}{a^2}, \\ &C_{11} = \frac{2}{a^2 - r^2}, \quad C_{22} = \frac{C_{33}}{\sin^2\theta} = \frac{2r^2}{a^2}, \\ &C = \frac{6}{a^2} > 0. \end{aligned} \tag{40}$$

The components C_{ijkl} (40) satisfy the condition (22), where the three-dimensional Gaussian curvature is $q = \frac{1}{a^2}$, consequently the reference space of the vacuum bubble is a three-dimensional sphere of the real radius $a = \frac{1}{\sqrt{q}}$. We have shown above that the de Sitter space (30) possesses negative four-dimensional Gaussian curvature $K = -\frac{1}{a^2} = -q$, consequently it is a four-dimensional sphere with the imaginary radius $\Re = iq$.

Comparing the obtained results with the analogical ones for the liquid sphere (11), we find that both reference spaces possess positive constant curvature, but the four-dimensional de Sitter space possesses constant negative curvature. Calculating the physically observable components of the Riemann-Christoffel tensor X_{ik} (28) for the de Sitter vacuum bubble, we find

$$X_{11} = -\frac{c^2}{a^2 - r^2} < 0, \quad X_{22} = \frac{X_{33}}{\sin^2\theta} = -\frac{c^2 r^2}{a^2} < 0. \tag{41}$$

We conclude therefore that the sign of curvature of the de Sitter vacuum bubble coincides with the signs of the $R_{\alpha\beta\gamma\delta}$ projections onto time (the "negative curvature of time").

Comparing the component X_{11} (41) with the expression of the gravitational inertial force (37), we find that these quantities satisfy the condition (29), i.e. the signs of the F_1 and X_{11} are opposite. We conclude that **the non-Newtonian force of attraction inside the liquid sphere (11) is due to the positive curvature of time, the force of repulsion inside the vacuum bubble (30) is due to the negative curvature of time.**

These results are connected with the geometric structure of the physically observable curvature components X_{ik}. Generally speaking, they depend on the deformation, rotation, and gravitation of the reference space [2]. If locally the space does not deform and rotate, the components X_{ik} take the form

$$X_{ik} = \frac{1}{2}({}^*\nabla_i F_k + {}^*\nabla_k F_i) - \frac{1}{c^2} F_i F_k, \tag{42}$$

where ${}^*\nabla_i$ is the chr.-inv. operator of covariant differentiation [2].

We have thus shown that the collapsing liquid bubble (11) transforms instantly into the vacuum bubble (30) by the special case of collapse: $a = r_{br}$. The surface $r = a$ in this case is simultaneously: 1) the breaking surface; 2) the surface of the inflation collapsar.

Calculating the elementary observable interval of time for the metrics (11) and (30), we find, respectively:

1) the Schwarzschild liquid bubble

$$d\tau_l = \pm\frac{1}{2}\left(3\sqrt{1-\frac{\varkappa\rho a^2}{3}} - \sqrt{1-\frac{\varkappa\rho r^2}{3}}\right)dt; \qquad (43)$$

2) the de Sitter vacuum bubble

$$d\tau_v = \pm\frac{1}{2}\left(\sqrt{1-\frac{r^2}{a^2}}\right)dt. \qquad (44)$$

Assuming in (43) $a = \sqrt{\frac{3}{\varkappa\rho}} = r_{br}$, we obtain

$$d\tau_l = \mp\frac{1}{2}\left(\sqrt{1-\frac{r^2}{a^2}}\right)dt. \qquad (45)$$

We have obtained as a result that the observable time τ inside these bubbles flows in the opposite direction. We consider usually the observable time as flowing in the positive direction — from the past to the future. In order to determine one of the two signs in the formulaes (43–44), it is necessary to ask, which of the two bubbles is more applicable as the model of the observed Universe: the Schwarzschild liquid bubble or the de Sitter vacuum bubble? This question will be studied in detail in the next section.

4 The de Sitter bubble as a proposed cosmological model

Consider the Schwarzschild and de Sitter bubbles as the two possible cosmological models. The choice of such a model must be in accordance with astronomical data. The most important criterion for the choice is the observed red-shift. In other words, the model, which allows the red-shift, can be chosen as the cosmological model. The effect of the spectral line displacement is calculated exactly for every gravitational field configuration.

As known, the world-lines of light-like particles (null geodesic lines) are described by the equations of the parallel transfer of the isotropic (null) four-dimensional wave vector K^α

$$\begin{gathered}\frac{dK^\alpha}{d\sigma} + \Gamma^\alpha_{\mu\nu}K^\mu\frac{dx^\alpha}{d\sigma} = 0, \quad K^\alpha = \frac{\omega}{c}\frac{dx^\alpha}{d\sigma} = 0,\\ K_\alpha K^\alpha = 0,\end{gathered} \qquad (46)$$

where ω is the cyclic frequency, $\Gamma^\alpha_{\mu\nu}$ is the Christoffel symbols of the second kind, σ is the parameter of differentiation, $\frac{dx^\alpha}{d\sigma}$ is the isotropic (null) vector of the 4-velocity, which is tangent to the world-lines ($g_{\alpha\beta}\frac{dx^\alpha}{d\sigma}\frac{dx^\beta}{d\sigma} = 0$).

These equations have the form in terms of the physically observable quantities (viz. the theory of chronometric invariants) [9]

$$\frac{1}{\omega}\frac{d\omega}{d\tau} + \frac{1}{c^2}D_{ik}\frac{dx^i}{d\tau}\frac{dx^k}{d\tau} - \frac{1}{c^2}F_i\frac{dx^i}{d\tau} = 0, \qquad (47)$$

$$\begin{gathered}\frac{d}{d\tau}\left(\omega\frac{dx^i}{d\tau}\right) + 2\omega(D^i_k + A^{\cdot i}_{k\cdot})\frac{dx^k}{d\tau} -\\ -\omega F^i + \omega\Delta^i_{nk}\frac{dx^n}{d\tau}\frac{dx^k}{d\tau} = 0,\end{gathered} \qquad (48)$$

$$h_{ik}\frac{dx^i}{d\tau}\frac{dx^k}{d\tau} = c^2. \qquad (49)$$

The system of equations (47–49) is the chr.-inv. form of the parallel transfer equations of the four-dimensional wave vector $K^\alpha = \frac{\omega}{c}\frac{dx^\alpha}{d\sigma}$, where the equations (47–48) are linked by the relation (49). Solving the system for every metric, we find the frequency of the photon and the associted spatial trajectory in the given space-time.

If the reference space does not rotate and deform, the equations (47–48) take the form

$$\frac{1}{\omega}\frac{d\omega}{d\tau} - \frac{1}{c^2}F_i\frac{dx^i}{d\tau} = 0, \qquad (50)$$

$$\frac{1}{\omega}\frac{d}{d\tau}\left(\omega\frac{dx^i}{d\tau}\right) - F^i + \Delta^i_{nk}\frac{dx^n}{d\tau}\frac{dx^k}{d\tau} = 0. \qquad (51)$$

Substituting into (50) the expressions for gravitational inertial force F_1 (13) and (40), we obtain the equations describing the behaviour of the cyclic frequency inside both the condensed matter and physical vacuum bubbles, respectively:

1) the Schwarzschild bubble

$$\frac{1}{\omega}\frac{d\omega}{d\tau} = -\frac{\varkappa\rho c^2}{3}\frac{r}{\left(3\sqrt{1-\frac{\varkappa\rho a^2}{3}} - \sqrt{1-\frac{\varkappa\rho r^2}{3}}\right)\sqrt{1-\frac{\varkappa\rho r^2}{3}}}\frac{dr}{d\tau}; \qquad (52)$$

2) the de Sitter bubble

$$\frac{1}{\omega}\frac{d\omega}{d\tau} = \frac{r}{a^2 - r^2}\frac{dr}{d\tau}. \qquad (53)$$

Integrating (52–53), we obtain, respectively:

1) the Schwarzschild bubble

$$\omega = \frac{P}{3\sqrt{1-\frac{\varkappa\rho a^2}{3}} - \sqrt{1-\frac{\varkappa\rho r^2}{3}}}, \quad P = const; \qquad (54)$$

2) the de Sitter bubble

$$\omega = \frac{Q}{\sqrt{1-\frac{r^2}{a^2}}}, \quad Q = const, \qquad (55)$$

where P and Q are integration constants.

Cosmologists have introduced the quantity z — the relative variation of the frequency

$$z = \frac{\omega_{em} - \omega_{obs}}{\omega_{obs}}, \tag{56}$$

where ω_{em} is the frequency, emitted by the source, located at the radial distance r_{em} relative to the observer, ω_{obs} is the observable (observed, registered) frequency of this source at the place, where the observer is located: r_{obs}. The condition $z < 0$ means that the observable frequency is more than the emitted, consequently the observable light seems shifted more towards the blue than the emitted one (the phenomenon of blue-shift). The condition $z > 0$ implies a red-shift, because in this case the observable frequency is less than the emitted one.

Calculating the value z for the expressions (54–55), we obtain

1) the Schwarzschild bubble

$$z = \frac{\sqrt{1 - \dfrac{\varkappa\rho r_{em}^2}{3}} - \sqrt{1 - \dfrac{\varkappa\rho r_{obs}^2}{3}}}{3\sqrt{1 - \dfrac{\varkappa\rho a^2}{3}} - \sqrt{1 - \dfrac{\varkappa\rho r_{em}^2}{3}}} < 0; \tag{57}$$

2) the de Sitter bubble

$$z = \frac{\sqrt{a^2 - r_{obs}^2} - \sqrt{a^2 - r_{em}^2}}{\sqrt{a^2 - r_{em}^2}} > 0. \tag{58}$$

It follows from (58) that the red-shift takes place inside the de Sitter bubble, therefore namely this space-time can be considered as a cosmological model.

Let us study more exactly the behavior of the frequency of photons emitted by distant sources. Assume that the photons from the source move to the observer in the radial r-direction. Then (49) takes the form

$$\frac{a^2}{a^2 - r^2}\left(\frac{dr}{d\tau}\right)^2 = c^2. \tag{59}$$

Taking the root of (59), we obtain

$$\frac{dr}{\sqrt{a^2 - r^2}} = \pm\frac{c}{a}d\tau = \pm H d\tau, \tag{60}$$

where H is the Hubble constant. Assuming $H = 75\,\text{Mps/sec} = 2.3 \times 10^{-18}\text{sec}^{-1}$, we find $a = 1.3 \times 10^{28}$ cm.

Choose the sign + or −, respectively, if the distance between the observer and the source is taken into account: 1) from the observer to the source; 2) from the source to the observer. Integrating (60) from r (the distance from the source) until $r = 0$ (the location of the observer), we find

$$\int_r^0 \frac{dr}{\sqrt{a^2 - r^2}} = -\arcsin\frac{r}{a} = -H\tau, \tag{61}$$

where τ is the observable time, in the course that the signal from the source comes to the observer. It follows from (61) the expression for r:

$$r = a\sin H\tau, \tag{62}$$

i.e. the photometric distance is harmonic (sinusoidal) oscillation with the amplitude a and the period $T = \frac{2\pi}{H}$. The amplitude a is the maximal distance from any observer — the so called "event horizon". It is easy to find that the three-dimensional observable vector of the light velocity $c^1 = \frac{dr}{d\tau}$ has the form

$$c^1 = \frac{dr}{d\tau} = aH\cos H\tau = c\cos H\tau, \tag{63}$$

where

$$h_{11}c^1c^1 = \frac{a^2}{a^2 - r^2}\left(\frac{dr}{d\tau}\right)^2 = c^2.$$

This formula means that the radial component of the vector of the light velocity oscillates with a frequency H and an amplitude c. This oscillation is shifted for $\frac{\pi}{2}$ with respect to the oscillation of the radial distance r (62).

Substituting (63) into (55), we obtain

$$\omega = \frac{Q}{\cos H\tau}, \quad 0 \leqq \tau \leqq \frac{\pi}{2H}. \tag{64}$$

As seen, $\omega \to \infty$ if $\tau \to \frac{\pi}{2H}$, i.e. by $r \to a$. It follows from (58) that the value of z increases infinitely by $r \to a$. This effect takes place from the viewpoint of the real observer, because the observable time depends on the photometric distance r from the event horizon:

$$d\tau = \frac{1}{2}\left(\sqrt{1 - \frac{r^2}{a^2}}\right)dt. \tag{65}$$

Thus the tempo of the observable time decreases by $r \to a$, and the observable time is stopped at the event horizon. Therefore the observable cyclic frequency of photons increases infinitely by $r \to a$.

It was shown above, the coordinate (photometric) distance r is the sinusoidal (harmonic) oscillation (wave) with the amplitude a and the cyclic frequency $H = \frac{2\pi}{T}$. The quantity $T = \frac{2\pi}{H}$ is the full period of the oscillation, the maximal value a (amplitude) is the event horizon. Taking into account only the positive values of r, we are restricted only to the semi-period of the oscillation. The maximal value of $r = a$ takes place at $\tau = \frac{\pi}{2H} = \frac{T}{4}$. Introducing the used-in-contemporary cosmology value $H = 2.3 \times 10^{-18}\text{sec}^{-1}$, we find $T_a = \frac{\pi}{2H} = 21.6 \times 10^9$ years — the time of passing of the light signal from the event horizon to the observer. Contemporary cosmologists calculate the time of the life of the Universe as the interval of time after the Big Bang. They obtained the age of the Universe approximately 13.75×10^9

years. If we'll introduce H as the ordinary (not the cyclic) frequency $H = \frac{H_c}{2\pi} = \frac{1}{T}$, we find $T = 13.74 \times 10^9$ years.

As is well known, the mathematical basis of contemporary relativistic cosmology is the theory of a non-stationary (extending) universe. It is founded on Friedman's cosmological models, which belong to a particular class of solutions to Einstein's field equation, obtained by the imposing condition that the space of the observable Universe is homogeneous and isotropic. This class of solutions is described by the metric

$$ds^2 = c^2dt^2 - R^2(t)\frac{dx^2 + dy^2 + dz^2}{\left[1 + \frac{k}{4}(x^2 + y^2 + z^2)\right]^2}, \quad k = 0, \pm 1, \quad (66)$$

where $R(t)$ is the scale factor: $\frac{1}{R}\frac{dR}{dt} = H$. In accordance with the value k of the three-dimensional space: 1) is flat ($k = 0$); 2) has negative curvature ($k = -1$); 3) has positive curvature ($k = +1$). Models with $k = 0, -1$ are called open, and models with $k = +1$ are closed ones. Friedman's spaces are both empty ($T_{\alpha\beta} = 0$) and filled by ideal liquid described by (10).

The special reference space (68) does not rotate and gravitate, but it does deform. The tensor of the rate of deformation is described by the formula $D_{ik} = R\frac{dR}{dt}$. The observable time flows uniformly: $d\tau = dt$, in particular, it does not depend on the photometric distance r in contrast to the interval of the observable time in the de Sitter bubble. Friedman's models are: 1) extending; 2) compressing; 3) oscillating; 4) stationary [2]. The cosmological term λ can be: 1) positive, 2) negative, 3) zero. Cosmologists explain the observable red-shift by the Doppler effect which is due to the expansion of the space of the Universe. The generally accepted model of the non-stationary (extending) Universe is the Standard Cosmological Model. The age of the Universe is determined by means of extrapolation of the uniformly flowing time from the present to the past — the beginning of the Universe caused by the Big Bang. The age of the observable Universe, according to Friedman's theory, is determined approximately as 13×10^9 years — the interval of the time from the Big Bang of the initial singularity (the "point" consisting of super-compact initial substance).

Now we come to the essential question: What cosmological model is more applicable for the description of the observable Universe: the stationary de Sitter space or the extending Friedman's space? The criterium of the choice must be the results of astronomical observations. It follows from the observations of spectra of galaxies that the observable red-shift is linear for more near galaxies and it rapidly increases for the most distant objects. Most cosmologists explain this result as the accelerated expansion of space, while routinely avoiding some principal weaknesses. The correct theoretical explanation of this fact has not been obtained until now. Moreover, contemporary cosmologists do not calculate variations of frequencies as exact solutions to the general relativistic equation of motion of null geodesic lines. The observable phenomena of the red-shift is explained by the temporal variations of the scale factor $R(t)$. It is necessary to note that the exact solution(s) to the equations (47–49) can be found only for concrete metrics. In particular, the expression of the cyclic frequency ω for Friedman's metric can be obtained only if the exact expression for $R(t)$ is known and the value of k is chosen. In other words, in order to study variations of frequencies of cosmic objects, it is necessary before hand to assign the function $R(t)$, which determines the kind of deformation, and the value of k, which determines the geometry of the reference space.

The exact value of the frequency (55) is obtained here as the solution to equation of motion of null geodesic lines (47–49). It follows from (55, 59) that the observable frequency ω and the quantity z increase infinitely while approaching the event horizon. If $r \ll a$, the quantity z can be transformed as

$$z \approx \frac{r_{em}^2 - r_{obs}^2}{2a^2}. \quad (67)$$

It means that the red-shift in the spectra of near-to-the observer objects ($r \ll a$) is subject to the parabolic law. In other words, the linear red-shift cannot be explained in the de Sitter space. The gravitational inertial force of repulsion inside the de Sitter bubble causes the parabolic red-shift for near sources and the infinite increase at the maximal distance from the observer — the event horizon. Thus the red-shift in the de Sitter bubble is due to the non-Newtonian force of repulsion, which is proportional to the radial (photometric) distance r.

We conclude: neither the Friedman expansion, which is caused by the deformation of the reference space, nor the de Sitter force of repulsion can explain simultaneously both the linear red-shift for near sources and the sharp, non-linear increase for most distant sources. Probably, this problem can be solved in frames of a generalized metric which includes both Friedman's expansion and the de Sitter repulsion. It is possible that the de Sitter space is applicable near the event horizon ($r \backsim a$), while the Friedman extending space correctly describes more near-to-the observer regions ($r \ll a$).

5 The past, the present, and the future are three multispace aspects of the observable time

Now, let us consider in detail the collapse mechanism of the liquid bubble into the vacuum bubble. We have obtained above the key rôle in the very process the condition (36) plays. If such a state is realized, then the interval of the observable time interior to Schwarzschild's liquid bubble $d\tau_{\text{l}}$ transforms into the interval of the observable time inside de Sitter's vacuum bubble $d\tau_{\text{v}}$; moreover, each of these intervals possesses the opposite sign:

$$d\tau_{\text{l}} = -d\tau_{\text{v}}.$$

It means that the observable time inside the vacuum de Sitter bubble flows in the opposite direction. We have assumed in the previous section that once the de Sitter bubble is

applicable as a cosmological model, the flow of the τ in this space is positive: the observable time flows from the past to the future. Then the observable time inside the Schwarzschild liquid bubble flows from the future to the past, and its interval has the form:

$$d\tau_{\rm l} = -\frac{1}{2}\left(3\sqrt{1-\frac{a^2}{r_{br}^2}} - \sqrt{1-\frac{r^2}{r_{br}^2}}\right)dt < 0. \qquad (68)$$

If $a = r_{br}$, then (70) transforms into the expression

$$d\tau_{\rm v} = \frac{1}{2}\left(\sqrt{1-\frac{r^2}{a^2}}\right)dt > 0, \qquad (69)$$

which is the interval of the observable time inside the de Sitter bubble.

Thus the surface $a = \sqrt{\frac{3}{\varkappa\rho}} = r_{br}$ is the mirror dividing two worlds — the space of the future and the space of the past. It means, this surface is the space of the present. As was shown above, the surface a is singular. It means, the present is the *instantaneous state* between the future and the past, where the *future transforms into the past by means of passing through the singulary state*. The space of the future is here the vacuum de Sitter liquid bubble, where the observable time flows from the future to the present: that is, the future "goes to us". The future, after the passage through the said singulary surface, becomes the past: the present "leaves us". Thus the singular surface is not only a mirror (a reflecting surface). It is simultaneously a membrane: a telemetric, multispace membrane connecting the worlds of the past and the future. The future penetrates into the inflation collapsar namely through this "mirror-like membrane" — the *interior layer* between the past and the future. This situation can be illustrated in terms of the well-known description of the interaction between a light beam and some incident surface (as the light beam falls upon the surface). This beam splits into three beams: 1) the reflected; 2) the refracted; 3) the absorbed. The light beam within the framework of General Relativity is the trajectory of photons — the world-line of the null four-dimensional length $ds = 0$, where here every individual photon is said to be the event itself. The world-lines with $ds \neq 0$ also consist of four-dimensional world-points. It is possible to say therefore that the light beam of events, falling onto the singular surface, splits into: 1) the reflected light beam (returned into the space of the future); 2) the refracted light beam (directed into the space of the past); 3) the absorbed light beam, by the said singularity surface. The first light beam describes those events, which cannot be realized (*materialized*) in the present (for example, using analogy with daily life, certain ideas or epochs which are far too advanced for the time). The second light beam describes those events, which could be realized in principle, but they can not actually be realized (in part, these are not readily perceived by the bulk human consciousness). Finally, those events in the likeness of the absorbed light-beam represent the world of the present, which is uniquely perceived by our consciousness (taking into account varying internal degrees of consciousness) as "reality". The said non-realized (for a while) events can be called *virtual events*.

An event in General Relativity is the four-dimensional point of the space-time V_4 — the three-dimensional point, which is expanded into a "thread". This thread is the four-dimensional trajectory of the event — the world-line. These lines can be: 1) non-null (trajectories of mass-bearing particles, both real and imaginary); 2) null (trajectories of light-like particles; in particular, photons). Interlacing of these threads creates the "material of the space". Because we assume here fundamental interactions between the past, the present, and the future, we must introduce a "medium", which realizes these interactions. We will consider in this paper only null world-lines, i.e. we will study events of the "life of photons".

It is evident that those particles, which realize the transfer of energies between the future into the past, must penetrate the singularity surface. As known, regular photons cannot pass through the singularity surface, but this surface is penetrable for *zero-particles*, introduced in [3]. These particles exist in the generalized space-time $\widetilde{V}_4$, which is determined as an immediate generalization of the Riemannian space-time V_4 of General Relativity (both at the differential-geometric manifold and sub-manifold levels): $\widetilde{V}_4 = V_4 \cup Z$, where Z is the *zero-space*. Zero-particles have zero rest-mass m_0, zero relativistic mass m, and non-zero gravitational-rotational mass M, which is described in the $\widetilde{V}_4$ as

$$M = \frac{m}{1-\dfrac{\mathrm{w}+v_i u^i}{c^2}}, \quad u^i = \frac{dx^i}{dt}. \qquad (70)$$

The four-dimensional metric of $\widetilde{V}_4$ satisfies the condition $g = \det|g_{\alpha\beta}| \leqslant 0$, i.e. it allows the versatile degeneration of the metric. The manifold $\widetilde{V}_4$ is the ordinary space-time V_4 by $g < 0$ and it is the zero-space Z by $g = 0$. Zero-particles transfer instantaneously ($d\tau = 0$), from the viewpoint of a real observer, along three-dimensional lines of null observable length ($d\sigma = 0$), i.e. they are mediums for the *long-range-action*. Zero-particles can be considered as the *more tenuous and thinner structures* than the photon. The condition (5) takes for zero-particles the form $d\sigma = d\tau = 0$.

The four-dimensional null wave vector K^α of the $\widetilde{V}_4$ can be expressed both in the corpuscular form and in the wave form

$$K^\alpha = \frac{\omega}{c}\frac{dx^\alpha}{d\sigma}, \quad K_\alpha = \frac{\partial\psi}{\partial x^\alpha}, \qquad (71)$$

where ψ is the phase of the wave (the eikonal).

The physically observable characteristics of K^α are [3]

$$\frac{K_0}{\sqrt{g_{00}}} = \pm\omega = \frac{{}^*\partial\psi}{\partial t}, \quad K^i = \frac{\omega}{c^2}\frac{dx^i}{d\tau} = -h^{ik}\frac{{}^*\partial\psi}{\partial x^k}, \qquad (72)$$

where

$$\frac{{}^*\partial}{\partial t} = \frac{1}{\sqrt{g_{00}}}\frac{\partial}{\partial t}, \quad \frac{{}^*\partial}{\partial x^i} = \frac{1}{\sqrt{g_{00}}}\frac{\partial}{\partial x^i} + \frac{v_i}{c^2}\frac{{}^*\partial}{\partial t}$$

are the chr.-inv. operators of differentiation along the temporal and spatial coordinates, respectively [2]. The signs (+) and (−) are related to the spaces possessing the direct and reverse flow of time, respectively.

The wave form of the condition $K_\alpha K^\alpha = 0$ is the well-known eikonal equation

$$g^{\alpha\beta}\frac{\partial\psi}{\partial x^\alpha}\frac{\partial\psi}{\partial x^\beta} = 0. \tag{73}$$

Expressing (73) in terms of physically observable values, we obtain

$$\frac{1}{c^2}\left(\frac{{}^*\partial\psi}{\partial t}\right)^2 - h^{ik}\frac{{}^*\partial\psi}{\partial x^i}\frac{{}^*\partial\psi}{\partial x^k} = 0. \tag{74}$$

The cyclic frequency of zero-particles is $\omega = 0$, consequently the equation (74) takes the form of the standing wave [3]

$$h^{ik}\frac{{}^*\partial\psi}{\partial x^i}\frac{{}^*\partial\psi}{\partial x^k} = 0, \tag{75}$$

which can certainly be interpreted as a hologram, i.e., a standing wave of the extended space-time. Thus the present, in the sense of geometric optics, is a **holographic picture perceived by our consciousness as the material (real) world.**

We conclude therefore that zero-particles are the **mediums of the long-range-action** in the space of the present — the boundary between the spaces of the future and the past. Zero-particles can be considered as a result of the fundamental interaction between the photons themselves, moving in time in the two above-mentioned opposite directions and possessing certain cyclic frequencies of the opposite signs. In other words, the standing wave can be interpreted as a result of the summarization of the two waves ψ_+ and ψ_-, directed from the past to the future and from the future to the past, respectively. Let photons, moving in the space of the past, possess positive frequencies ω_+, and photons moving in the space of the future, possess negative frequencies ω_-, respectively. The interaction between the ψ-waves, oppositely oriented in time, generates information, which is transmitted instantaneously by means of zero-particles. This information creates a hologram (the unique "reality" of the present moment), which exists during the infinitely small interval of time as well as after it is substituted by the next hologram. By analogy, the perception of the continuity (and solidity) of the present is due to the fact that the successive frames of a movie are substituted very quickly.

We do not consider here the whole unique process of the chain of sequential materializations: zero-particles → photons → mass-bearing particles, because this problem is very difficult and impractical to be considered in further detail. We introduce here instead the problem of observation of cosmic objects. Consider the information which comes to us from stars and galaxies in the form of light beams. Because the cosmic objects are distant from us, we register the photons later than they were first emitted. It means, the observer, registering the electromagnetic radiation of the source, studies the **past state of this cosmic object**. This state corresponds to the moment of radiation of the electromagnetic signal. The information about the present state of the object can be obtained by means of registration of zero-particles, emitted by the source at the moment of observation. But the observer does not perceive it, because he does not use corresponding intermediary instruments. Contemporary astronomers use instruments, which can register only different ranges of electromagnetic radiation transferring at the light velocity.

6 Newtonian and non-Newtonian forces in the Universe

We have studied until now only non-Newtonian forces:

1) the force of attraction (13), created by the homogeneous liquid sphere (11);

2) the force of repulsion (37), created by the vacuum bubble (30);

3) the values of these forces are proportional to the radial coordinate r;

4) both forces are connected to the observable components of the Riemann tensor by the correlation (29).

The metrics (11) and (30) describe the gravitational fields created by the continuous bodies (bubbles). It is necessary to note that the force of attraction (13) transforms into the force of repulsion (37) as a result of the collapse of the liquid bubble, and both forces are non-Newtonian. The force of attraction (13) is created by the liquid sphere, which was initially introduced by Schwarzschild for the description of the Sun. On the other hand, the Sun as an attracting body is described by the well-known Schwarzschild metric of a single mass (mass-point) in emptiness ($R_{\alpha\beta} = 0$) [8]. This metric has the form

$$\begin{aligned} ds^2 &= \left(1-\frac{r_g}{r}\right)c^2dt^2 - \frac{dr^2}{1-\dfrac{r_g}{r}} - r^2(d\theta^2+\sin^2\theta d\varphi^2), \\ r_g &= \frac{2GM}{c^2} \end{aligned} \tag{76}$$

where r_g is the gravitational (Hilbert) radius and M is the mass of the gravitating mass-point.

The space-time (76) collapses by the condition $r = r_g$, and the surface $r = r_g$ is called the *Schwarzschild surface*. Besides this, the space experiences breakage by the same condition. Thus the mass-point stops the time and breaks the space by $r = r_g = r_{br}$.

The metric (76) is applied for the description of the gravitational field of the Sun and the motion of the planets of the Solar System. It allows the post-Newtonian approximation, consequently it must include Newtonian gravitation. Let us study in detail the physical and geometrical characteristics

of the gravitational field of the mass-point in order to compare the obtained results with the analogous results for the metric (11), which describes the continuous body — a liquid sphere. This approach allows us to determine the problem of the connection between the local geometry of space-time and the character of attractive forces therein.

We have obtained for the metric (11) that the radial non-Newtonian force of attraction (13) is linked to the radial projection of the "curvature of time" (28) by the correlation (29). As follows from (29), the force of attraction is due to the positive curvature of time. Let us study the connection between the observable components of the Riemann tensor and the gravitational inertial force for the space-time (76).

The reference space described by (76) does not rotate and deform, but it gravitates. Calculating the gravitational inertial force F_i by the formula $F_i = \frac{c^2}{c^2-\mathrm{w}}\frac{\partial \mathrm{w}}{\partial x^i}$, we obtain

$$F_1 = -\frac{c^2 r_g}{2r^2}\frac{1}{1-\dfrac{r_g}{r}}, \quad F^1 = -\frac{c^2 r_g}{2r^2}. \tag{77}$$

Substituting into the expression for F^1 the value $r_g = \frac{2GM}{c^2}$, we rewrite (77) in the form

$$F_1 = -\frac{GM}{r^2}\frac{1}{1-\dfrac{2GM}{c^2 r}}, \quad F^1 = -\frac{GM}{r^2}. \tag{78}$$

We see that the component F^1 is the ordinary Newtonian force of attraction. Calculating the observable components of the Riemann tensor X_{11} by the formula (42), we find

$$X_{11} = -\frac{c^2 r_g}{r^3}\frac{1}{1-\dfrac{r_g}{r}} < 0. \tag{79}$$

It follows from (78–79) the relation between the force of attraction and the "curvature of time" in the radial direction:

$$F_1 = \frac{r}{2}X_{11}. \tag{80}$$

The signs of F_1 and X_{11} coincide in contrast to the analogous relation (29), which is satisfied for both the de Sitter and Schwarzschild bubbles. It means that the Newtonian force of attraction is due to the "negative curvature of time". The point is that the Non-Newtonian and Newtonian gravitational forces of attraction are originated by different sources. As shown earlier, the non-Newtonian force of attraction is connected to the *continuous body* (the liquid sphere). The Newtonian force is connected usually to the mass, which is *concentrated inside a small volume*, so called a " mass-point" [8]. Meanwhile, it is evident that continuous bodies possess the said Newtonian force, because they attract bodies with smaller masses. Therefore, it is necessary to state correctly the criterium, which will determine what kind of cosmic bodies must be described as "continuous bodies" and what kind — as "mass-points".

The gravitational field of the mass-point is described by the Schwarzschild metric (76), which includes Newtonian gravitation (as well as the post-Newtonian approximation). The motion of cosmic bodies, which move around the attracting center (mass-point), is usually studied in either the framework of Newtonian gravitation or that of the post-Newtonian theory of gravitation. In the second case, the motion of cosmic objects is calculated in the Schwarzschild mass-point field by the condition $r_g \ll r$. This condition means that the Hilbert radius is very small in comparison to the distance between the attracting center and the object moving around the center. This approach is applicable both to the Sun and to the planets, asteroids, etc. On the other hand, continuous bodies also possess gravitational attraction. In part, the gravitational inertial force of attraction in the reference space of the homogeneous liquid sphere is described by (13). The question now arises: what are the conditions, by which the Newtonian force of attraction is the partial case of the non-Newtonian force (13)?

It follows from (77–78) that the gravitational inertial force coincides with the Newtonian force of attraction if $r_g \ll r$. Because the Newtonian theory of gravitation is constructed in the flat three-dimensional (Eucledian) space, we can assume that the homogeneous gravitating mass M has the form

$$M = \rho V, \quad V = \frac{4\pi a^3 \rho}{3}, \tag{81}$$

where V is the volume of the mass, a is its radius, $\rho = const$ is the density of mass. This assumption is admissible also for any homogeneous sphere. Using (81), we can rewrite the expression (13) in the form

$$F_1 = -\frac{c^2 r_g}{a^3}\frac{r}{\left(3\sqrt{1-\dfrac{r_g}{a}} - \sqrt{1-\dfrac{r_g r^2}{a^3}}\right)\sqrt{1-\dfrac{r_g r^2}{a^3}}}. \tag{82}$$

Let $r_g \ll r \leqq a$. Expressing the value $\sqrt{1-\frac{r_g r^2}{a^3}}$ into series, neglecting the members of the second kind and assuming $\sqrt{1-\frac{r_g}{a}} \approx 1-\frac{r_g}{2a}$, we obtain, after transformations, the expression for the F_1 in the form

$$F_1 \approx -\frac{c^2 r_g r}{2a^3} = -\frac{GMr}{a^3}. \tag{83}$$

If $r = a$, then (83) transforms into the expression for the Newtonian force of attraction, created by the sphere of radius a

$$F_1 = -\frac{GM}{a^2}. \tag{84}$$

The expression (84) coincides completely with (78) by $r_g \ll r = a$. Thus the Newtonian gravitational force is the

partial case of the non-Newtonian force of gravitation (82) by the condition $r_g \ll r = a$. But this fact does not mean that we must use the Newtonian theory of gravitation for the description of the gravitational field of the single body, whose Hilbert radius is small in comparison with its radius. The point is that the application of the relativistic mass-point metric (76) allows us to calculate the well-known effects (e.g. the perihelion motion of Mercury, the gravitational shift of light beams, the gravitational shift of spectral lines). It is possible that many other effects, unknown until now, will be explained by means of this metric.

We have studied until now only the case $r_g \ll r = a$. This condition corresponds to a single body, whose Hilbert radius r_g is negligible in comparison with its geometrical radius a. Consider now the case $r_g \ll r$, where the radial coordinate r can possess any values. Then the value $\frac{\varkappa\rho r^2}{3} = \frac{r_g r^2}{a^3}$ is not infinitely small for $r \gg a$. It follows from (11) that the condition $\frac{\varkappa\rho r^2}{3} = 1$ is the *condition of space breaking*, consequently the quantity $r_{br} = \sqrt{\frac{3}{\varkappa\rho}}$ is the breaking radius. Using the expressions for the r_g and r_{br}, we can rewrite (13) in the form

$$F_1 = -\frac{2GM}{c^2 a^3} \frac{r}{\left(3\sqrt{1-\dfrac{2GM}{c^2 a}} - \sqrt{1-\dfrac{r^2}{r_{br}^2}}\right)\sqrt{1-\dfrac{r^2}{r_{br}^2}}}. \quad (85)$$

The formula (85) describes the gravitational inertial force of the liquid sphere, whose Hilbert radius is small in comparison with the radius of the sphere ($\frac{r_g}{a} \ll 1$) and the sphere of space breaking $r = r_{br}$ is outside the liquid sphere ($r_{br} > a$). It follows from (85) that the force $F_1 \to \infty$ by $r \to r_{br}$. It is evident that the force (85) is the non-Newtonian force of attraction, manifesting a curvature dicontinuity in the environment.

The condition of space breaking was initially studied in [6]. The Sun was introduced as a liquid homogeneous sphere. It was shown that the Sun would break the surrounding space, with the breaking radius $r_{br} = 3.43\times10^{13}$ cm = 2.3 AU (1 AU = 1.49×10^{13} cm), where 1 AU is the distance between the Sun and the Earth. Thus the breaking (curvature discontinuity) of the Sun's space is located inside the asteroid strip, i.e. outside the gravitating body (the Sun). The Hilbert radius of the Sun is $r_g = 2.9 \times 10^5$ cm, the proper radius being $a = 6.95 \times 10^{10}$ cm. It is easy to calculate $\frac{r_g}{a} = 4.2 \times 10^{-6} \ll 1$, and $\frac{r_{br}}{a} = 4.9 \times 10^2$. It is possible that this non-Newtonian force creates the additional effect on the motion of the bodies in the Solar System. In partial, those bodies, which recede from the Sun in the radial direction, must possess additional negative (directed to the Sun) acceleration.

Analogous calculations were realized for all the planets of the Solar System [6]. It is important to note that the breaking spheres of the Earth, Mars, and Jupiter intersect with the asteroid strip near the hypothetical planet Phaeton, according to the Titus-Bode law at $r = 2.8$ AU. It is possible that the breaking of the Solar System space by the Sun and the mentioned planets plays an important rôle in the very formation of the Solar System itself. It means that not only the Sun, but also other planets of the Solar System exert an effect on the motion of different objects, including artificial satellites, moving in the orthogonal direction with respect to the orbits of planets. The additional non-Newtonian force of attraction is proportional to the radial distance r, and the Newtonian force decreases as $\frac{1}{r^2}$. It means that the more distant the body moves away from the center of attraction, the more appreciable the effect of the non-Newtonian part of the force is. It is possible that the Pioneer anomaly can be explained by the existence of non-Newtonian forces: this effect is registered near the boundary of the Solar System, because Newtonian attraction here decreases (with radial distance), and non-Newtonian attraction increases.

Thus the gravitational field of a single mass, whose Hilbert radius is considerably smaller than its radius, can be described by the Schwarzschild mass-point metric (76) by way of performing calculations of the orbital motions of the test bodies. The analogical field must be described by the metric of a continuous body (such as the simplest metric of the homogeneous liquid sphere), i.e. if we consider the radial motion of the moving test body.

Consider now a cosmic body whose Hilbert radius is comparable with its proper radius: $r_g \sim a$. A model of the observable Universe whose whole radius matches the Hilbert radius was first suggested by Stanyukovich [10]. He studied some geometric properties of the liquid body in the state of gravitational collapse, but he did not introduce the concrete metric. Stanyukovich assumed that the space of the Universe was a collapsar, whose Hilbert radius r_g was equal to the distance up to horizon of events a. According to this concept, the mass of the Universe could be calculated by the formula $M = \frac{ac^2}{2G}$. Assuming $a = 1.3\times10^{28}$ cm (the maximal observed distance), we should find $M = 8.78 \times 10^{55}$ g. This value coincides approximately with estimates obtained by way of other sorts of reasoning.

The average value of the density of the liquid substance is $\rho = \frac{M}{V}$. Calculating the value of the density of the mass-point collapsar $M = \frac{ac^2}{2G}$ by the assumption $V = \frac{4\pi a^3}{3}$, we obtain

$$\rho = \frac{3c^2}{8\pi G a^2} = \frac{3H^2}{8\pi G} = 9.5 \times 10^{-30} \frac{\text{g}}{\text{cm}^3}, \quad H = \frac{c}{a}. \quad (86)$$

This value corresponds to the range of values obtained from observational data. Moreover, it corresponds to the theoretical value of the critical density ρ_{cr} by the condition $H = 2.3 \times 10^{-18}$ sec^{-1}.

It is necessary to note that the critical density is determined in standard cosmology as the density of the Friedman model (66), whose three-dimensional space is flat: $k = 0$. It is evident that this space-time is not a collapsar, because the observable time τ coincides with the coordinate time t: $d\tau = dt$,

consequently $g_{00} = 1$. (Recall that the collapse condition is $\sqrt{g_{00}} = 0$). Calculating the volume of the gravitational collapsar by the formula $V = \frac{4\pi a^3}{3}$, we have assumed in fact that the space inside the collapsar is flat. Let us study this problem in detail below.

Recall once again that Stanyukovich considered the Universe as the result of the collapse of the space-time (76), created in emptiness by the mass-point, because he actually used the Hilbert radius r_g [10]. We have introduced in this paper the collapse of a specific continuous body — a homogeneous liquid sphere (liquid bubble). It follows from (12) that the radius of the liquid sphere (11) in the collapse condition r_c equals its proper radius a and the breaking radius r_{br}, if

$$r_c = a = r_{br} = \sqrt{\frac{3}{\varkappa\rho}}. \tag{87}$$

Substituting into (87) $\varkappa = \frac{8\pi G}{c^2}$ and $\rho = \frac{3M}{4\pi a^3}$, we find, after elementary transformations,

$$r_c = a = r_{br} = r_g = \frac{2GM}{c^2}, \tag{88}$$

where M is the mass of both the liquid and vacuum bubbles, because the liquid bubble in the state of collapse is precisely the vacuum bubble.

We have interpreted above that the liquid and vacuum bubbles are the spaces of the future and the past, respectively. This is partly how we geometrize the reality of time in terms of its flows (successive states) and in a cosmological framework. Then the space of the present must: 1) belong to these states simultaneously; 2) be situated between the future and past spaces. Of special interest, the singular surface $r = a$ (the event horizon) satisfies both conditions. Firstly, the event horizon belongs to the gravitational and inflation collapsars; secondly, it is between the future and the past, since the observable time at the surface of the collapsar is stopped.

Since the event horizon is the characteristic surface of both the gravitational and inflation collapsars, it is simultaneously the surface of both the "white" and "black" holes. The collapsing liquid bubble transforms **instantaneously** into the de Sitter vacuum bubble — the **inflation collapsar**. Besides, the space inside the inflation collapsar (the "white hole") is simultaneously also the space inside the gravitational collapsar (the "black hole"). The white and black holes possess the generic surface $r = a$, which is simultaneously: 1) the radius of the liquid sphere and its breaking radius; 2) the event horizon itself and the radius of curvature of the vacuum bubble; 3) the Hilbert radius of the whole mass-point, which equals both the masses of the liquid and vacuum bubbles. The transformation of the liquid into the vacuum is accompanied by the inversion of the observable time: the **flow of time changes the direction by way of transformation**. Let us consider the causes of this transformation in detail. The question is: where, in the reality of time, is the mass M? The answer is: the liquid and vacuum bubbles are reflections of one other, where the mirror is the singular surface, therefore the mass is in the very present state of time, i.e. at the singular surface. Thus the materialization of the present ("reality") is the transfer of time flows through the said singularity.

Let us return for a moment to the "black-and-white" model of the Universe. This object is the result of some transformations: 1) the liquid substance transforms **instantly** into the physical vacuum in the state of inflation; 2) the "curvature of time" changes its sign; 3) the Non-Newtonian force of attraction transforms into the force of repulsion. In fact, the liquid sphere overturns itself in time. This overturning is similar to the transfer of a time flow from one side of the Möbius strip onto the other side where the respective time on each of these sides flows in the opposite direction (compared to the other). We know that the Möbius strip is a two-dimensional one-sided surface which can be included (embedded) in three-dimensional Eucledian space E_3 (otherwise, it is generally non-orientable).

It is possible to say, therefore, that the observable time has three dimensions: the past, the present, the future. Time is perceived by human consciousness as one-dimensional and directed from the past to the future. Meanwhile, similar events are repeated for different epochs, demonstrating that the past and the future are mirror images of one other, where the mirror is the present. But these events are not identical. It is possible to say that the spaces of the past and the future are created from "different cosmic substances", which depends on the time of creation of each space. Thus the past, present, and future are the three dimensions of the temporal volume, and these dimensions are different in principle. The past contains the consequence of holograms — physically realized (materialized) events. Besides, it also contains non-realized events. The future is virtual, because it contains only non-materialized events. Some events will be physically realized, others will be virtual. Such materialized events create the hologram (standing-wave picture) of the events, which is perceived by human consciousness as the (present) "reality".

As such, our Universe transforms the space of the future through the singular surface (the present) into the space of the past, consequently the *following materialization is none other than time transfer through the pertinent singularity — the event horizon*. This singular surface is the place of interaction of two opposite forces — attraction and repulsion. The energy of physical vacuum creates the force of attraction, appearing as the "scattering of galaxies". It can be called "radiant energy". The energy of compression, which is due to the force of attraction, can be called "dark energy". These two types of energy are divided and connected at the same time by said singular surface, which transforms the future into the past. When the course of the future reaches an end, the radiant energy will not develop, and the observable Universe will be compressed into the state of initial singularity. The cos-

mos will exist the way it does at present until it transforms all the virtual realities of the future time (as it flows from the future to the past). When this mechanism is exhausted, the observable Universe will compress itself into a Schwarzschild black hole, namely the initial singularity. It is possible that the mass of the singularity itself is the hypothetical "hidden mass", which exerts a definite effect on the motion of stars and galaxies.

Let us now calculate the values r_{br} and r_g for the Earth, the Galaxy, and the observable Universe: see Table 1. Besides, let us include into Table 1 the relative values r_{br}/a and r_g/a for the mentioned objects. It follows from the Table that the physical-geometric properties of the Universe differ in principle from the analogous properties of other objects (the Earth, the Sun, the Milky Way). In reality, only the Universe is simultaneously both a white hole and a black hole, because its Hilbert radius r_g equals the radius of the inflation collapsar a. These values coincide completely with the radius of space breaking in the curvature of time. It is possible to say that the forces of attraction and repulsion in the cosmos are in the state of equilibrium. It is evident that the observable Universe must be described as a stretched meta-body filled with matter (physical vacuum in the given case).

The other objects (the Earth, the Sun, the Milky Way) contain black holes, whose Hilbert radiuses r_g are very small in comparison to their radiuses a. In addition, these objects break the surrounding space, and the respective spheres of spatial discontinuities are located out of the bodies (sources), far away from them. Since the Hilbert radius $r_g \ll a$ depends only on the mass of the body, we will consider these bodies as mass-points, for example, by studying test bodies motion in their gravitational fields. But if we want to study this case in detail, we must consider the sources as stretched bodies filled with matter. This approach applied in [6] to the Solar System allows us to study the coupling between them. It is easily obtained from the formula (12), that the Earth, the Sun, and the Galaxy cannot be "white holes", since the value r_c is imaginary. Therefore, these objects include Hilbert "black holes" inside their spaces, but the resepctive space breakings are outside of them.

7 Conclusion

The seminal process of time-transfer transformation of the future into the past has been considered in this paper. The future and past spaces are introduced geometrically as two telemetric spheres (bubbles), filled with ideal substances — liquid vacuum and physical vacuum respectively. These bubbles are mirror reflections of each other, where the mirror is the singular surface. It means that the transfer of time from the future to the past is realized through the singular state — the very space of the present. The singular surface is simultaneously the surface of both the gravitational and inflation collapsar, which can be called the dual "black-white hole". Thus, the present is the result of the collapse of the future space, where the singular surface (the present) is the event horizon. The collapsar is in the state of equilibrium, because the two oppositely directed forces equalize each other. They are 1) the gravitational force of attraction; 2) the force of repulsion, which can be called the "force of anti-gravitation". The present is stable, until these forces neutralize one other. If the force of attraction is greater than the force of repulsion, the event horizon approaches the observer in space-time: the space of the observable Universe "compresses". If the force repulsion is greater than the force of attraction, the event horizon recedes from the observer: the space of the Universe observable "expands".

We have obtained that observable time flows in the opposite directions inside the liquid and vacuum bubbles. As was shown in [3], spaces with the opposite directions of time are mirror reflections of each other. In essence, the very term the "mirror space" is linked immediately to the "arrow of time". The widely accepted opinion is that the "arrow of time" can be directed only from the past to the future. The mathematical apparatus of General Relativity does not prohibit the reverse flow of time, i.e. from the future to the past. Nevertheless the reverse flow of time is not introduced in contemporary physics and cosmology, because modern scientists refer to Hans Reichenbach's "arrow of time", which is directed always to the future [4]. However, Reichenbach stipulating unidirectional time also implied a world process of evolution (transfer of energy). In particular, in the geometric framework of General Relativity, time can be stopped (as light can also be frozen) or be directed to the past or the future. Setting free cosmology from the unidirectional time concept gives us a definite advantage as to introduce the pontentially revolutionary Mirror Universe into General Relativity.

It is therefore more correct to introduce time as an ultimate kind of energy, although formally time is one of the coordinates of the four-dimensional Riemannian manifold — the space-time of General Relativity. But the three spatial coordinates are measured by lines, while time is measured by clocks, consequently space and time are two aspects of the indivisible manifold — the space-time. Clearly speaking, space-time can be considered as *material* (space), which is filled with time (time-energy). Time-filled spaces exists only in pseudo-Riemannian spaces, because the principal difference between coordinates exists, namely in spaces where the basis vectors possess both real and imaginary lengths.

It is necessary to mention "rulers" of a special kind, which are used in contemporary astronomy and cosmology, namely light rays. Because light transfers at the finite velocity c, observation of electromagnetic radiation ensuing from cosmic objects allows us to study only the past states of these objects. It is evident that the present states of these cosmic objects could be studied by means of instruments, which could register a long-range action. The unfortunate negation of a long-range action allows us to consider only the past states

of the Universe. In reality, our telescopes perceive only those light rays from stars and galaxies, emitted in the past. But if we'd only virtually reflect on the very boundaries of the observable Universe, that the present exists simultaneously in the whole space of the Universe, we might be able to build a space-time apparatus capable of registering the momentary (present) action of cosmic objects. (For example, such apparatuses have been constructed and tested by Nikolai Kozyrev). It is well-known that the consensual opinion exists that General Relativity prohibits a long-range action due to the "light barrier". This opinion is fundamentally incorrect: only the typical human consciousness produces this imaginary barrier. In fact, the mathematical apparatus of General Relativity allows the existence of zero-particles possessed of instantenous transfer. The rejection of the notion of the "light barrier" allows us to construct, in principle, instruments for the registration of zero-particles.

All the innovative techniques in this paper are substantially based on Riemannian geometry only. The usual imaginary prohibitions (e.g., the speed of light barrier) by way of consensus in the field of General Relativity retard the development of General Relativity and science as a whole on the furthest horizon, which is a way to negate General Relativity as a whole. Clearly, those typical conditions restricting Special Relativity (as in the usual particle physics) do not ultimately exist in General Relativity as a whole by way of the vastness and versatility of the underlying Riemannian geometry (in our extensive case as shown in [3], the basic Riemannian geometry of General Relativity is extended at the sub-manifold level by the presence of degenerate, generally rotating zero-spaces and zero-particles). Meanwhile, in principle, the fundamental elements of Riemannian geometry allow for the existence of both the long-range action and the reverse flow of time: the long-range action is realized by null-particles, while the reverse flow of time is due to gravitation and rotation. It is necessary to note that these results are obtained by the condition that gravitation and rotation are rather strong. Meanwhile, most specialists in General Relativity consider gravitation and rotation as weak factors. For example, the gravitational potential w and the linear velocity of rotation v_i from the expression of $d\tau$ (3) are taken into account by the usual problem of the synchronization of clocks as merely small corrections. Moreover, contemporary cosmologists assume that the reality of time of the Universe is the same in the whole space (being limited usually by the Hubble volume), since the observable time in the Friedman cosmological model flows uniformly: $d\tau = dt$. But, as shown here, even using very simple non-rotating model of the gravitating Universe (the de Sitter bubble) as a start, we have seen that gravitation causes the accelerated extension of the space of the Universe near the event horizon.

All that has been said above is similar to the observation of a thunderstorm: we first see a lightning flash, only then the thunderpeal is registered by our ears. This is because light and sound travel at different speeds. A blind observer will, however, perceive only the thunderpeal. Moreover, having not a visual connection to the source of this sound (which is the lightning flash), he will be unable to determine the distance to the lightning. (A normal, sighted observer merely multiplies the sound speed in the air by the duration between the observed lightning and the heard thunderpeal, thus calculating the distance to the lightning.) Most astronomers may now be compared to the previous blind researcher of the thunderstorm: the instruments they use in their astronomical observations register only electromagnetic radiations of different sorts (visible light, radio-waves, x-rays, etc.), while all these radiations travel at the speed of light (in vacuum) or even slower than light (if travelling in a medium); their current instruments are not able to register real cosmic signals which are faster than light. In other words, those astronomers merely focus on the registration of the "short-range action" (transferred by photons, in particular). They do not take the possibility of the "long-range action" (instantaneous geometric interactions) into account. The key role in this primitive approach is played by the psychological wall erected against superluminal (and instantaneous) interactions. There is an easily popular bias that this prohibition is due to Einstein, whose prior postulate of the Special Theory of Relativity stipulated that signals travelling faster than light was practically impossible. This is, however, not true in the bigger picture. Einstein claimed this postulate in his early "positivistic" publication prior to General Relativity, in the framework of his theory of observable phenomena registered by means of signals of light: superluminal (and instant) signals were naturally out-of-access for such an observer. However, the geometric (if not hypergeometric) structure of the four-dimensional pseudo-Riemannian space (which is the basic space-time of Einstein's General Theory of Relativity, being geometrically more complete, vast, and versatile in comparison to the Special Theory of Relativity) allows more diverse paths along which particles (signals) of different kinds may travel. For instance, particles bearing non-zero rest-mass/energy inhabit the sub-light speed region of the space-time (located "inside" the light cone); meanwhile, particles bearing imaginary masses and energies inhabit the superluminal space-time region (located "outside" the light cone); subsequently, there exist light-like particles bearing zero rest-mass (they are always in motion), while their relativistic masses and energies ("kinetic" masses and energies of motion) are non-zero, as they travel along space-time trajectories located along the light cone. There are also the so-called "zero-particles": they are the ultimate case of light-like particles, and travel along the fully degenerate light-like trajectories which seem to have zero length and duration to an external observer; as a result zero-particles seem to be travelled instantaneously, thus transferring long-range action such as that in the case of the geometric non-quantum teleportation as shown in [3].

Object	Mass, gram	Proper radius, cm	Density, g/cm^3	Space breaking radius, cm	Hilbert radius, cm	r_g/a	r_{br}/a
Earth	5.97×10^{27}	6.38×10^{8}	5.52	1.64×10^{13}	0.88	1.4×10^{-9}	2.6×10^{4}
Sun	1.98×10^{33}	6.95×10^{10}	1.41	3.43×10^{13}	2.9×10^{5}	4.2×10^{-6}	4.9×10^{2}
Milky Way	6.0×10^{45}	4.5×10^{22}	6.58×10^{-23}	4.95×10^{25}	8.9×10^{17}	2.0×10^{-5}	1.1×10^{3}
Universe	8.8×10^{55}	1.3×10^{28}	9.5×10^{-30}	1.3×10^{28}	1.3×10^{28}	1.0	1.0

A real observing human whose body is made of regular substance such as atoms and molecules cannot travel at the speed of light. At the same time, he perceives light by his physical organs and the other (artificial) instruments of observation: there is not a barrier dividing him and light. In analogy to this case, instruments registering zero-particles (which seem to be travelling instantaneously) may be invented. All that the innovative engineers need to do it is set themselves free of the psychological prohibition and limitation in traveling at the light speed, as to be professionally equipped with the full extent of the General Theory of Relativity which has already theoretically predicted zero-particles carrying the long-range action (geometric non-quantum teleportation).

Again, there are unfortunately many popular biases about Einstein's General Theory of Relativity. Most of them originated in the non-technically equipped reporters of pop-science, or the pop-science authors themselves whose knowledge in this field is limited with those "first-grade" rudimentary textbooks on the the Theory of Relativity. Such books present Einstein's theory rather very shallowly, paying attention to mostly the native examples based on Einstein's early postulates revolving around his theory of exchanging light signals. The greater true meaning of Einstein's theory — the deeper picture of space-time geometry as the basis of all the physical world — is regularly out-of-scope in such books due to the psychological threshold of the need to master Riemannian geometry and tensor calculus at a certain great level of mathematical and physical depth (which is not a trivial task for a beginner and indeed most would-be specialists, with the exception of very few gifted and versatile ones). As a result, we have such a popular bias (not based on geometry) as the above-mentioned aforementioned myth about the insurpassable nature of the light speed limit, and also the myth about the irreversibility of the arrow of time (which naturally depends on the physical conditions of observation in different space-time regions). There is also another myth saying that the General Theory of Relativity can result in only small corrections to Classical Mechanics and Electrodynamics (this is not true on cosmological scales where the effects of General Relativity greatly rule), and many other biases concerning Einstein's theory.

Setting ourselves free from these popular, primitive, anti-progressive biases, and following the deeper versatile trajectory (geometry) of the theory of space-time-matter established by Albert Einstein, no doubt certain researchers could arrive at new instruments of observation based on the geometric resurgence of the long-range action (in parallel with certain gravitational and gauge field instantons of the Plebanski type). These new developments, based on completely different principles than the usual electromagnetic interactions, could lead to certain cosmic engines allowing for (geometric) non-quantum teleportation, as well as other new exotic technologies in order to carry the human species to an unprecedented Golden Age in the cosmos.

Submitted on September 30, 2012 / Accepted on October 10, 2012

References

1. Raschewski P. K. Riemannische Geometrie und Tensoranalysis. Deutscher Verlag der Wissenschaften, Berlin, 1959 (translated by W.Richter); reprinted by Verlag Harri Deutsch, Frankfurt am Main, 1993.
2. Zelmanov A. Chronometric invariants. Dissertation, 1944. American Research Press, Rehoboth (NM), 2006.
3. Borissova L. and Rabounski D. Fields, Vacuum and the Mirror Universe. 2nd edition, Svenska fysikarkivet, Stockholm, 2009. Also, in parallel, see: Rabounski D. and Borissova L., Particles Here and Beyond the Mirror. 2nd edition, Svenska fysikarkivet, Stockholm, 2008.
4. Reichenbach H. The Direction of Time. University of California Press, Berkeley (CA), 1956.
5. Schwarzschild K. Über das Gravitationsfeld einer Kugel aus inkompressibler Flüssigkeit nach der Einsteinischen Theorie. *Sitzungberichte der Königlich Preussischen Akademie der Wissenschaft*, 1916, 426–435.
6. Borissova L. The Gravitational Field of a Condensed Matter Model of the Sun: the Space Breaking Meets the asteroid Strip. *The Abraham Zelmanov Journal*, 2009, vol.2, 224–260.
7. Borissiva L. De Sitter Bubble as a Model of the Observable Universe. *The Abraham Zelmanov Journal*, 2010, vol.2, 208–223.
8. Schwarzschild K. Über das Gravitationsfeld eines Massenpunktes nach der Einsteinischen Theorie. *Sitzungberichte der Königlich Preussischen Akademie der Wissenschaft*, 1916, 189–196.
9. Zelmanov A. On the relativistic theory of an anisotropic inhomogeneous universe. The Abraham Zelmanov Journal, 2008, vol. 1, 33–63 (originally presented at the 6th Soviet Meeting on cosmogony, Moscow, 1959).
10. Stanyukovich K. On the Problem of the Existence of Stable Particles in the Metagalaxy. *The Abraham Zelmanov Journal*, 2008, vol. 1, 99–110.

A Single Big Bang and Innumerable Similar Finite Observable Universes

Nilton Penha Silva
Departamento de Física (Retired Professor), Universidade Federal de Minas Gerais, Belo Horizonte, MG, Brazil.
E-mail: nilton.penha@gmail.com

Gravity dominated Universe until it was 3.214 Gyr old and, after that, dark energy dominates leading to an eternal expansion, no matter if the Universe is closed, flat or open. That is the prediction of the expansion factor recently proposed by Silva [2]. It is also shown that there is an upper limit for the size of the Observable Universe *relative radial comoving coordinate*, beyond which nothing is observed by our fundamental observer, on Earth. Our Observable Universe may be only a tiny portion of a much bigger Universe most of it unobservable to us. This leads to the idea that an endless number of other fundamental observers may live on equal number of Observable Universes similar to ours. An unique Big Bang originated an unique Universe, only part of it observable to us.

1 Introduction

Since 1929, with Hubble [1], we learned that our Observable Universe has been continuously expanding. Nearly all galaxies are moving away from us, the further they are, the faster they move away. If the galaxies are moving apart today, they certainly were closer together when the Universe was younger. This led to the idea of the Big Bang theory, which is the most accepted theory for the explanation on how the Universe began. According to it, all started from a physical singularity where all Universe matter-energy-space were extremely concentrated with temperature well above 10^{32} K, when a cataclismic expansion ocurred and the size of it went from a Planck's length to some Gigayears (Gyrs) in an extremely tiny fraction of a second.

According to the theory, as the Universe cooled, the first building blocks of matter, quarks and electrons, were formed, followed by the production of protons and neutrons. In minutes protons and neutrons aggregated to produce nuclei.

Around 380,000 years after the Big Bang, there was the so called recombination era in which matter cooled enough to allow formation of atoms transforming the Universe into a transparent eletrically neutral gas. The first photons that managed to be traveling freely through the Universe constitute the so called Cosmic Microwave Background (CMB) which are detected today. This "afterglow light" study is very important because they show how was the the Primeval Universe. Next step is the formation of the structure which gave rise to the astronomical objects [4–10].

Today the Universe keeps expanding, but since 1998 we learned that it has a positive acceleration rate. This indicates that there is something overcoming the gravity and that has been called dark energy. A completely characterization of the dark energy is not done yet. Most researchers think it comes from the vacuum.

In previous papers [2, 3], we have succeeded in obtaining an expression for the Universe scale factor or the Universe expansion factor as you may well call it too:

$$\begin{aligned} a(t) &= \exp\left(\frac{H_0T_0}{\beta}\left(\left(\frac{t}{T_0}\right)^{\beta}-1\right)\right), \\ \beta &= 1+H_0T_0\left(-\frac{1}{2}\Omega_m(T_0)+\Omega_\Lambda(T_0)-1\right) \end{aligned} \tag{1}$$

and H_0 is the so called Hubble constant, the value of the Hubble parameter $H(t)$ at $t = T_0$, the current age of the Universe. Expression (1) is supposed to be describing the expansion of the Universe from the beginning of the so called *matter era* ($t \approx 10^{-4}$ Gyr, after the Big Bang). Right before that the Universe went through the so called *radiation era*. Only the role of the matter (baryonic and non-baryonic) and the dark energy, both treated as perfect fluids are considered. In our work the dark energy was associated to an *a priori* time dependent $\Lambda(t)$ (cosmological "constant").

Figure 1 shows the expansion factor $a(t)$ as function of the Universe age. In Figure 2 the behaviour of the expansion factor acceleration, $\ddot{a}(t)$, is reproduced. Before $t = T_\star = 3.214$ Gyr, acceleration was negative, and after that, acceleration is positive. To perform the numerical calculations we

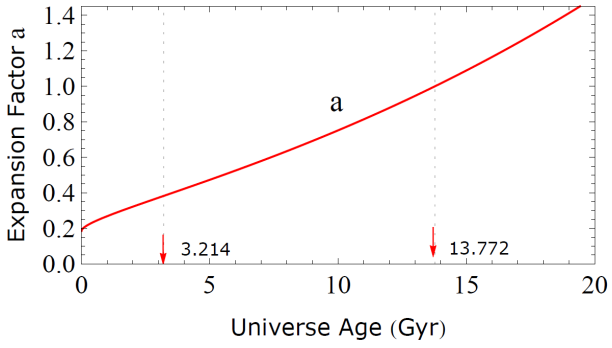

Fig. 1: $a(t) = \exp\left(\frac{H_0T_0}{\beta}\left(\left(\frac{t}{T_0}\right)^{\beta}-1\right)\right)$.

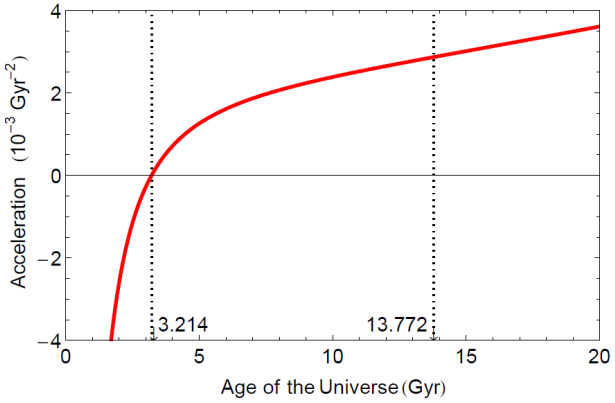

Fig. 2: $\ddot{a}(t) = a(t)\left(H_0\left(\frac{t}{T_0}\right)^{\beta} - (1-\beta)\frac{1}{t}\right)H_0\left(\frac{t}{T_0}\right)^{\beta-1}$.

have used the following values [11]:

$$\begin{aligned} H_0 &= 69.32\ \text{kms}^{-1}\text{Mpc}^{-1} \\ &= 0.0709\ \text{Gyr}^{-1}, \\ T_0 &= 13.772\ \text{Gyr}, \\ \Omega_m(T_0) &= 0.2865, \\ \Omega_\Lambda(T_0) &= 0.7135. \end{aligned} \tag{2}$$

In reference [2], some properties such as Gaussian curvature $K(t)$, Ricci scalar curvature $R(t)$, matter and dark energy density parameters $(\Omega_m, \Omega_\lambda)$, matter and dark energy densities (ρ_m, ρ_λ), were calculated and plotted against the age of the Universe, for $k = +1, 0, -1$. It was found that the current curvature radius $\mathfrak{R}(T_0)$ has to be larger than 100 Gly, for $k = \pm 1$. Obviously, for $k = 0$, $\mathfrak{R} = \infty$. So, arbitrarily [2], we have chosen $\mathfrak{R}(T_0) = 102$ Gly. None of the results were sufficient to decide which value of k is more appropriate for the Universe. The bigger the radius of curvature, the less we can distinguish which should be the right k among the three possible values. Considering that, we pick the most intuitive geometry, at least in our view, we work here with the closed Universe version.

2 Closed Universe

The closed Universe Friedmann - Lemaitre - Robertson - Walker (FLRW) spacetime metric is given by [4–10]:

$$\begin{aligned} ds^2 &= \mathfrak{R}^2(t)\left(d\psi^2 + \sin^2\psi\left(d\theta^2 + \sin^2\theta d\phi^2\right)\right) - c^2dt^2 \\ &= \mathfrak{R}^2(T_0)\,a^2(t)\left(d\psi^2 + \sin^2\psi\left(d\theta^2 + \sin^2\theta d\phi^2\right)\right) \\ &\quad - c^2dt^2, \end{aligned} \tag{3}$$

where ψ, θ and ϕ are comoving space coordinates ($0 \le \psi \le \pi$, $0 \le \theta \le \pi$ and, $0 \le \phi \le 2\pi$), t is the time shown by any observer clock in the comoving system. $\mathfrak{R}(t)$ is the scale factor in units of distance; actually it is *radius of curvature* of the Universe as already said in previous section. The time t is also known as the cosmic time. The function $a(t)$ is the usual expansion factor

$$a(t) = \frac{\mathfrak{R}(t)}{\mathfrak{R}(T_0)}, \tag{4}$$

here assumed to be that of Equation 1.

The FLRW metric embodies the so called Cosmological Principle which says that the Universe is spatially homogeneous and isotropic in suficient large scales.

We have to set that our "fundamental" observer (on Earth) occupies the $\psi = 0$ position in the comoving reference system. To reach him(her) at cosmic time T, the CMB photons spend time T since their emission at time $t \approx 380,000$ yr, after the Big Bang, at a specific value of the comoving coordinate ψ. Let us call ψ_T this specific value of ψ. We are admitting that the emission of the CMB photons occured simultaneously for all possible values of ψ. Although that happened at $t \approx 380,000$ yr, for purposes of integrations ahead it is assumed to be $t \approx 0$ with no considerable loss.

Having said that, we can write, for the trajectory followed by a CMB photon ($ds^2 = 0, d\phi = d\theta = 0$), the following:

$$-\frac{cdt}{\mathfrak{R}(t)} = d\psi, \tag{5}$$

$$-\int_0^T \frac{c}{\mathfrak{R}(t)}dt = \int_{\psi_T}^0 d\psi, \tag{6}$$

$$\psi_T = \frac{c}{\mathfrak{R}(T_0)}\int_0^T \frac{1}{a(t)}dt, \tag{7}$$

The events ($\psi = 0$, $t = T$) and ($\psi = \psi_T$, $t = 0$) are connected by a null geodesics. The first event is relative to the fundamental Observer, while the second event refers to the emission of the CMB photons at $t \approx 0$ as explained above. ψ_T gets bigger as T increases which means that *the older the Universe gets, the further the referred Observer sees from the CMB*.

The comoving coordinate which corresponds to the current "edge" (horizon) of our Observable Universe is

$$\begin{aligned} \psi_{T_0} &= \frac{c}{\mathfrak{R}(T_0)}\int_0^{T_0}\frac{1}{a(t)}dt \\ &= \frac{c}{\mathfrak{R}(T_0)}\int_0^{T_0}\exp\left(\frac{H_0T_0}{\beta}\left(1-\left(\frac{t}{T_0}\right)^{\beta}\right)\right)dt \\ &= 0.275\ \text{Radians} = 15.7\ \text{Degrees}. \end{aligned} \tag{8}$$

where, again, $\mathfrak{R}(T_0)$ is assumed to be 102 Gly for the reason exposed in reference [2] ($\mathfrak{R}(T_0) > 100$ Gly). Very much probably $\mathfrak{R}(T_0)$ should be much greater than that. The value of the current curvature radius is crucial in the sense of determining the coordinate ψ_{T_0}.

So CMB photons emitted at ψ_{T_0} and $t = 0$ should arrive at $\psi = 0$ and $t = T_0$, the current age. Along their

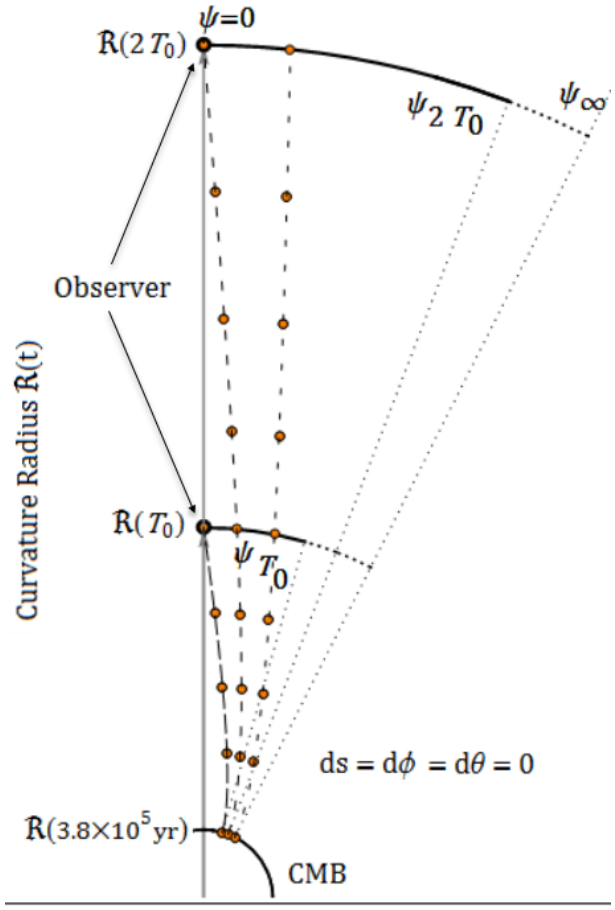

Fig. 3: The null geodesics connecting two events: $(\psi_{T_0},\ t \approx 0)$ and $(\psi = 0, t = T_0)$; $(\psi_{2T_0},\ t \approx 0)$ and $(\psi = 0,\ t = 2T_0)$. The null geodesic between $(\psi_\infty = 1.697\ \psi_{T_0},\ t \approx 0)$ and $(\psi = 0,\ t = \infty)$ will never be accomplished. $\mathfrak{R}(T)$ is radius of curvature at age T.

whole trajectory, other photons emitted, at later times, by astronomical objects that lie on the way, join the troop before reaching the fundamental observer. So he(she) while looking outwards deep into the sky, may see all the information 'collected' along the trajectory of primordial *CMB* photons. Other photons emitted at the same time $t \approx 0$, at a comoving position $\psi > \psi_{T_0}$ will reach $\psi = 0$ at $t > T_0$, together with the other photons provenient from astronomical objects along the way. As the Universe gets older, its "edge" becomes more distant and its size gets bigger. See Figure 3.

The current value for ψ_{T_0} should actually be smaller than 0.275 Radians, because, as we said above, $\mathfrak{R}(T_0)$ should be greater than the assumed value (102 Gly).

To get rid of such dependence on $\mathfrak{R}(T_0)$, we find convenient to work with the ratio r

$$r \equiv \frac{\psi}{\psi_{T_0}}, \tag{9}$$

which we shall call the *relative radial comoving coordinate*.

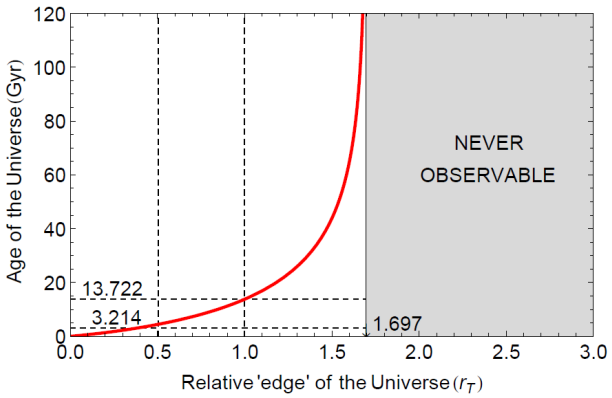

Fig. 4: $r_T = \int_0^T \frac{1}{a(t)}dt \Big/ \int_0^{T_0} \frac{1}{a(t)}dt$. The relative radial comoving coordinate r_T, from which *CMB* photons leave, at $(t \approx 0)$, and reach relative comoving coordinate $r = 0$ at age $t = T$ gives the relative position of the "edge" of the Observable Universe $(r_{T\to\infty} \to 1.697)$. (Axes were switched.)

Obviously, at age T, r_T is the *relative* measure of the "edge" position with respect to the fundamental observer $(\psi = 0)$

$$r_T = \int_0^T \frac{1}{a(t)}dt \Big/ \int_0^{T_0} \frac{1}{a(t)}dt, \tag{10}$$

and $r_{T_0} = 1$. For a plot of r_T see Figure 4.

3 Observable Universes

One question that should come out of the mind of the fundamental observer is: "Is there a maximum value for the relative comoving coordinate r?" What would be the value of r_∞?

By calculating r_∞, we get

$$r_\infty = \int_0^\infty \frac{1}{a(t)}dt \Big/ \int_0^{T_0} \frac{1}{a(t)}dt = 1.697. \tag{11}$$

To our fundamental observer (Earth), there is an upper limit for the relative comoving coordinate $r = r_\infty = 1.697$, beyond that no astronomical object can *ever* be seen by such fundamental observer.

This should raise a very interesting point under consideration.

Any other fundamental observer placed at a relative comoving coordinate $r > 2r_\infty$ $(\psi > 2\psi_\infty)$, with respect to ours, will never be able to see what is meant to be our Observable Universe. He (she) will be in the middle of another visible portion of the same whole Universe; He (she) will be thinking that he (she) lives in an Observable Universe, just like ours. Everything we have been debating here should equally be applicable to such an 'other' Observable Universe.

The maximum possible value of ψ is π (Equation 3), then the maximum value of r should be at least 11.43. Just recall that $r = 1$ when $\psi = \psi_{T_0}$. This ψ_{T_0} was overevaluated as being 0.275 Radians = 15.7 Degrees, in equation (8)

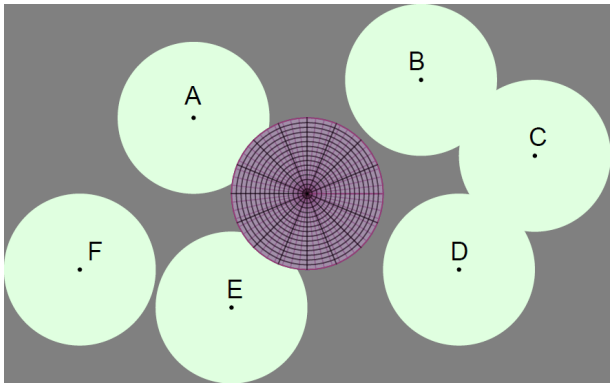

Fig. 5: This illustration tries to show schematically a hypersurface at time T with our Observable Universe surrounded by other similar Observable Universes, arbitrarily positioned, some of them overlapping.

when considering the current radius of curvature as $\Re(T_0) =$ 102 Gly. As found in reference [2] $\Re(T_0)$ should be bigger than that, not smaller. Consequently the real ψ_{T_0} should be smaller than 0.275 Radians = 15.7 Degrees, not bigger. One direct consequence of this is that there is room for the ocurrence of a large number of isolated similar *Observable Universes* just like ours.

We may say that the Big Bang gave birth to a large Universe, of which our current Observable Universe is part, perhaps a tiny part. The rest is unobservable to us and an endless number of portions just the size of our Observable Universe certainly exist, each one with their fundamental observer, very much probably discussing the same Physics as us.

Of course, we have to consider also the cases of overlapping Observable Universes.

One important thing is that we are talking about **one Universe**, originated from **one Big Bang**, which is not observable as a whole, and that may contain **many** other Observable Universes **similar** to ours. Would it be a *Multiverse*? See Figure 5.

4 Conclusion

The expansion factor $a(t) = exp\left(\frac{H_0 T_0}{\beta}\left(\left(\frac{t}{T_0}\right)^{\beta} - 1\right)\right)$, where $\beta = 1 + H_0 T_0\left(-\frac{1}{2}\Omega_m(T_0) + \Omega_\Lambda(T_0) - 1\right) = 0.5804$ [2], is applied to our Universe, here treated as being closed ($k = +1$). Some very interesting conclusions were drawn. One of them is that the radial relative comoving coordinate r, measured from the fundamental observer, $r = 0$ (on Earth), to the "edge" (horizon) of our Observable Universe has an upper limit. We found that $r \to 1.697$ when $T \to \infty$. Therefore all astronomical objects which lie beyond such limit would never be observed by our fundamental observer ($r = 0$). On the other hand any other fundamental observer that might exist at $r > 2 \times 1.697$ would be in the middle of another Observable Universe, just like ours; he (she) would never be able to observe our Universe. Perhaps he (she) might be thinking that his (her) Observable Universe is the only one to exist. An endless number of other fundamental observers and an equal number of Observable Universes similar to ours may clearly exist. Situations in which overlapping Universes should exist too. See Figure 5.

The fact is that the Big Bang originated a big Universe. A tiny portion of that is what we call our Observable Universe. The rest is unobservable to our fundamental observer (Earth). Equal portions of the rest may be called also Observable Universes by each of their fundamental observers if they exist. So we may speak about many Observable Universes - a Multiverse - or about only one Universe, a small part of it is observable to the fundamental observer.

By using the expansion factor here discussed we have also succeeded in finding a generalization of Hubble's Law, which may be found in reference [13].

The expansion factor, Equation 1, proposed in reference [2] has been shown to be a very good candidate to be describing the expansion of the Universe.

Submitted on January 2, 2017 / Accepted on January 4, 2017

References

1. Hubble E. A relation between distance and radial velocity among extragalactic nebulae, *Proceedings of the National Academy of Sciences of the United States of America*, 1929, v. 15(3), 168–173.
2. Silva N.P. A Model for the Expansion of the Universe. *Progress in Physics*, 2014, v. 10(2), 93–97.
3. Silva N.P. A Closed Universe Expanding Forever. *Progress in Physics*, 2014, v. 10(3), 191–195.
4. Raine D. An Introduction to the Science Of Cosmology. Institute of Physics Publishing Ltd, 2001.
5. Peacock J.A. Cosmological Physics. Cambridge University Press, 1999.
6. Harrison E.R. Cosmology: The Science of the Universe. Cambridge University Press, 2^{nd} ed., 2000.
7. Islam J.N. An Introduction to Mathematical Cosmology. Cambridge University Press, 2002.
8. Ellis G.F.R. Relativistic Cosmology. Cambridge University Press, 2012.
9. Springel V., Frenk C.S. and White S.D. The Large-scale Structure of the Universe. *Nature*, 2006, v. 440(7088), 1137–1144.
10. Luminet J.P. Cosmic Topology: Twenty Years After. *Gravitation and Cosmology*, 2014, v. 20(1), 15–20.
11. Bennett C.L. et al. Nine-Year Wilkinson Microwave Anisotropy Probe (WMAP) Observations: Final Maps and Results. arXiv: astro-ph.CO. 2013.
12. Peebles P.J.E. The Large-scale Structure of the Universe. Princeton university press, 1980.
13. Silva N.P. Beyond the Hubble's Law. *Progress in Physics*, 2017, v. 13(1), 5–6.

Physical Properties of Stars and Stellar Dynamics

Yuri Heymann

3 rue Chandieu, 1202 Geneva, Switzerland. E-mail: y.heymann@yahoo.com

The present study is an investigation of stellar physics based on observables such as mass, luminosity, radius, and photosphere temperature. We collected a dataset of these characteristics for 360 stars, and diagramed the relationships between their characteristics and their type (white dwarf, red dwarf, main sequence star, giant, supergiant, hypergiant, Wolf-Rayet, carbon star, etc.). For stars dominated by radiation pressure in the photosphere which follow the Eddington luminosity, we computed the opacity and cross section to photon flux per hydrogen nuclei in the photosphere. We considered the Sun as an example of star dominated by gas pressure in the photosphere, and estimated the density of the solar photosphere using limb darkening and assuming the adiabatic gradient of a monoatomic gas. We then estimated the cross section per hydrogen nuclei in the plasma of the solar photosphere, which we found to be about 2.66×10^{-28} m^2, whereas the cross section of neutral hydrogen as given by the Bohr model is 8.82×10^{-21} m^2. This result suggests that the electrons and protons in the plasma are virtually detached. Hence, a hydrogen plasma may be represented as a gas mixture of electrons and protons. If the stellar photosphere was made of large hydrogen atoms or ions such as the ones we find in gases, its surface would evaporate due to the high temperatures.

1 Introduction

The present study is an investigation of stellar physics based on characteristics such as mass, luminosity, radius, and photosphere temperature. We analysed a set of 360 stars for which we collected available data from the literature. The set included white dwarfs, red dwarfs, main sequence stars, giant stars, Wolf-Rayet stars, carbon stars, etc. Let us introduce the basics to get a sense of how stars regulate fusion reactions and the basic principles of stellar dynamics.

We can easily infer that stellar equilibrium is driven by hydrostatic pressure. The internal pressure of a star is determined by the radiation pressure and gas pressure, which counterbalance the hydrostatatic pressure from gravitation and prevent the star from collapsing. Radiation pressure and gas pressure are temperature dependent. When a star cools, it experiences a drop in internal pressure that causes the star to contract. This contraction will cause an increase in the hydrostatic pressure within the star. The gravitational force exerted by the inner mass of the star on a particule at a given radius is $F_g = \frac{GM_r m_p}{r^2}$, where r is the radius, M_r the interior mass of the star up to radius r, m_p the mass of the particule, and G the gravitational constant. Therefore, the more the star contracts, the higher the hydrostatic pressure. The increase in hydrostatic pressure increases the rate of fusion, which produces excess heat. In return, this excess heat increases the gas and radiation pressure in the star causing the star to expand. This process repeats until the star reaches a certain equilibrium.

Nuclear fusion, therefore, is driven by the hydrostatic pressure in stars. There are three possible mechanisms by which hydrostatic pressure could affect the fusion power of stars:

- Assuming that a minimum pressure or temperature is required to sustain fusion, the volume of the fusing core increases as hydrostatic pressure increases. According to the Arrhenius equation, reaction kinetics are highly dependent on temperature. Note that the Arrhenius equation assumes the Maxwell-Boltzmann distribution, and the relationship would be different for a Fermi gas.
- The density in the core of the star increases as hydrostatic pressure increases. Hence, a larger quantity of matter would be subject to fusion in the core of the star.
- The kinetic rate of fusion (i.e. the reaction rate or speed) may increase as pressure increases.

These are the mechanisms we propose regulate a star. In some instances the volume and luminosity of the star oscillates. These are the so-called variable stars. A notable example of variable stars are the Cepheid variables. They are known for a method to measure distances based on the period of their oscillation. As there is a relationship between the period of the star's oscillations and its luminosity, one can infer the intrinsic luminosity and compute the distance. Several different theories explain the oscillations of variable stars. We enumerate some possible mechanisms below:

- The κ-mechanism or Eddington valve is the most popular theory explaining variable Cepheids [1]. According to this theory, doubly ionized helium is more opaque than single ionized helium. As helium in the star heats, it becomes more ionized and less transparent so that the heat is retained longer. As the star expands, it cools and its helium becomes less ionized and hence more transparent, allowing the heat to escape. Then the star contracts again and the process repeats.

- Another mechanism would be a change in the regime of the fusion reactions for certain thresholds in the hydrostatic pressure of the star. For example, fusion of heavier elements in the core of large stars could ignite at a certain temperature threshold and produce large temperature spikes causing the star to oscillate. This theory would be applicable to massive stars where fusion of heavy elements in the core occurs.
- The ageing model of the core could also explain variable stars. Let us consider a star fusing hydrogen into helium when the star has too low a mass to ignite helium fusion. As the star ages, the helium core grows, and the shell of fusing hydrogen around the core thins. Let us say the hydrogen shell heats the core, making it expand and push the hydrogen shell to the exterior; the temperature of the shell would fall below the ignition point, and switch off hydrogen fusion. Then the core would cool, returning the hydrogen shell to the ignition point and switching hydrogen fusion on again. This pattern would repeat in cycles. This theory would apply to stars with small cores and explain the type II Cepheids, which have about half the mass of the Sun and therefore are not massive enough to fuse helium.
- Temperature driven kinetics for fusion reactions may also induce stellar oscillations. If the kinetic rate of fusion increases as temperature increases, a small increase in temperature at the core would cause large temperature spikes. Then the star would expand over a long period of time before cooling and contracting again. Note that this process would cause stars to be unstable. The fact that the Sun is stable with very low oscillations of order 0.1 % of its luminosity would be a counter example of temperature driven fusion kinetics, unless the sensitivity of the fusion-kinetic rate with respect to temperature is very small.

When a star has exhausted the nuclear supply at its core, it will cool. This will eventually trigger a gravitational collapse. When the star contracts, the depleted nuclear fusion at its core would not be able to counterbalance the hydrostatic pressure. As the radius of the star diminishes, the gravitational force acting on the particles of the star increases proportionally to $\frac{1}{r^2}$. The gravitational collapse of the star can lead to the formation of a black hole on one extreme or a supernova at the other. The latter occurs if at a certain point during the collapse the pressure is so high that it triggers fusion reactions in series at a very fast rate, causing the star to explode and leading to the formation of up to the heaviest elements of the Mendeleev table such as uranium. A black hole would form if fusion does not halt the gravitational collapse. In some instances gravitational collapse stops before the formation of a black hole, producing a neutron star or white dwarf. These are intermediary stages before the formation of a black hole. White dwarfs are less dense than neutron stars, at an earlier stage of matter compression than neutron stars. Neutron stars are composed of neutronium, a compact pack of neutrons, and have densities around 4×10^{17} kg/m^3. White dwarfs have densities around 10^7 to 10^{10} kg/m^3. Electron degeneracy pressure is the mechanism which supposedly prevents the further collapse of white dwarfs. Degeneracy of matter from gravitational collapse starts at the core of the star. Sometimes the core of the star collapses into a neutron star or a black hole while the outer shell of the star explodes into a supernova. Red giants of masses comparable to the Sun generally blow out their outer layer at the end of their life to form planetary nebulae, leaving a white dwarf in the core.

We find that stellar photosphere dynamics are crucial in the determination of the power of stars as measured by their luminosity. We cannot miss the notable work of Arthur Eddington on the dynamics of stars dominated by radiation pressure in the photosphere, according to which, the luminosity of such stars is proportional to their mass. Using data from stars dominated by radiation pressure in their photosphere, we can estimate the opacity parameter. We also discuss models and factors which may affect opacity, as this is a preponderant parameter for radiative heat transfer, a key component of stellar models. For stellar models we also need boundary conditions such as the density of the photosphere. We show how to estimate the density of the solar photosphere using limb darkening. According to the standard solar model, there is a layer at the surface of the Sun where radiative heat transfer is not efficient enough and convection takes place. The photosphere can be viewed as a plasma surface; hence using a model of the surface we can compute the cross section per hydrogen nuclei in the photosphere. We computed the cross section per hydrogen nuclei from radiation pressure and gas pressure, and found that both values match closely. From the cross section per hydrogen nuclei we obtained, we can infer that in stellar plasma the electrons and nuclei are virually detached. Therefore, stellar plasma may be represented as a gas mixture of electrons and nuclei. We discuss the modelling implications of this representation of stellar plasma.

2 Overview of stellar data

Stars form a very heterogeneous group having various luminosities, masses, temperatures, and densitities. In the below diagrams we show the relationships between these characteristics for the stars in our catalog. In section 2.1 we introduce the classification of stars we used for the diagrams. Section 2.2 shows the stellar diagrams we obtained with a emphasise on their interpretation.

2.1 Classification of stars

Stars can be classified according to their spectra, color, and size. Stellar spectra provide precious information about their atmospheric composition by analyzing their spectral lines, and surface temperature from Planck's law of black-body

spectrum. We divided the stars in our catalog according to the below groups:

- White dwarfs are degenerated stars which are very dense and composed mostly of electron-degenerate matter. They have masses comparable to that of the Sun, volumes comparable to that of Earth, and are very faint. Some white dwarfs are classified as helium stars as they have very strong helium lines and weak hydrogen lines [2].
- Brown dwarfs have masses comprised in the range of 13 to 80 Jupiter masses. Their mass is below the threshold needed to fuse hydrogen, but enough to fuse deuterium.
- Red dwarfs have masses in the range of 0.075 to 0.6 solar masses, and surface temperatures below 4,000 K. A count the stars nearest to earth, it was estimated that red dwarfs comprise about 80% of the stars in the Milky Way.
- Yellow dwarfs are main-sequence stars of comparable mass to the Sun, with a surface temperature between 5,300 and 6,000 K. We created a broader group that we called yellow main sequence stars to include all stars with masses between 0.6 and 1.7 solar masses, and a temperature between 4,200 and 7,200 K.
- A-type stars are main-sequence stars of spectral type A of 1.4 to 2.1 solar masses, and a surface temperature between 7,600 and 11,500 K. Their spectra have strong hydrogen Balmer absorption lines.
- B-type stars are main-sequence stars of 2 to 16 solar masses, and a surface temperature between 10,000 and 30,000 K. Their spectra have non-ionized helium lines.
- Subgiants are stars at an intermediary stage of evolution before becoming giants. These stars are brighter than main-sequence stars but not as bright as giants.
- Red giants are evolved stars of 0.8 to 8 solar masses which have exhausted the hydrogen supply in their core and are fusing helium into carbon. They have high luminosities compared to their main-sequence peers, and inflated atmospheres making their radii large, resulting in low surface temperatures between 3,200 and 4,000 K. Orange giants are distinguished from red giants by their temperature, which ranges from 4,000 to 5,500 K.
- Carbon stars are red giants whose atmosphere contains more carbon than oxygen.
- S-type stars are giant stars with approximately equal quantities of carbon and oxygen. These are intermediaries between giants and carbon stars.
- Blue giants are hot giant stars with masses in the range of ten to hundreds of solar masses, and surface temperatures between 22,000 and 45,000 K.
- Supergiants are stars with luminosities between those of the giants and hypergiants on the Hertzsprung-Russell diagram. They are divided into red supergiants, orange supergiants, and blue supergiants according to their surface temperatures. The red ones have surface temperatures between 3,200 and 4,000 K, the orange ones between 4,000 and 7,000 K, and the blue ones between 7,000 and 50,000 K.
- Hypergiants are stars with tremendous luminosities on the high end of the Hertzsprung-Russell diagram. They are divided into red hypergiants, yellow hypergiants, and blue hypergiants according to their surface temperatures. The temperature ranges are the same as for supergiants with the yellow group replacing the orange stars of the supergiant category.
- Wolf-Rayet stars are evolved massive stars which are fusing helium or heavier elements in the core. They have spectra showing broad emission lines of highly ionized helium and nitrogen or carbon. Most Wolf-Rayet stars have lost their outer hydrogen and have an atmosphere predominantly made of helium. Their surface temperature ranges between 30,000 and 200,000 K. A subgroup of Wolf-Rayet stars referred to as WO stars have strong oxygen emission lines, indicating the star is on the oxygen sequence.

2.2 Stellar diagrams

In the current section we display several diagrams showing the relationship among the characteristics of stars along with their classification. Figure 1 shows the relationship between the luminosity and mass of stars, Figure 2 the relationship between the volume and the luminosity of stars, and Figure 3 the relationship between the average density of stars and temperature of the photosphere.

Figure 1 shows that red giants are much more luminous than their main-sequence star counterparts for the same mass. As red giants are evolved stars which fuse helium in the core, we can infer that the fusion of helium into carbon is much more exothermic than the fusion of hydrogen into helium. Red giants are also less dense than their main-sequence counterparts, meaning that helium fusion occurs in a domain at lower pressure than hydrogen fusion and produces more heat. In Figure 2, we see that main sequence stars expand when shifting on the helium burning sequence to form red giants, and contract when shifting from the main-sequence branch to Wolf Rayet stars. For Wolf-Rayet stars which fuse helium or heavier elements in the core, fusion occurs in a domain at higher pressure than their counterparts. This is especially pronounced for OW Wolf-Rayet stars on the oxygen sequence, where the fusion pressure domain is clearly higher than for helium fusion.

There are also mass threadshods for fusion to occur. For example, red giants of mass less than 0.9 solar mass are never

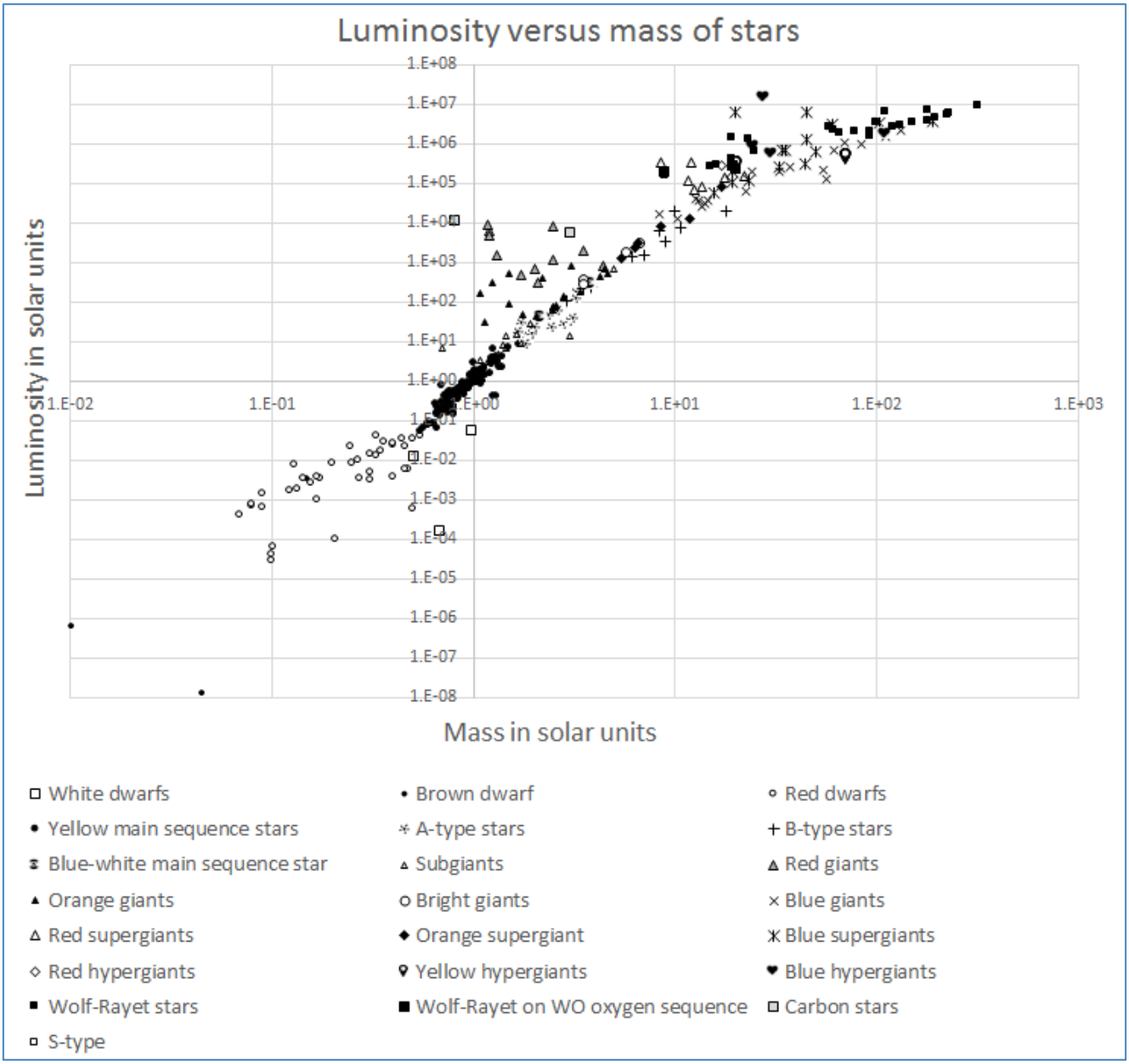

Fig. 1: Luminosity versus mass of stars. Mass and luminosity are in solar units.

observed. This limit is commonly attributed to the age of the universe, because low mass main-sequence stars take longer to fuse the hydrogen in their core, and therefore it is hypothesized that stars below 0.9 solar masses did not have sufficient time to become red giants. However, this limit could also represent the minimum mass required to obtain the necessary conditions for helium fusion. Similarly, Wolf-Rayet stars have masses above the 8.0-9.0 solar mass limit. Thefore, low mass stars do have the necessary conditions to fuse elements heavier than helium in the core.

The red dwarfs in Figure 1, show a distribution in their luminosities. This might be due to ageing, as red dwarfs haven't sufficient mass to fuse the helium accumulating in their core. As a star exhausts its hydrogen supply and accumulates helium in its core, the core cools and contracts. As the core contracts, a new shell of fresh hydrogen fuel is formed at the periphery of the core. Fusion of this hydrogen shell maintains the temperature of the core, preventing it from contracting further. The fact that the atomic mass of helium is greater than that of hydrogen also plays a role.

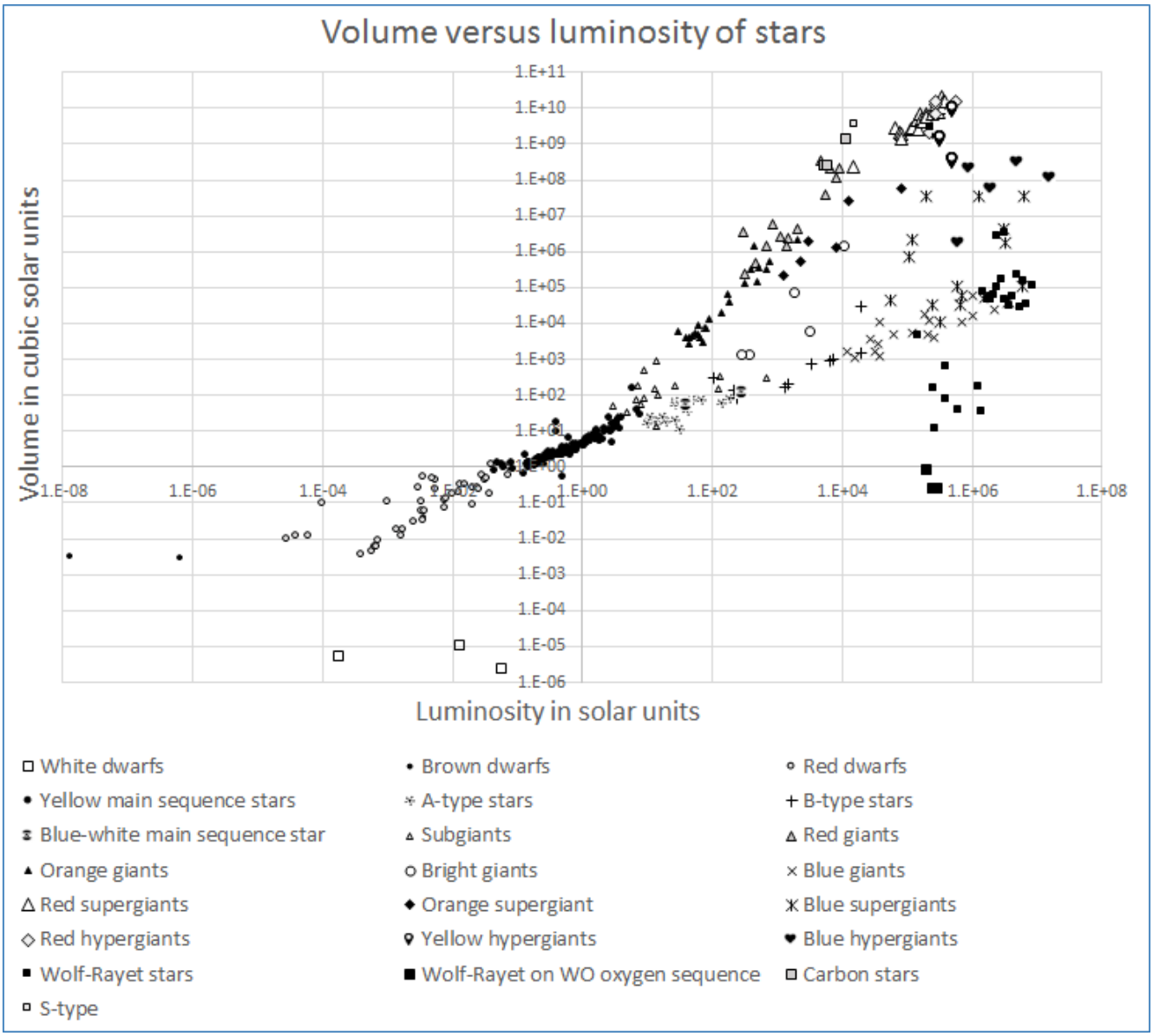

Fig. 2: Volume versus luminosity of stars. Volume and luminosity are in solar units.

Helium nuclei are formed of four nucleons (two protons and two neutrons). Therefore, there is four times more mass in a helium gas than in a hydrogen gas at a given pressure, provided they obey the ideal gas law. As the star gets older, the core shrinks and grows ever denser by accumulating helium. Therefore, as red dwarfs age, they should become denser and less luminous. Common stellar age-dating methods, based on the main-sequence turnoff, are focused on main-sequence stars that become red giants. Such age calculation methods do not yield stellar ages older than about 15 billion years, perhaps because this is when a solar type main-sequence star becomes a red giant. No methods have been developed so far to estimate the age of red dwarfs, which could possibly be much older. Using stellar models would be an approach for age-datating of red dwarfs.

3 Stars dominated by radiation pressure in the photosphere

3.1 Eddington luminosity

Inside a star, the internal pressure acting against the hydrostatic pressure is the sum of the radiation pressure and gas pressure, hence:

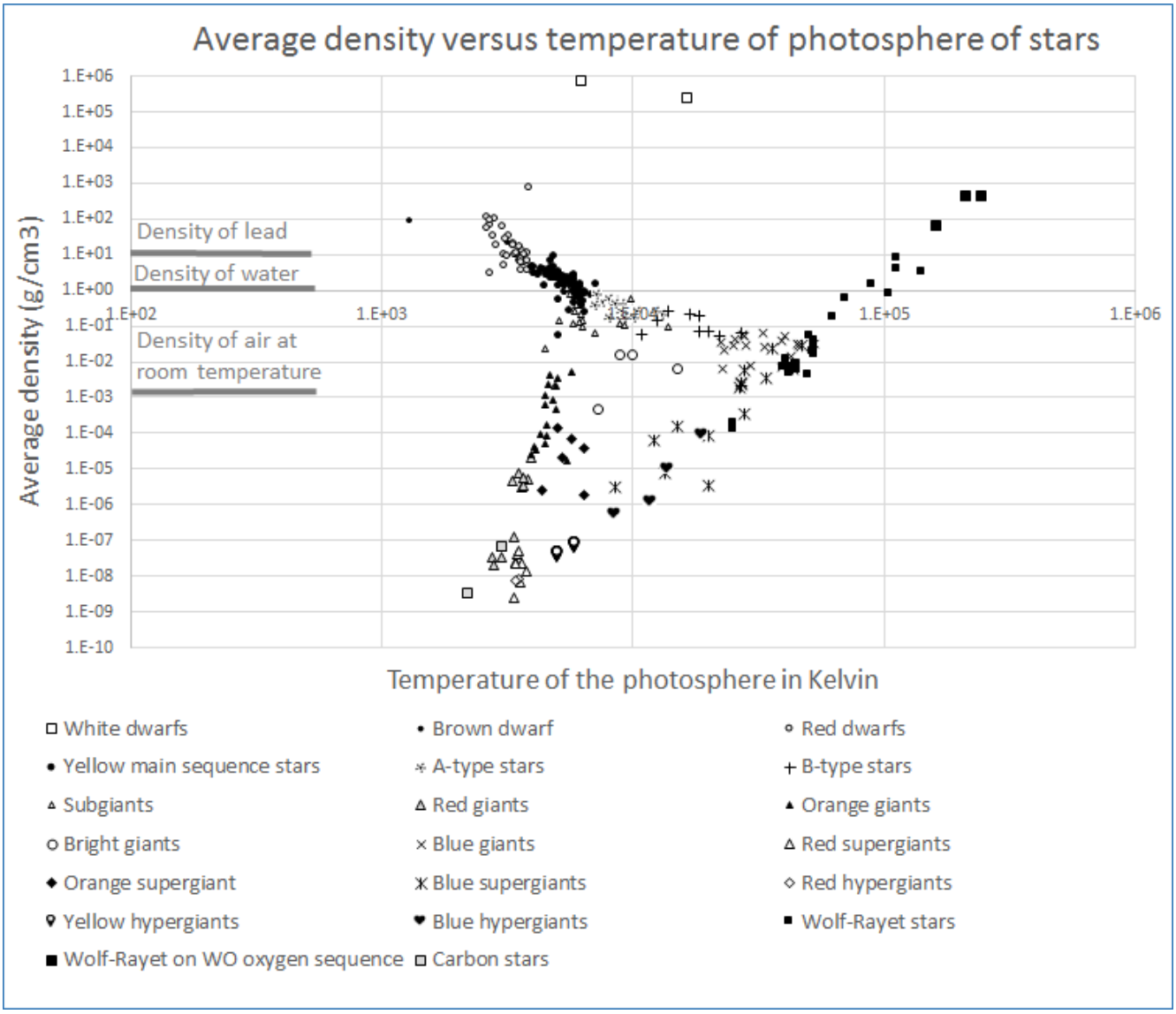

Fig. 3: Average density versus temperature of the photosphere of stars. Density is given in g/cm^3, and temperature in Kelvin.

$$P = \rho_n kT + \frac{1}{3}aT^4 , \tag{1}$$

where $\rho_n = \frac{N}{V}$, N is the number of molecules in the gas, V is the volume, $a = \frac{4\sigma}{c}$ is the radiation constant, k is the Boltzmann constant, σ is the Stefan-Boltzmann constant, T is the temperature, and c the speed of light.

When the radiation pressure is considerably higher than the gas pressure, the gas pressure term can be neglected, therefore we get:

$$\frac{\partial P_r}{\partial T} = \frac{4}{3}aT^3 , \tag{2}$$

The equation for radiative heat transfer is expressed as follows:

$$\frac{\partial T}{\partial r} = -\frac{3}{4}\frac{1}{ac}\frac{\kappa\rho}{T^3}\frac{L}{4\pi r^2} , \tag{3}$$

where κ is the opacity, L is the luminosity, T is the temperature, r is the radius, ρ is the density, c is the speed of light, and a the radiation constant.

Rewriting (2), we get:

$$\frac{\partial P_r}{\partial r}\frac{\partial r}{\partial T} = \frac{4}{3}aT^3 , \tag{4}$$

Combining (3) and (4) we get:

$$\frac{\partial P_r}{\partial r} = -\frac{\kappa\rho}{c}\frac{L}{4\pi r^2}\,, \tag{5}$$

From hydrostatic equilibrium:

$$\frac{\partial P}{\partial r} = -\frac{GM_r\rho}{r^2}\,, \tag{6}$$

where G is the gravitational constant, M_r is the interior mass of the star at radius r, and ρ is the density.

By combining (5) and (6) we get:

$$L = \frac{4\pi cG}{\kappa}M\,, \tag{7}$$

which is the Eddington luminosity. Stars dominated by radiation pressure in their photosphere are fully determined by the photosphere, meaning that their luminosities will adjust to match the Eddington luminosity. For such stars luminosity is proportional to mass as shown by the Eddington luminosity equation. Should excess heat be generated, the star will lose matter through its photosphere, which may explain why many Wolf-Rayet stars have lost their outer hydrogen layer.

We can also express this equation in terms of temperature using Stefan-Boltzmann as:

$$Flux = \frac{L}{4\pi r^2} = \sigma T^4\,. \tag{8}$$

Hence, combining (7) and (8), we get:

$$T = \left(\frac{cG}{\kappa\sigma}\right)^{1/4}\frac{M^{1/4}}{R^{1/2}}\,. \tag{9}$$

3.2 Cross section of an hydrogen ion from photon flux

There are two different methods to calculate the cross section of an ion exposed to photon flux in the photosphere; these are known respectively as the optical and the radiation pressure cross section approaches.

The optical cross section calculation considers the obscuration of a radiative flux travelling in an isotropic medium. Let us consider an isotropic gas with a radiative flux going through a surface A in the x-direction orthogonal to the surface. The flux at step $x + dx$ is equal to the flux at step x multiplied by one minus the proportion of the area that is obscured by the cross section of the atoms in the volume Adx. The number of atoms in the volume Adx is $\rho_n Adx$. We multiply the number of atoms in the volume by the cross section of the atom σ_p to give the total area obscured by the gas. Hence, we get:

$$F(x + dx) = F(x)\left(1 - \sigma_p\rho_n dx\right)\,, \tag{10}$$

where $F(x)$ is the flux at step x, $F(x + dx)$ is the flux at step $x + dx$, ρ_n is the density in number of particles per volume, and σ_p is the cross section per particle.

As $dF = F(x + dx) - F(x)$, we get:

$$\frac{dF}{F} = -\sigma_p\rho_n dx\,. \tag{11}$$

We integrate (11) to obtain:

$$F(x) = F_0\exp(-\sigma_p\rho_n x)\,. \tag{12}$$

The opacity is defined from the attenuation of radiation intensity through a medium and is given by $I(x) = I_0\exp(-\kappa\rho x)$, where I is the intensity, therefore:

$$\kappa = \frac{\sigma_p}{m_p}\,, \tag{13}$$

where κ is the opacity, σ_p is the cross section of a particle, and m_p is the mass of a particle.

The radiation pressure cross section considers an ion above the surface of a star. Let us assume that the ion is in equilibrium, meaning that the gravitational force exerted by the star on the atom is equal to the radiation pressure from the radiation flux coming from the surface of the star times the cross section of the ion. Therefore, we get:

$$\frac{GMm_p}{R^2} = \sigma_p\frac{1}{3}aT^4\,, \tag{14}$$

where G is the gravitational constant, M the mass of the star, R the radius of the star, m_p the mass of an ion, σ_p the cross section of an ion, T the temperature, and a the radiative constant.

Note that the radiation pressure just above the surface is the same as the radiation pressure below the surface. This can be proven but is outside scope of our discussion.

Combining (9) and (14) we get:

$$\kappa = \frac{4}{3}\frac{\sigma_p}{m_p}\,. \tag{15}$$

This equation differs slightly from (13) due to factors introduced in the derivation of the radiative heat transfer equation (3). The factor 3/4 in equation (3) comes from the fact that a collimated radiation flux was used to compute the radiation pressure dependency on the flux [3]. The two cross section calculation approaches provide a consistency check across the different models. We see that the optical and radiation pressure cross sections mean the same thing; it is the cross section of an ion exposed to photon flux.

3.3 Opacity and cross-section calculations

Now let us confront the model for stars dominated by radiation pressure in the photosphere with actual data. The stars dominated by radiation pressure must be those with low average densities and high photosphere temperatures and include the most massive stars. We included in this group blue giants, carbon stars, all the supergiants and hyper giants (red to blue), and all the Wolf-Rayets. Then we did a linear regression of

photosphere temperature against $M^{1/4}R^{-1/2}$, where temperature is in Kelvin, mass M in kilograms, and radius R in meters (see figure 4). We obtained a linear equation with slope $\alpha = 35.87$ [K kg$^{-1/4}$ m$^{1/2}$] and determination coefficient R^2 standing at 93%. Using the formalism of equation (14), we obtain the below cross section to particle mass ratio function of the slope α:

$$\frac{\sigma_p}{m_p} = \frac{3G}{a\alpha^4} . \tag{16}$$

The cross section σ_p expresses the surface of the ion exposed to photon flux.

By considering a hydrogen ion having a mass $m_p = 1.67\times 10^{-27}$ kg, we obtain a cross section $\sigma_p = 2.67 \times 10^{-28}$ m^2. This cross section is equal to four times the Thomson cross section for the scattering of a free electron by radiation. The Thomson cross section of free electron scattering is expressed as follows:

$$\sigma_T = \frac{8\pi}{3}\left(\frac{q^2}{4\pi\epsilon_0 mc^2}\right)^2 = 6.65 \times 10^{-29}\,\mathrm{m}^2 , \tag{17}$$

where q is the charge of the electron, ϵ_0 is the permittivity of free space , m is the mass of the electron, and c is the speed of light.

For comparison purpose, the radius of a proton is about 8.8×10^{-16} m, which works out to a cross section of 2.43×10^{-30} m^2, which is about hundred times less than the cross section we computed. The radius of a hydrogen atom from the Bohr model is about 5.3×10^{-11} m, or a cross section of 8.82×10^{-21} m^2, which is about 33 million times larger than the cross section we computed. In contrast, the cross section of hydrogen ion exposed to photon flux we computed is four times the Thomson cross section for the scattering of free electrons.

The corresponding opacity κ is 0.160 m^2 kg^{-1} given (13) or 0.213 m^2 kg^{-1} given (15). Opacity remains fairly consistent across the range of photosphere temperatures (2,200 K to 245,000 K), and photosphere compositions (different hydrogen to helium ratio) for the stars in our sample. Wolf-Rayet stars generally exhibit strong helium lines in their atmosphere. For example, Wolf-Rayet star WR136 which is among our sample set was determined to have an atmospheric composition of 86.5% helium, 12% hydrogen and 1.5% nitrogen by mass based on analysis of its spectra [4]. The red hypergiant star WOH G64 has a broad number of emission lines in its spectrum including Hα , $H\beta$, [O I], [N I], [S II], [N II], and [O III] [5]. Despite the limited data available on helium to hydrogen ratio estimates for these stars, the variability of stellar spectra in our sample would suggest that opacity is not sensitive to the composition of the photosphere, unless all of these stars have lost their outer hydrogen layer. For example, if the ratio $\frac{\sigma_p}{m_p}$ is higher for hydrogen than for helium, according to (14), stars dominated by radiation pressure in the photosphere would preferentially lose hydrogen through their surface while retaining their helium.

Ionisation supposedly depends on temperature. However, the wide range of photosphere temperatures in the sample would suggest that the degree of ionisation is not relevent. This could be indicative of the process contributing to radiative opacity in the photosphere. For bound-free transitions which consist of the absorption of radiation by an electron bound to an ion, and free-free transitions which consist of the absorption of a photon by an unbound electron moving in the field of an ion, the Rosseland opacity is a function of the temperature and hydrogen fraction, and exhibits the dependency with temperature $\kappa \propto \rho T^{-7/2}$ as per Kramers' law. This is quite unexpected as the data do not show such a dependency; otherwise, the regression in Figure 4 would not be linear. Instead, temperature would be proportional to the square of $M^{1/4}R^{-1/2}$. As this is not the case, these opacity models do not seem to adequately describe stellar photosphere plasma.

4 Stars dominated by gas pressure in the photosphere

4.1 Estimation of the density in the solar photosphere

The density of the photosphere is an important parameter required to solve the heat transfer equation for stars. A way to probe the density of the photosphere of the Sun is by using limb darkening. Limb darkening is the observation of the center part of a star appearing brighter than the edge or limb of the luminous disk. This effect is due to the thermal gradient and transparency of the photosphere. The intensity of light at the center of the disk corresponds to the black-body spectrum at an optical depth of 2/3 because of the transparency of the photosphere. The intensity of light at the edge of the disk corresponds to the black-body spectrum at the surface of the photosphere, which is cooler than the temperature at an optical depth of 2/3. The intensity of light travelling through a semi-transparent medium is expressed as follows:

$$I(x) = I_0 \exp(-\kappa\rho x) , \tag{18}$$

where κ is the opacity, ρ the density, and x the depth of the medium.

Therefore, the distance from the surface at an optical depth of 2/3 corresponding to 1/3 of the intensity going through is expressed as follows:

$$l = -\frac{\ln(1/3)}{\kappa\rho} . \tag{19}$$

Let us say T_0 is the temperature at the limb which is the surface of the photosphere, and $T_{2/3}$ is the temperature at the center of the disk or an optical depth of 2/3. Hence, the temperature gradient is expressed as follows:

$$\frac{dT}{dr} = \frac{T_0 - T_{2/3}}{l} , \tag{20}$$

where l is given by (19).

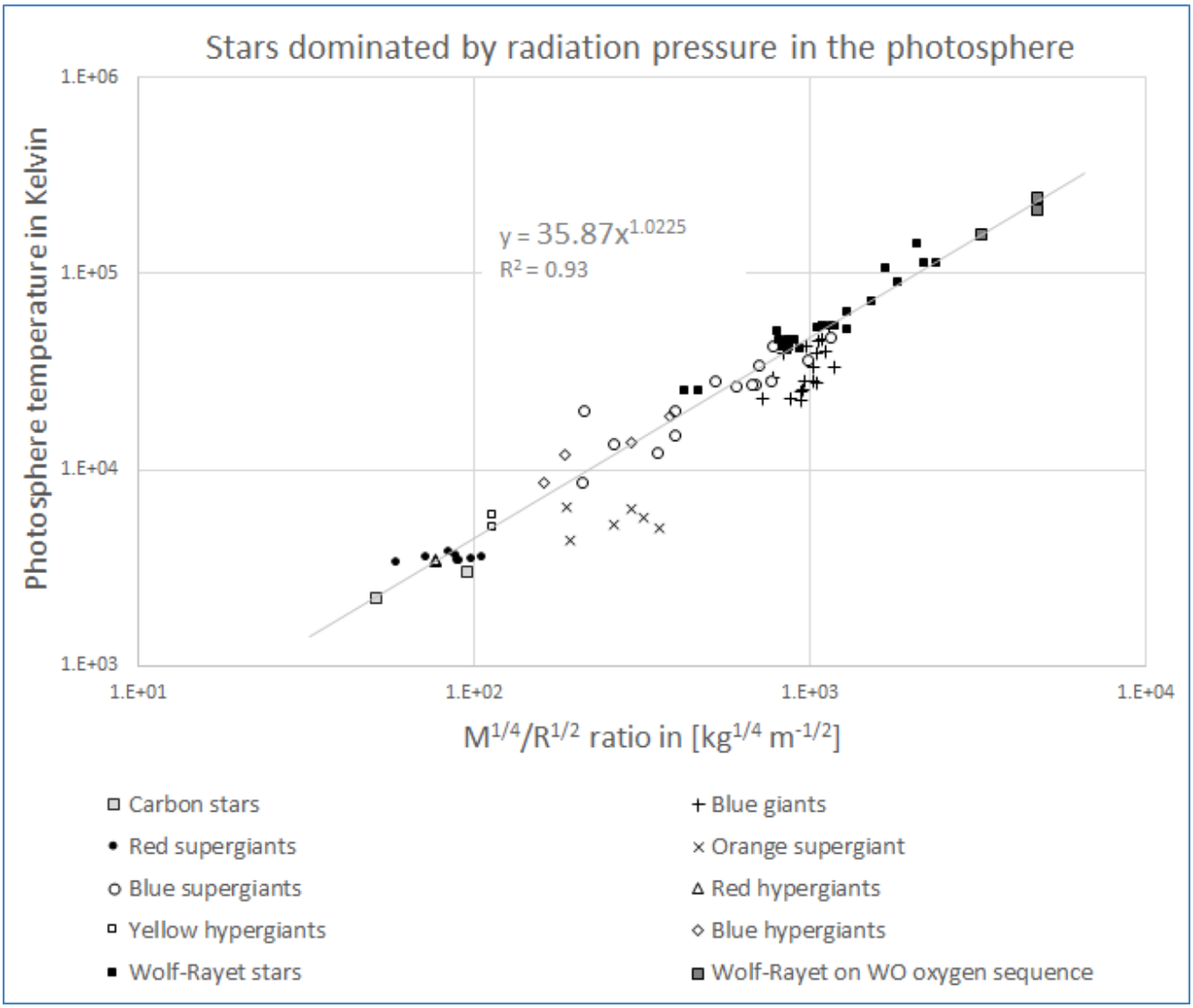

Fig. 4: Photosphere's temperature versus $M^{1/4}R^{-1/2}$ ratio for stars dominated by radiation pressure in the photosphere.

Within a star heat transfer is dominated by the process having the lowest thermal gradient. We know that for the external layer of the Sun, the temperature is too low for radiative heat transfer to be efficient, and convective heat transfer dominates. The thermal gradient of convective heat transfer in a gas is the adiabatic gradient. From limb darkening we get T_0 and $T_{2/3}$. Therefore, using (19) and (20), we can estimate the density of the photosphere.

The ratio of the intensity at an angle θ to intensity at the center of the star from limb darkening is expressed as follows [6]:

$$\frac{I(\theta)}{I(0)} = \frac{2}{5} + \frac{3}{5}\cos(\theta)\,. \tag{21}$$

The intensity at the limb is the intensity at an angle $\theta = \frac{\pi}{2}$. Therefore, the ratio of the intensity at the limb to the intensity at the center of the star is 0.4. From Stefan-Boltzmann law, we get the ratio of the temperature at the limb to the temperature at the center:

$$\frac{T_0}{T_{2/3}} = 0.4^{1/4}\,. \tag{22}$$

The average temperature of the solar photosphere is about 5,800 K. Let us say the temperature at the center of the disk is $T_{2/3}$ = 6,300 K. Hence, the temperature at the limb is T_0= 5,010 K.

The adiabatic gradient is the temperature gradient obtained for a gas parcel as it rises, assuming an ideal gas. For an ideal gas we have $P = (R/\mu)\rho T$, where R is the ideal gas constant and μ the molar weight. As we move a gas parcel

upwards an infinitesimal distance, the variation in pressure is given by:

$$\frac{dP}{dr} = \frac{R}{\mu}\left(\rho\frac{dT}{dr} + T\frac{d\rho}{dr}\right) = \frac{P}{T}\frac{dT}{dr} + \frac{P}{\rho}\frac{d\rho}{dr}\,. \tag{23}$$

For an adiabatic gas, we also have $P = K\rho^{\gamma}$, hence:

$$\frac{dP}{dr} = K\gamma\rho^{\gamma-1}\frac{d\rho}{dr} = \gamma\frac{P}{\rho}\frac{d\rho}{dr}\,. \tag{24}$$

Combining (23) and (24) we get:

$$\frac{dT}{dr} = (\gamma-1)\,\frac{T}{P}\frac{P}{\rho}\frac{d\rho}{dr} = \left(\frac{\gamma-1}{\gamma}\right)\frac{T}{P}\frac{dP}{dr}\,. \tag{25}$$

From hydrostatic pressure, we have:

$$\frac{dP}{dr} = -\frac{GM}{R^2}\rho\,. \tag{26}$$

Combining (25) and (26) with $P = \frac{\rho}{m_p}kT$ we get:

$$\frac{dT}{dr} = -\left(\frac{\gamma-1}{\gamma}\right)\frac{GM}{R^2}\frac{m_p}{k}\,, \tag{27}$$

which is the adiabatic gradient at the stellar surface, where k is the Boltzmann constant, G the gravitational constant, M the mass of the star, R the radius of the star, m_p the mass of a gas molecule.

For a monoatomic gas $\gamma = \frac{5}{3}$. Hence, the adiabatic gradient at the surface of the sun is 0.013 K/m. In contrast, the standard solar model uses an adiabatic gradient of 0.010 K/m.

Hence, the density of the photosphere of the Sun from (19) and (20) is:

$$\rho = -\frac{1}{\kappa}\frac{\ln(1/3)}{(T_{2/3} - T_0)}\frac{dT}{dr}\,, \tag{28}$$

which yields a density of 6.92×10^{-5} kg/m^3, whereas the standard solar model uses a photosphere density of about 10^{-6} kg/m^3 [7]. For the calculation, we used the opacity obtained in section 3.3.

4.2 Calculation of the cross section per hydrogen nuclei from gas pressure

Let us consider an ion above the stellar surface. A condition to have a stable surface is that the gravitational force exerted by the star on the ion is offset by the repulsive force due to gas pressure. Assuming an ideal gas, we get:

$$\frac{GMm_p}{R^2} = \sigma_{ef}\frac{\rho\,k\,T}{m_p}\,, \tag{29}$$

where σ_{ef} is the effective cross section, m_p is the mass per hydrogen nuclei, M is the mass of the star, G is the gravitational constant, R is the radius of the star, ρ is the mass density in the photosphere, k is the Boltzmann comstant, and T is the temperature.

Although the photosphere is about 500 km thick, modelling the photosphere as a surface makes sense. As shown in figure 5, we can see a clear surface of dense plasma at the photosphere of the Sun. Note that in equation (29) we did not consider the electromagnetic forces. Because free electrons are lighter than the protons, they should tend to escape the surface much easier. However, the plasma may have mechanisms in place to keep its neutrality. For example, a positively charged surface would retain the electrons while pushing out the protons. Equation (29) provides a net cross section from gravity alone and does not model such an effect.

The gas pressure due to molecular collisions is somehow different than radiation pressure. When a photon collides with a surface, the momentum vector is applied in the direction of the trajectory of the photon. For molecular gas collisions, it is like playing pool. Considering molecules of spherical shape, the momentum vector is normal to the sphere, meaning it is applied along the axis between the point of impact of the collision and the center of the sphere. Therefore, we need to introduce a shape coefficient to relate the effective cross section to the geometrical cross section of the molecule.

Let us consider a force f exerted on a sphere of radius r. The surface element is $dS = r^2\sin(\theta)\,d\theta\,d\varphi$. The projection of the force f on the z-axis is $f_z = f\cos(\theta)$, where θ is the angle between the z-direction and and the vector f. The effective force is the average of f_z over the half sphere. Hence, the effective force is computed as follows:

$$f_{ef} = \frac{1}{2\pi r^2}\int_{\varphi=0}^{2\pi}\int_{\theta=0}^{\pi/2} f\cos(\theta)r^2\sin(\theta)\,d\theta\,d\varphi\,. \tag{30}$$

Because $\sin(\theta)\cos(\theta) = \frac{\sin(2\theta)}{2}$, we get:

$$f_{ef} = \frac{f}{4\pi}\int_{\varphi=0}^{2\pi}\int_{\theta=0}^{\pi/2}\sin(2\theta)\,d\theta\,d\varphi\,. \tag{31}$$

We get:

$$f_{ef} = \frac{f}{2}\,. \tag{32}$$

Therefore, the geometric cross section is twice the effective cross section from gas pressure: $\sigma_g = 2\sigma_{ef}$, where σ_g is the geometric cross section and σ_{ef} the effective cross section.

From (29) and the density we obtained in section 4.1, we get an effective cross section of 1.33×10^{-28} m^2 or a geometric cross section of 2.66×10^{-28} m^2. In section 3.3, we obtained a cross section to photon flux of 2.67×10^{-28} m^2. Hence, in the plasma the cross section per hydrogen nuclei from gas pressure is virtually the same as the cross section from radiation pressure.

Neutral hydrogen atoms in the Bohr model are represented with the nucleus at the center and an electron in orbit around the nucleus. The Bohr model yields a radius of

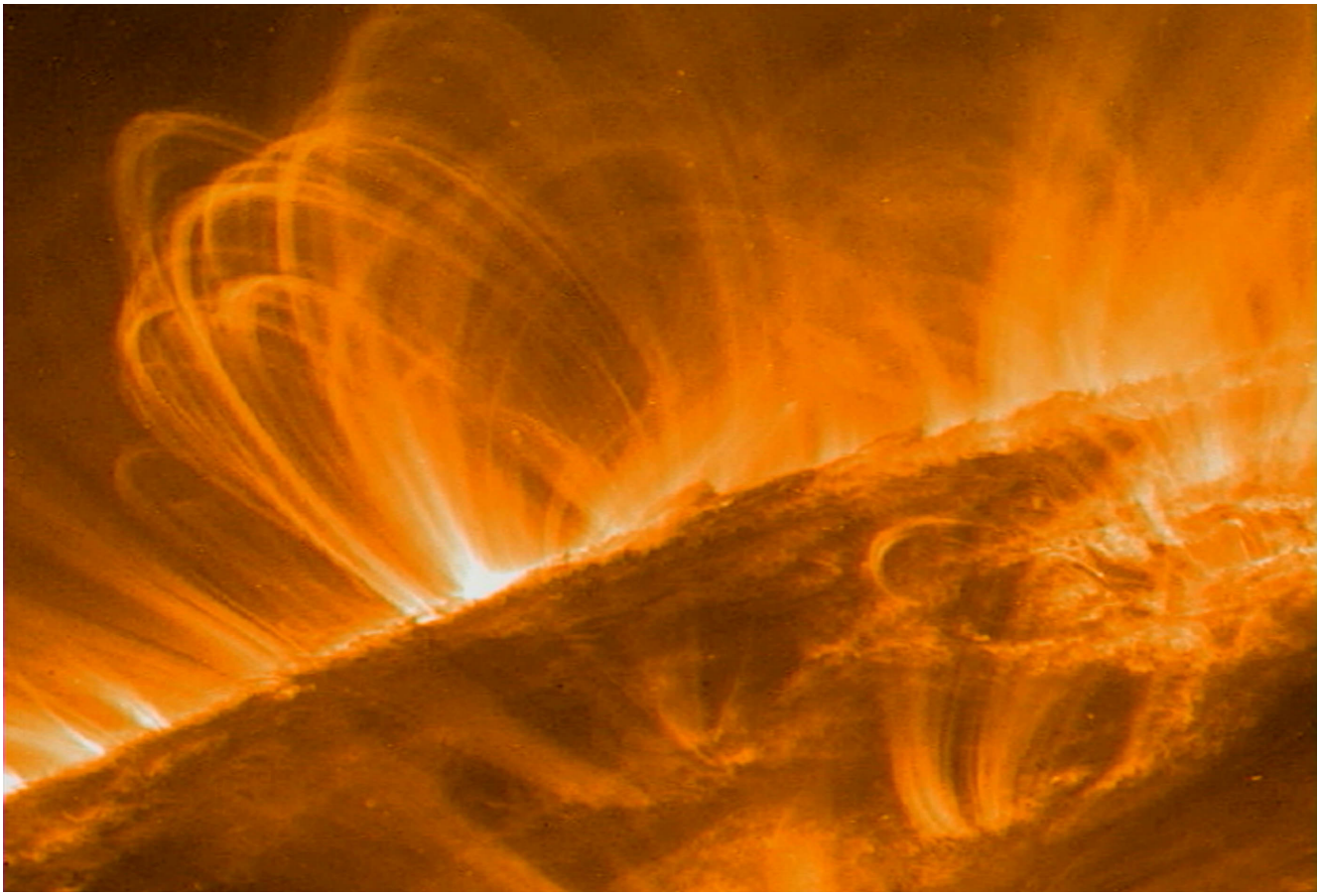

Fig. 5: Image of the solar surface. Credit: NASA/GSFC (December 2000)

5.3×10^{-11} m for the hydrogen atom with a corresponding cross section of 8.82×10^{-21} m^2. Hydrogen cross sections have been obtained from electron collisions yielding cross sections on the order of 10^{-21} m^2 for ionized hydrogen [8]. A precise value was measured by [9], who obtained a cross section of 3.86×10^{-21} m^2 using photodetachment of negatively charged hydrogen ions H^-, that is in close agreement with the Bohr model. The fact that we obtained a much smaller cross section per hydrogen nuclei suggests that in a plasma, the electrons are virtually detached from the nuclei. Therefore, a hydrogen plasma may be represented as a gas mixture of electrons and protons. Hence, the total pressure would be equal to the sum of the partial pressure of the electrons and protons.

Assuming that the electrons and protons are at the same temperature, the adiabatic gradient we computed with eq. (27) should be divided by two, and the density in the photosphere would be half the estimate we obtained, leaving the cross section unchanged. For the proton and electron temperatures to equilibrate, the Coulomb collision rates would need to dominate to allow energy transfer between the electrons and protons. Most plasmas are considered weakly collisional, which means that the Coulomb collision rates are negligible compared to other processes that control the velocity distributions. Therefore, if we assume that the temperature of the electrons is much lower than the temperature of the protons, we can neglect the electron pressure; and if it is the reverse, then we can neglect the proton pressure, provided that both particles are on the ideal gas domain.

Electrons and protons are fermions, meaning they are modelled as a Fermi gas. Fermions are particles described by the Fermi-Dirac distribution thus obeying the Pauli exclusion principle. Whenever the average interparticular separation is much larger than the average de Broglie wavelength of the particules, the Fermi-Dirac distribution can be approximated by the Maxwell-Boltzmann distribution, and the Fermi gas behaves similarly to an ideal gas [10]:

$$\bar{R} \gg \frac{h}{\sqrt{3mkT}}\,, \tag{33}$$

where $\bar{R}$ is the average interparticle separation, h the Planck's constant, m the mass of the particle, k the Boltzmann constant, and T the temperature.

This condition is satisfied in the solar photosphere for

both the electrons and protons, hence we can use the ideal gas equation as an approximation in the photosphere.

Note that if the particles in the plasma of the solar photosphere were made of large ions or atoms such as the ones we find in gases, according to (29), the surface of the Sun would evaporate due to the high temperatures.

5 Conclusion

In the present study we collected stellar data (mass, radius, luminosity and surface temperature) for a set of 360 stars. From stars dominated by radiation pressure in the photosphere, we estimated the opacity, a key parameter for radiative heat transfer. As radiative heat transfer is no longer efficient in the solar convective zone where heat transfer occurs by convection, we assumed the adiabatic gradient of a monoatomic gas for the solar photosphere. We then estimated the density in the photosphere of the Sun using limb darkening. Photosphere density is a boundary parameter required for the solar model. We also considered that the stellar photosphere can be modelled as a surface. Hence, for an hydrogen ion in equilibrium in the photosphere, the force exerted by the gravitation of the star on the ion should be offset by the radiation and gas pressure. Therefore, we computed the cross section per hydrogen nuclei from radiation pressure for stars dominated by radiation pressure in the photosphere, and from gas pressure for stars dominated by gas pressure in the photosphere. We found that the cross section per hydrogen nuclei in stellar plasma is about 2.66×10^{-28} m^2 from both radiation and gas pressure. The cross section of neutral hydrogen as given by the Bohr model for an electron in orbit around the nucleus is 8.82×10^{-21} m^2, which suggests that the electrons and protons in the plasma are virtually detached. Hence, a hydrogen plasma may be represented as a gas mixture of electrons and protons. If the stellar photosphere was made of large hydrogen atoms or ions such as the ones we find in gases, the surface of the photosphere would evaporate due to the high temperatures. This result could impact stellar models as we would have to add together the partial pressures of the electrons and the protons in the plasma.

Submitted on January 10, 2017 / Accepted on January 14, 2017

References

1. Smith D.H. Eddington's Valve and Cepheid Pulsations. *Sky and Telescope*, 1984, v. 68, no. 6, 519.
2. Liebert J., Bergeron P., Eisenstein D., Harris H.C., Kleinman S.J., Nitta A., and Krzesinski J. A Helium White Dwarf of Extremely Low Mass. *The Astrophysical Journal*, 2004, v. 606, L147.
3. Salaris M., and Cassisi S. Evolution of Stars and Stellar Populations. John Wiley & Sons Ltd., 2005, p. 53.
4. Hamann W.-R., Wessolowski U., and Koesterke L. Non-LTE spectral analyses of Wolf-Rayet stars: The nitrogen spectrum of the WN6 prototype HD 192163 (WR136). *Astronomy and Astrophysics*, 1994, v. 281, no. 1, 184–198.
5. Levesque E.M., Massey P., Plez B., and Olsen K.A.G. The Physical Properties of the Red Supergiant WOH G64: The Largest Star Known? *Preprint arXiv:0903.2260*, 2009.
6. Carroll B.W., and Ostlie D.A. An Introduction to Modern Astrophysics Addison-Wesley Publishing Co, Inc., 1996, p. 292.
7. Eddy J.A. A New Sun. The Solar Results from Skylab. *Ed. Rein Ise*, 1979, p. 37.
8. Yoon J.-S., Song M.-Y., Han J.-M., Hwang S.H., Chang W.-S., Lee B., and Itikawa Y. Cross Sections for Electron Collisions with Hydrogen Molecules. *Journal of Physical and Chemical Reference Data*, 2008, v. 37, 913.
9. Frolov A.M. Photodetachment cross-section of negatively charged hydrogen ion *Preprint arXiv:1510.04766*, 2015.
10. Reif F. Fundamentals of Statistical and Thermal Physics. *Levant Books*, 2010, p. 247.

Flyby Anomaly via Least Action

Arto Annila
Department of Physics, University of Helsinki, Gustaf Hällströmin katu 2 FI-00014, Helsinki, Finland.
E-mail: arto.annila@helsinki.fi

The observed but unexpected changes in velocity during spacecraft flybys of Earth are examined using the principle of least action in its original dissipative form. In general, the spacecraft's momentum will change when it travels through an energy density gradient of space that is enfolding a gravitating, orbiting and rotating body. When space is understood as a physical substance that embodies quanta of actions, rather than being modeled by a mere metric, it becomes apparent that the changes in momentum couple with flux of quanta from the local system of bodies to the universal surroundings or vice versa. In this way the original least-action principle accounts also for the 'anomalous' change in velocity by an equation of motion which complies with the empirical relation that has been deduced from Earth-flybys.

1 Introduction

Even a slight deviation from a common rule may entail an error in the very rule. Here, in the context of flyby anomaly, the rule – perhaps at stake – is conservation of momentum. It is a corner stone of physics, whence the flyby anomaly is worth attention.

The law of conservation of momentum asserts, for example, that when a spacecraft is passing by a planet, it will gain momentum as much as the planet will lose momentum. The momentum transfer is a minute drop for the massive planet but a giant boost for the tiny spacecraft. The spacecraft's velocity v will change relative to the Sun as much as its flight direction will change relative to orbital velocity u of the planet [1–3]. The gain can be at most $2u$ when the planet is moving straight at the spacecraft which will subsequently swing a full U-turn around the planet. Curiously though, it seems as if spacecraft had acquired more speed during certain flybys than the planet's orbital momentum could possibly grant them [4, 5]. The origin of this anomaly is unknown.

However, it has been inferred from meticulously monitored flybys of Earth [6–10] that the anomalous change in velocity Δv complies closely with relation [5]

$$\frac{\Delta v}{v} = \frac{2\omega_\oplus R_\oplus}{c}(\cos\delta_i - \cos\delta_o), \qquad (1)$$

where c is the speed of light, $R_\oplus$ is Earth's radius and $\omega_\oplus$ angular velocity of rotation, δ_i is the spacecraft's inbound and δ_o outbound declination, so that $2\omega_\oplus R_\oplus/c = 0.49\times10^{-6}$. The relationship (Eq. 1) implies that the anomalous gain Δv in the spacecraft's velocity stems from Earth's angular velocity $\omega_\oplus$ depending on how the spacecraft's inbound and outbound asymptotes align relative to the axis of rotation. Yet, the effect of Earth's gravito-magnetic field on the spacecraft's velocity has been calculated to be many orders of magnitude smaller than the measured anomaly [11, 12]. Other explanations have also been considered [13–17] and found feasible [18], but there is currently no consensus what exactly underlies the phenomenon. Also the general validity of Eq. 1 has been questioned [19–22]. Moreover, it should be noted that anomalies, when without radar monitoring, are difficult to detect along flybys of other planetary bodies.

As long as the case is open there ought to be room for attempts to explain the measurements. Thus, we would like to contribute to the puzzle of flyby anomaly by maintaining that the spacecraft does move along a geodesic, i.e., a path of least action, also when it is subject to the unknown force that causes the unaccounted change in momentum. So, it should be possible to infer the cause of anomaly from the principle of least action. However, the familiar Lagrangian form when without dissipation applies only to closed stationary orbits such as ellipses or to ideal paths with symmetrical inbound and outbound trajectories. In contrast, the general form of the least action principle by Maupertuis [23–25] accounts also for open paths, most notably for hyperbolic flyby trajectories that are asymmetric relative to the planet's rotation. Furthermore, we are motivated to apply this general principle that distinguishes itself from particular models of celestial mechanics, because it has already accounted for anomalous perihelion precession [26], rotation of galaxies [27], geodetic and frame dragging drift rates [28] as well as for frequency shifts and bending of light [29], as well as for propagation of cosmic rays [30] and the thrust of electromagnetic drive [31]. Thus, our examination of the flyby anomaly using the universal principle is not a standalone study. It can be seen as a further test of our approach yet in another physical situation.

2 The least-action principle

The spacecraft is customarily pictured to move along a hyperbolic path as if it was coming from a distant asymptotic state of free space and returning via periapsis back to the asymptotic state. Per definition this ideal, i.e., fully reversible passage cannot accommodate any net change in momentum in the planet's frame of reference, because the initial and final asymptotic states are taken as indistinguishable from

each other in energetic terms. In other words, the Lagrangian having only kinetic and potential energy terms does not allow for any change in the total energy, i.e., dissipation. But in reality the unaccounted increase (or decrease) in kinetic energy reveals that during the flyby the spacecraft does descend down (or move up) along a potential energy gradient, so that the initial and final states are not equal in energetic terms. Therefore, to account for the flyby anomaly as a non-conserved phenomenon we will use Mauperutuis's rather than Lagrange's principle of least action. Then it remains for us to identify among conceivable gradients in energy, the one that lies asymmetrically with respect to the spacecraft's inbound and outbound trajectories, and hence is responsible for the net change in energy.

In all cases, the spacecraft treks at least through the gravitational potential of free space. The all-embracing vacuum potential energy $GM^2/R = Mc^2$ totals from the mass M of all bodies in the Universe within Hubble's radius $R = cT$ at its current age $T = 13.8$ billion years where G is the gravitational constant [32]. In terms of geometry the free space energy density is characterized by the universal L^2-norm [33] that manifest itself in the quadratic form c^2. Physically speaking, the norm means that in the free space there is no shorter path than that taken by light. Thus, the energy density of free space, on the order of one nJ/m^3, is the ultimate reference for any other energy density.

A local potential energy, known as the local gravitational potential energy is in balance with the bound energy density of a body, for example, a planet, just as the universal gravitational potential is energy is in balance with all bodies in the Universe [34]. Thus, the spacecraft when moving past by the planet, will be subject to energy density gradients, i.e., forces that will show as changes in its momentum. We acknowledge that general relativity accounts for the space without energy density due to the gravitational field itself. General relativity expresses gravity in terms of the geometrical properties of spacetime through the Einstein field equations. This mathematical model is excellent for many data, but when without dissipation, it does not account accurately for irreversible changes in momentum, for instance, for the spacecraft anomalous gain in momentum during the flyby.

To work out the energy density gradient responsible for the dissipative change in momentum we will express the local energy density at a distance r from the body relative to the universal energy density by the ratio of light's universal velocity to its local velocity $n = c/v$. The index n has been used earlier to describe the gravitational potential in terms of an optical medium [35] consistently with the fact that gravity and electromagnetism share the same functional forms [34, 36]. The local excess in energy density is miniscule in the vicinity of an ordinary celestial body. This is to say that when light is grazing the planet Earth, its speed $v \leq c$ will hardly deviate from c. Therefore, light will experience only a minute change in momentum that will manifest itself as a tiny blue shift and next-to-negligible bending.

However, the spacecraft with velocity $v \ll c$ will be subject to a marked change in its momentum during its passage through the local potential of space imposed by the gravitating, orbiting and rotating Earth. This is to say that the spacecraft will gain momentum when inbound and conversely it will lose momentum when outbound. The inbound gain and outbound loss will sum up to zero in the case the open hyperbolic trajectory through a spherically symmetric field. A net change in momentum will accrue only if the flight path is open asymmetric relative to energy density gradients of space due to the planet's orbital and rotational motion.

In general the index n for a locus of space can be obtained from the least action principle in its original form by Maupertuis. The principle [23, 25–27, 29] equates a change in kinetic energy $d_t 2K$ with changes in scalar potential energy $\partial_t U$ and vector potential energy $\partial_t Q$,

$$d_t 2K = -\partial_t U + i\partial_t Q, \tag{2}$$

where we emphasize, although self-evidently, the orthogonal relationship between the gradients of scalar and vector potential energy by the imaginary quotient i. The equation of motion (Eq. 2) containing both real and imaginary parts ensures that any (formal) solution is non-conserved. Moreover, orthogonality is familiar from electrodynamics, for instance, as defined by Poynting theorem. Accordingly, when the spacecraft accelerates in the gravitational field of a planet, the quanta will dissipate to the surrounding free space from the local gravitational potential orthogonally to the acceleration.

The equation for the dissipative changes in energy [25,31] (Eq. 2) corresponds to Newton's second law of motion for a change in momentum $\mathbf{p} = m\mathbf{v}$ when multiplied with velocity $\mathbf{v}$, i.e.,

$$\begin{aligned} \mathbf{F} &= d_t \mathbf{v} \quad | \cdot \mathbf{v} \\ \mathbf{F} \cdot \mathbf{v} &= d_t(m\mathbf{v}) \cdot \mathbf{v} = \mathbf{v} \cdot m\mathbf{a} + v^2 \partial_t m \\ d_t 2K &= -\mathbf{v} \cdot \nabla U + i\partial_t Q, \end{aligned} \tag{3}$$

where kinetic energy, i.e., vis viva is $2K = mv^2$, and where the spatial gradient of U relates to the familiar term $m\mathbf{a}$ of acceleration and the change in mass $dm = dE/c^2$ equals dissipation $n^2 d_t Q = d_t E$ to the free space. As usual, the mass-energy equivalence converts mass-bound energy to energy E of freely propagating photons in the vacuum. In short, Eqs. 2 and 3 simply state that at any position along the spacecraft's least-time path the momentum will follow the force $\mathbf{F} = -\nabla U + i\nabla Q$, where the energy density gradient subsumes both the scalar and vector components. In this way our account on gravity is physical rather than merely mathematical and consistent with electromagnetism. However, in what follows, the orthogonality of the two components remains only implicit when we work out only the magnitude of the total

potential energy in any given position along the spacecraft's path.

3 Passages through gradients

The general principle of least action in its original form allows us to examine the flyby trajectories by specifying the energy density of space by the index n at a particular position r of space from the center of a gravitating body with mass $M_\oplus$. Also earlier the gravitational field has been described in terms of an optical medium [35], but we do not model space by an explicit metric, instead present it in energetic terms. When approximating the total potential energy U only with the local gravitational potential energy $GmM_\oplus/r$, Eq. 3 can be solved for the index of space

$$\begin{aligned} d_t(mv^2) &= -\partial_t \frac{GmM_\oplus}{r} + i\partial_t mc^2 \\ n^2 = \frac{c^2}{v^2} &= \left(1 - \frac{GM_\oplus}{c^2 r}\right)^{-1} \approx 1 + \frac{GM_\oplus}{c^2 r} = 1 + \varphi_\oplus \end{aligned} \tag{4}$$

at a locus r. The squared index sums the universal density (unity) and the local excess $\varphi_\oplus$ as experienced by a test body of vanishing mass, i.e., a photon. The first order approximation means that n^2 does not differ much from the asymptotic ($r \to r_\infty$) unity of free space. Explicitly, a ray of light will bend hardly at all even when grazing the Earth of radius $R_\oplus$, since $\varphi_\oplus = GM_\oplus/c^2 R_\oplus \approx 0.7 \times 10^{-9}$.

However, the spacecraft with its minute velocity v relative to the speed of light, i.e., $v^2/c^2 \ll 1$, will accelerate considerably when traversing through the gradient $d(n^2)/dr = \nabla\varphi_\oplus = -GM_\oplus \mathbf{r}_o/c^2 r^2$ where the unit vector $\mathbf{r}_o = \mathbf{r}/r$ points to the center of mass. According to Eqs. 2 and 3 the spacecraft will fly past by the planet when $\mathbf{v} \cdot d_t\mathbf{p}/c^2 > -\mathbf{v} \cdot \nabla\varphi_\oplus$. Conversely, when $\mathbf{v} \cdot d_t\mathbf{p}/c^2 < -\mathbf{v} \cdot \nabla\varphi_\oplus$, the spacecraft will spiral down to a crash on the planet. Eventually, when $\mathbf{v} \cdot d_t\mathbf{p}/c^2 = -\mathbf{v} \cdot \nabla\varphi_\oplus$, Eq. 2 can be integrated to a closed form. Then the net flux from to the system to its surroundings vanishes $d_t Q = 0$, and hence the integration yields the familiar stationary condition $2K + U = 0$, i.e., the virial theorem. This is to say, the spacecraft has settled on a stable Keplerian orbit about the planet.

When the planet is not only gravitating but both orbiting and rotating, then the excess in energy density of space at r is in balance also with energy that is bound in both the orbital and rotational motion as much as $\mathbf{r}_o$ aligns along the planet's orbital u and rotational $\mathbf{w}_\oplus = \omega_\oplus R_\oplus$ velocities, denoted by $u_r = \mathbf{u} \cdot \mathbf{r}_o$ and $w_r = \|\mathbf{w}_\oplus \times \mathbf{r}_o\|$, i.e.,

$$\begin{aligned} n^2 = \frac{c^2}{v^2} &= \left(1 - \frac{GM_\oplus}{c^2 r} - \frac{u_r^2 R_\oplus}{c^2 r} - \frac{w_r^2 R_\oplus}{c^2 r}\right)^{-1} \\ &\approx 1 + \varphi_\oplus + \varphi_u + \varphi_w. \end{aligned} \tag{5}$$

Again the first order approximation means that n^2 does not differ much from the free space unity. Explicitly when setting for the Earth with $r \approx R_\oplus$ and $u_r = u_\oplus$, the orbital $\varphi_u = u_\oplus^2/c^2 \approx 10^{-8}$ and rotational $\varphi_w = w_\oplus^2/c^2 \approx 0.6 \times 10^{-13}$ contributions are tiny. This means that the Earth hardly drags the vacuum along with its orbital and rotational motion.

However, the spacecraft with velocity $v^2/c^2 \ll 1$ will acquire momentum markedly during its way through the gradient $\nabla\varphi$. The gain in momentum from the orbital motion is the well-known gravity assist. Obviously this gravitational slingshot cannot be used when the spacecraft moves too slowly to catch the planet, i.e., $\mathbf{v} \cdot d_t\mathbf{p}/c^2 < -\mathbf{v} \cdot \nabla\varphi_u$. Eventually, when $\mathbf{v} \cdot d_t\mathbf{p}/c^2 = -\mathbf{v} \cdot \nabla\varphi_u$, dissipation vanishes, and hence Eq. 2 can be integrated to the stationary state condition $2K + U = 0$. It means that the spacecraft has settled on a stable Lagrangian point where it is coorbiting Sun along with Earth.

In addition to the gain in momentum from the planet's orbital motion, the spacecraft may gain a detectable amount of momentum when traversing through the gradient $\nabla\varphi_w$ due to the planet's rotation about its axis. Obviously this velocity excess will be deemed as anomalous when left unaccounted. Conversely, when the gradients along the inbound and outbound trajectories are opposite and equal, i.e., symmetric about the planet's rotation, there is no net dissipation and no net change in momentum. Eventually, when dissipation vanishes, $\mathbf{v} \cdot d_t\mathbf{p}/c^2 = -\mathbf{v} \cdot \nabla\varphi_w$, and hence Eq. 2 reduces to the steady-state condition $2K + U = 0$. It means that the spacecraft has settled on a geostationary orbit. When the spacecraft is in synchrony with the planet's rotation, obviously it will not be exposed to any energy density gradients due to the rotation.

4 Anomalous change in velocity

The above classification of spatial energy density in the gravitational, orbital and rotational terms (Eq. 5) serves us to specify the equation for the "anomalous" gain in velocity Δv. It accrues during the flyby through the energy density gradient of space $\nabla\varphi_w$ imposed by the rotating planet. In general the change in the spacecraft's momentum at any point along the trajectory is, according to Eq. 3, equal to the force $\mathbf{F} = d_t\mathbf{p} = d_t(m\mathbf{v}) = mc^2\nabla\varphi_w$. When the minute change in mass dm is neglected, the anomalous gain in velocity Δv due to the gradient ∂_w of rotational contribution φ_w can be obtained by summing up the changes in velocity dv

$$\begin{aligned} \Delta v &= \int_{v_i}^{v_o} \partial_w \varphi_w dv = \int_{\theta_i}^{\theta_o} v \frac{\partial(\omega_\oplus R_\oplus \cos\delta/c)^2}{\partial(\omega_\oplus R_\oplus \sin\delta/c)} \frac{R_\oplus}{r} d\delta \\ &= \int_{\delta_i}^{\delta_o} v \frac{2\omega_\oplus R_\oplus \sin\delta}{c} \frac{R_\oplus}{r} d\delta \\ &\approx v \frac{2\omega_\oplus R_\oplus}{c} (\cos\delta_i - \cos\delta_o) \end{aligned} \tag{6}$$

along the flight path from the inbound asymptotic velocity v_i to the outbound asymptotic velocity v_o. The equation 6 integrates the gradient ∂_w of the rotational contribution φ_w

given by Eq. 5 from the inbound asymptote with declination δ_i to the outbound asymptote with declination δ_o along the spacecraft's path. The gain in velocity will accrue only when the inbound and outbound trajectories through the energy gradients due to the planet's rotation are asymmetric. The trigonometric form of the energy density gradient $\partial_w = \partial/\partial(\omega_\oplus R_\oplus \sin\delta/c)$, where δ denotes declination (Figure 1), for the integration of declination from the inbound to outbound asymptote has been derived earlier [16]. It is easy to check by inspecting the following two points. At the Equatorial plane $\delta = 0$, where the quadratic factor $(\omega_\oplus R_\oplus \cos\delta/c)^2$ of φ_w peaks, the energy density gradient vanishes. Conversely, at poles $\delta = \pm\pi/2$, where φ_w in turn vanishes, the gradient in space due to the planet's rotation peaks. In addition to the declination by $\sin\delta$, the gradient depends on the angular velocity $\omega_\oplus$ and radius $R_\oplus$ relative to c. The product form of the three factors ensures the obvious fact that if any one of them vanishes, the gradient does not exist. The transformation from one variable of integration to another $dv = vd\delta$ follows from $vdt = rd\delta$, e.g., defining $dv = adt$ via acceleration $a = v^2/r$.

We motivate the approximation $R_\oplus/r \approx 1$ in Eq. 6 to recognize the empirical equation (Eq. 1) because the radial gradient of φ falls as $1/r^2$, and hence most of Δv accumulates when the spacecraft is near the periapsis whereas contribution from the long opposite inbound and outbound legs is negligible. The polar coordinate representation $R_\oplus/r = 1/2(1-R_\oplus/C+\cos\theta)/(1-R_\oplus/2C)$ reveals the decreasing contribution of a path position r in the sum (Eq. 6) as a function of increasing polar angle θ. The distance from the center of mass to the intersection of the inbound and outbound asymptotes of the hyperbola is denoted with C. Specifically, Eq. 6 yields the maximum change $\Delta v/v = 2\omega_\oplus R_\oplus/c$ for the flight along the rectangular hyperbola from the inbound arm $\delta_i = \pi$ to the outbound arm $\delta_o = -\pi/2$ via the periapsis at $\delta_a = \pi/4$ for a low altitude $r \to R_\oplus$ passage. Conversely, for a high altitude path, such as that of Rosetta's last flyby, the approximation $r \to R_\oplus$ underlying the empirical equation is less motivated, and hence the anomaly is negligible.

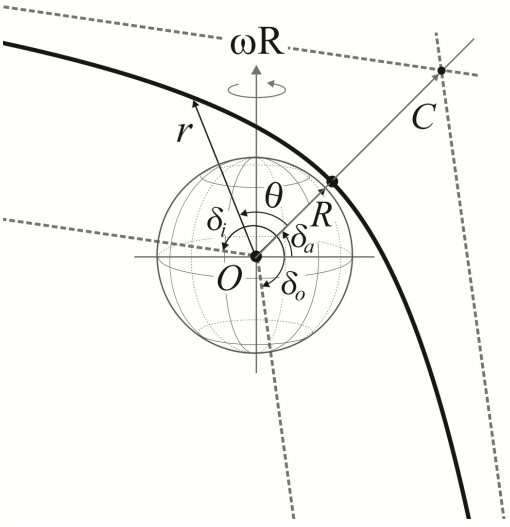

Fig. 1: Equatorial view of a grazing flyby trajectory. The hyperbolic flight path is defined by the planet's radius R extending nearly to the periapsis (solid dot) at declination δ_a and the distance C from the center of mass at the origin O to the intersection of inbound and outbound asymptotes (dashed lines) with declinations δ_i and δ_o. The path's radial coordinate is given by r and polar angle by θ as measured from δ_a. The planet's axis of rotation with angular velocity ωR stands upright.

Obviously the derived formula (Eq. 6) is not only an explicit approximation by $R_\oplus/r \approx 1$, but also implicit in modeling the planet as a rigid homogenous sphere. Moreover, the derivation also neglects apparent forces that are imposed on the spacecraft, such as a drag due to atmospheric friction. However, our study does not aim at producing a formula to calculate Δv due to the atmospheric drag or planet's geoid, instead it targets by the derivation of $\Delta v/v$ to explain the phenomenological formula (Eq. 1) and to identify the anomalous gain in momentum to result from the spacecraft traversing through the energy density gradient of space imposed by the rotation of the planet. Undoubtedly, when more flyby data accumulates, the empirical formula (Eq. 1) will be verified or falsified, thereby giving also a verdict on this study.

5 Discussion

The mathematical correspondence between the empirical relationship (Eq. 1) and the derived formula (Eq. 6) is reassuring, but not alone an explanation for the anomalous gain in velocity. Namely, the obtained consistency in energetic terms is by itself not a tangible explanation, because energy as such does not exist but it is an attribute of its carrier. Thus, the profound question is: What is the carrier substance that embodies the universal density of space and local gravitational potentials that the spacecraft is subject to during its flyby? Of course, this query is not relevant when general relativity is used as a mathematical model for measurements. But when one is after the cause, i.e., the force responsible for the flyby anomaly, the physical form of space must be considered.

The carrier of gravitational force has been sought for long. Nonetheless the graviton of quantum field theory remains a hypothetical elementary particle. In the past the photon was considered as the carrier, because gravity and electromagnetism share similar functional forms [34, 36, 38] as well as because the squared speed of light in the vacuum relates to the absolute electromagnetic characteristics of free space via $c^2 = 1/\varepsilon_o\mu_o$. Also the free space gauge $\partial_t\phi + c^2\nabla\cdot\mathbf{A} = 0$ implies physical existence of scalar ϕ and vector $\mathbf{A}$ potentials, so that ϕ will decrease with time when quanta move down

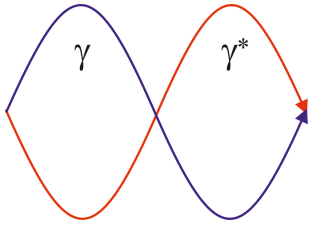

Fig. 2: The photon γ (blue) is the undividable quantum of action whose momentum resides on its wavelength, and equivalently, whose energy is within its period of time. The photon with opposite polarization (red) is the antiphoton γ^*. When γ and γ^* copropagate, the net electromagnetic force will vanish, but the compound boson continues to carry momentum and energy. These compound actions embody space universally and locally. Thus, the associated energy density appears as the universal gravitational potential energy, known as the vacuum density, which is in balance with all bodies. Likewise, a local potential energy is in balance with a local gravitating, orbiting and rotating body.

along the gradient of **A** or vice versa. Recently the old tenet of photon-embodied space has been revived so that the photons are considered to propagate in pairs of opposite polarization, and hence the pairs are without electromagnetic forces [28, 31, 39]. This destructive interference is, of course, familiar from diffraction. By the same token, Aharonov-Bohm experiment demonstrates how an applied vector potential will increase the energy density without introducing fields along the path [40]. According to this percept the two quanta of light do not vanish for nothing when interfering destructively, instead they continue in copropagation with opposite phases, and hence continue in carrying energy and momentum (Figure 2).

Our portrayal of the physical vacuum reminds of de Broglie's theory [41] about a spatially extended, particle centered pilot wave [42]. This view of the physical vacuum, as ours, makes sense of quantum mechanical phenomena without conceptual challenges [43]. In view of that, it has been understood also earlier that c, ε_o and μ_o are not constants, but properties when the vacuum has been considered to embody continuously appearing and disappearing fermion pairs [44, 45]. Instead of accounting for the vacuum's electromagnetic properties by transiently appearing paired charges we reason that when a charge appears in the vacuum, a corresponding force will appear. The force will move the paired photons away from the out-of-phase relation, and hence an electromagnetic field will appear around the charge. Thus, when an atom ionizes, the photons of the electromagnetic field will not appear out of the blue, but they have been around all the time, however in the out-of-phase configuration that manifests itself only as energy density.

The photon-embodied vacuum is understood to emerge from various processes, such as annihilation, where constituents of matter with opposite charge transform to mere radiation. For example, the annihilation of electron with positron will yield, in addition to the two readily observable photons of opposite polarization and directions of propagation, also pairs of co-propagating photons. Conversely, the photon-embodied vacuum is the source of quanta for pair production [37,39,46]. Likewise, electron capture where a proton turns to a neutron, pairs of co-propagating photons will emerge from annihilation of the constituents with opposite charges. When the space is understood to embody the oppositely paired photons, it is easy to envision that space around a body of high energy density houses a radially decreasing energy density, known as the local gravitational potential energy. In this way gravity can be understood as force, like any other force, to result from the energy density difference over a distance, i.e., from a gradient. Ensuing motions consume the free energy in least time. This evolution is expressed by the principle of least action in its original form (Eq. 2). Namely, all bodies move from one state to another along geodesics to diminish density gradients in the least time.

The least-time imperative means that the two bodies will move toward each other when the surrounding universal space is sparse enough to accept the paired quanta that are released from the dense gravitational potential of the bodies to the surrounding free space along the paths of least time. For example, an object falls straight down on the ground, i.e., along the least-time path, to consume the energy density difference between the local gravitational potential and the sparse surrounding vacuum. When the body is falling down, the oppositely paired photons are released from the local gravitational potential to the surrounding universal vacuum also along their paths of least time. Conversely, the two bodies will move away from each other when the surrounding potential is rich enough to grant paired quanta with energy to the local potential about the bodies.

In the same manner it is inescapable that it takes some form of free energy, ultimately carried by the photons that have been acquired from insolation, to lift up the fallen object from the ground back up on its initial height. So, the logic of reversibility says that the photons that were absorbed when the object was lifted up must have been emitted when the object was falling down. Thus, gravity is a dissipative phenomenon. When the bodies move toward each other, there is an efflux of quanta with energy to the surroundings, and conversely when the bodies move away from each other, there is an influx of quanta with energy from the surroundings. Manifestly, there is no net flux, i.e., no net dissipation from the system of bodies at a stationary state corresponding to an energetic balance with its surroundings.

This insight to gravity allows us to describe the spacecraft's flyby as an energy transfer process where quanta move from the local system of bodies to the surrounding space or vice versa. Flyby mission data show temporary maxima and minima in energy transfer that moderate toward the space-

craft's asymptotic courses [4]. We remind that oscillations are characteristics of least-time transitions from one state to another [47]. The oscillations are pronounced when the rate of energy transfer is rapid compared with the bound energy.

With this insight to gravity as a dissipative phenomenon, let us first consider the flight past a gravitating spherical body. The spacecraft treks along its inbound trajectory through an increasing energy density of space, i.e., the $1/r^2$-force field when the distance r closes toward the body. The increase in the spatial potential energy is balanced, according to Eqs. 2 and 3, by an increase in kinetic energy as well as by efflux of the oppositely paired quanta from the local gravitational potential comprising the body and the spacecraft to the universal gravitational potential due to all bodies in the Universe. The flux of quanta is often overlooked because the oppositely paired quanta without net electromagnetic field cannot be detected readily. However, the dissipation can be inferred recalling that the total gravitational potential energy of the body and the spacecraft at the periapsis is not exactly equal to the total potential energy when the spacecraft is at a point on the arm of hyperbola. The emission of quanta will cease, i.e., dissipation will vanish $d_t Q = 0$ momentarily, when the spacecraft arrives at the periapsis, where kinetic energy $2K$ matches the scalar potential energy U. Thereafter, along the outbound asymptote $2K$ will exceed U, and hence the paired quanta will be acquired from the surrounding vacuum to the local gravitational potential so that the balance with the surrounding density will be eventually regained far away from the planet. Since the passage from the inbound asymptotic state via the periapsis to the outbound asymptotic state is symmetric, the emission of quanta from the local system and the absorption to the local system match perfectly, and hence the net dissipation vanishes. Thus, the momentum of the two-body system is conserved.

Next, let us consider the flight past by an orbiting body. Along the inbound trajectory the spacecraft travels through the energy density of space that increases more rapidly than in the case of the merely gravitating body, namely at the rate that the planet orbits straight at the spacecraft. This more rapid increase in the potential energy is balanced, just as reasoned above, by a more rapid increase in kinetic energy concurrently with dissipation of the oppositely paired quanta to the surrounding space. First when at the periapsis, where the spacecraft moves orthogonal to the planetary orbit, dissipation vanishes momentarily. Thereafter, along the outbound asymptote $2K$ will exceed U, and hence quanta will be acquired from the surrounding vacuum to the local gravitational potential energy comprising the body and the spacecraft to regain the balance eventually when far away. Clearly the flyby about the approaching planet and the flyby about the departing planet differ from each by the rates of momentum and energy transfer from the system to the surrounding space. Thus, the spacecraft will pick up momentum in the former case and it will lose momentum in the latter case. The formula for the spacecraft's change in velocity can be derived in the same manner as Eq. 6 was derived. Consistently, also the (very slightly) perturbed planet will regain a stable orbit by processes where the paired quanta carry energy from the surroundings to the local potential and vice versa until the free energy minimum state has been attained.

Finally, let us consider the flight past a rotating planet that imposes an axially symmetric energy density gradient on the surrounding space. When the gradient along the inbound trajectory is equal in magnitude to the gradient along the outbound trajectory but of opposite sign, the emission and absorption of quanta from the system comprising the body and the spacecraft to the surrounding vacuum are equal. Thus, in that case the momentum is conserved, and hence no anomalous gain or loss in velocity will detected. Conversely, when the emission of quanta along the inbound trajectory and the absorption of quanta along the outbound trajectory do not cancel each other exactly, the spacecraft will either pick up or lose momentum depending on the sign of net dissipation. Likewise the concurrent (minute) perturbation of the planet's rotational momentum will damp down toward a stable state of spinning by energy transfer processes from the systemic potential to the surroundings and vice versa until the net dissipation finally vanishes at the free energy minimum state. Perhaps our account on gravity summons up the old abandoned idea of luminiferous ether [48]. Therefore, it is worth emphasizing that the proposed physical vacuum is not a medium that supports propagation of light, instead the photons constitute space. The paired photons without net polarization do not couple in electromagnetic terms, and hence the space is dark, but not illusive or only a mathematical metric. It reacts to every act. Any change in momentum is met with resistance, known as inertia, since the spatial energy density redistributes to regain balance among perturbed bodies [31].

6 Conclusions

We conclude that the flyby anomaly only appears as an odd phenomenon when not all components of force are included in its explanation. Specifically, we maintain that the law of conservation of momentum holds when the system of bodies associated with local potentials of space will in total neither lose nor gain quanta from the surrounding systems. The ultimate surroundings for any local system is the universal free space. It must be taken into account in the explanation of flyby anomaly.

We resort to the old idea that the vacuum is embodied by the quanta of light which pair in opposite polarization. Hence space is dark but it holds an energy density [32] on the order of one nJ/m^3. The non-zero energy density displays itself also in the Aharanov-Bohm experiment [40] and as the Casimir effect [49]. So in any closed system the conservation of momentum is a solid law. In fact, the law may seem universal, since the Universe as a whole may by definition seem like

a closed system. However, the quanta of light, that embody the space both in pairs of opposite polarization and solo, are open actions (Figure 2), whose momentum $\mathbf{p}$ may decrease concomitantly with increasing wavelength λ or vice versa so that the measure, known as Planck's constant, $h = \mathbf{p} \cdot \lambda$ remains invariant. Equivalently stated, a decrease in energy E is counterbalanced by an increase in time t, so that $h = Et$ is constant. Indeed, astronomical observations imply that the total energy density of the Universe is decreasing with increasing time. The photon that emerged from the nascent energy-dense Universe has shifted down in frequency $f = 1/t$ when adapting to ever more sparse surrounding densities on its way to us and eventually terminating at absorption to our detector. Conversely, when insisting on that energy is conserved, i.e., by applying a theory that conserves a symmetry, the ensuing interpretation of supernovae data will require an ad hoc patching, for instance, by dark energy [26].

Rules and regularities that are so apparent across scales of nature, are rightfully related to conservation laws. However, to avoid assigning phenomena as anomalous, it is necessary to include everything in an explanation. To this end among the laws of nature the truly superior and solid one is the conservation of the total number of quantized actions in the whole Universe.

Acknowledgements

I thank Dr. Pekka Teerikorpi for valuable comments.

Submitted on January 9, 2017 / Accepted on January 15, 2017

References

1. Flandro G.A. Fast Reconnaissance Missions to the Outer Solar System Utilizing Energy Derived from the Gravitational Field of Jupiter. *Astronautica Acta*, 1966, v. 12 329–337.
2. Wiesel W.E. Space flight Dynamics. McGraw-Hill, New York, NY, 1989.
3. Nieto M.M., Anderson J.D. Earth flyby anomalies. *Physics Today* 2009, v. 62 76–77.
4. Anderson J.D., Campbell J.K., Nieto M.M. The energy transfer process in planetary flybys. *New Astronomy*, 2007, v. 12 383–397.
5. Anderson J.D. et al. Anomalous Orbital-Energy Changes Observed during Spacecraft Flybys of Earth. *Physical Review Letters*, 2008, v. 100 091102.
6. Antreasian P.G., Guinn J.R. AIAA Paper No. 98-4287 presented at the AIAA/AAS Astrodynamics Specialist Conference and Exhibit, Boston, August 10-12, 1998. http://www2.aiaa.org/citations/mp-search.cfm.
7. Edwards C., Anderson J., Beyer P., Bhaskaran S., Nicholson F., Ottenhoff T., Stevens S. Tracking Gali-leo at Earth-2 perigee using the tracking and data relay satellite system. *Adv. Astron. Sci.*, 1994, v. 85 1609–1621.
8. Guman M.D., Roth D.C., Ionasescu R., Goodson T.D., Taylor A.H., Jones J.B. Cassini Orbit Determina-tion from First Venus Flyby to Earth Flyby. *Advances in Astronautical Sciences*, 2000, v. 105 1053–1072.
9. Morley T., Budnik F. Rosetta Navigation at its First Earth-Swingby. *Proceedings of the International Symposium on Space Technology and Science*, 2006, v. 25 59.
10. Williams B., Taylor A., Carranza E., Miller J., Stanbridge D., Page B., Cotter D., Efron L., Farquhar R., McAdams J., Dunham D. Early navigation results for NASA's Messenger mission to Mercury. *Advances in the Astronautical Sciences*, 2005, v. 120 1233–1250.
11. Iorio L. The Effect of General Relativity on Hyper-bolic Orbits and Its Application to the Flyby Anomaly. *Scholarly Research Exchange*, 2009, 807695, arXiv:0811.3924.
12. Acedo L. The flyby anomaly: A case for strong gravitomagnetism? *Advances in Space Research*, 2014, v. 54 788–796.
13. Cahill R.T. Resolving Spacecraft Earth-Flyby Anom-alies with Measured Light Speed Anisotropy. *Progress in Physics*, 2008, v. 3 9–15.
14. Adler S.L. Can the flyby anomaly be attributed to Earth-bound dark matter? *Physical Review D*, 2009, v. 79 023505.
15. Mbelek J.P. Special relativity may account for the spacecraft flyby anomalies. 2009, arXiv:0809.1888v3.
16. Hafele J.C. Causal Version of Newtonian Theory by Time–Retardation of the Gravitational Field Explains the Flyby Anomalies. *Progress in Physics*, 2013, v. 2 3–8.
17. Tajmar M., Assis A.K.T. Influence of Rotation on the Weight of Gyroscopes as an Explanation for Flyby Anomalies. *Journal of Advances in Physics*, 2016, v. 5 176–179.
18. McCulloch M.E. Modelling the flyby anomalies using a modification of inertia. *Monthly Notices of the Royal Astronomical Society*, 2008, v. 389 L57–L60.
19. Pinheiro M.J. Effect of TTC on Satellite Orbital Mechanics. *Physical Letters A*, 2014, v. 378 3007–3011.
20. Iorio L. A flyby anomaly for Juno? Not from stand-ard physics. *Advances in Space Research*, 2014, v. 54 2441–2445. arXiv:1311.4218.
21. Acedo L. The Flyby Anomaly in an Extended White-head's Theory. *Galaxies*, 2015, v. 3 113–128.
22. Pinheiro M.J. Some effects of topological torsion currents on spacecraft dynamics and the flyby anomaly. *Monthly Notices of the Royal Astronomical Society*, 2016, v. 461 3948–3953.
23. De Maupertuis P.-L.M. Les loix du mouvement et du repos déduites d'un principe metaphysique. *Histoire de l'Académie Royale des Sciences et des Belles-Lettres de Berlin*, 1746, 267–294.
24. Sharma V., Annila A. Natural process – Natural selection. *Biophysical Chemistry*, 2007, v. 127 123–128.
25. Tuisku P., Pernu T.K., Annila A. In the light of time. *Proceedings of Royal Society of London A*, 2009, v. 465 1173–1198.
26. Koskela M., Annila A. Least-time perihelion precession. *Monthly Notices of the Royal Astronomical Society*, 2011, v. 417 1742–1746.
27. Annila A. Rotation of galaxies within gravity of the Universe. *Entropy*, 2016, v. 18 191–205.
28. Annila A. Probing Mach's principle. *Monthly Notices of the Royal Astronomical Society*, 2012, v. 423 1973–1977.
29. Annila A. Least-time paths of light. *Monthly Notices of the Royal Astronomical Society*, 2011, v. 416 2944–2948.
30. Annila A. Cosmic rays reports from the structure of space. *Advances in Astronomy*, 2015, 135025.
31. Grahn P., Annila A., Kolehmainen E. On the exhaust of EM-drive. *AIP Advances*, 2016, v. 6 065205.
32. Feynman R.P., Morinigo F.B., Wagner W.G., Hatfield B. Feynman Lectures on Gravitation. Addison-Wesley, Reading, MA, 1995.
33. Bourbaki N. Topological vector spaces. Springer, Berlin, 1987. ISBN 3-540-13627-4.
34. Sciama D.W. On the origin of inertia. *Monthly Notices of the Royal Astronomical Society*, 1953, v. 113 34–42.
35. Evans J., Kamal K.N., Anwarul I. The Optical-Mechanical Analogy in General Relativity: Exact Newtonian Forms for the Equations of Motion of Particles and Photons. *General Relativity and Gravitation*, 1996, v. 28 413–439.

36. Heaviside O. A gravitational and electromagnetic analogy, Part I. *The Electrician*, 1893, v. 31 281–282.
37. Annila A. Natural thermodynamics. *Physica A*, 2016, v. 444 843–852.
38. Newton I. Opticks (1704) Excerpts of Queries 29 and 30 of Book III. Dover, New York, NY, 1979.
39. Annila A. The meaning of mass. *International Journal of Theoretical and Mathematical Physics*, 2012, v. 2 67–78.
40. Aharonov Y., Bohm D. Significance of electromag-netic potentials in quantum theory. *Physical Review*, 1959, v. 115 485–491.
41. De Broglie L. La mécanique ondulatoire et la structure atomique de la matière et du rayonnement. *Journal de Physique et Le Radium*, 1927, v. 8 225–241.
42. Bush J.W.M. The new wave of pilot-wave theory. *Physics Today*, 2015, v. 68 47–53.
43. Boyer T.H. Any classical description of nature requires classical electromagnetic zero-point radiation. *American Journal of Physics*, 2011, v. 79 1163–1167.
44. Urban M., Couchot F., Sarazin X., Djannati-Atai A. The quantum vacuum as the origin of the speed of light. *The European Physical Journal*, 2013, v. 31 281–282.
45. Leuchs G., Villar A.S., Sánchez-Soto L.L. The quantum vacuum at the foundations of classical electrodynamics. *Applied Physics B*, 2010, v. 100 9–13.
46. Annila A. All in action. *Entropy*, 2010, v. 12 2333–2358.
47. Mäkelä T., Annila A. Natural patterns of energy dis-persal. *Physics of Life Reviews*, 2010, v. 7 477–498.
48. Michelson A.A., Morley E.W. On the Relative Mo-tion of the Earth and the Luminiferous Ether. *American Journal of Science*, 1887, v. 34 333–345.
49. Casimir H.B.G., Polder D. The influence of retarda-tion on the London-van der Waals forces. *Physical Review*, 1948, v. 73 360–372.

The Proton Radius Anomaly from the Sheltering of Unruh Radiation

Michael Edward McCulloch

Plymouth University, Drake Circus, Plymouth, PL4 8AA, UK. E-mail: mike.mcculloch@plymouth.ac.uk

It has been found that in muonic hydrogen either the proton radius is 4% smaller than usual (a 7σ anomaly) or an unexplained extra binding energy of 320 μeV is present. Here it is shown that 55% of this extra energy can be explained if Unruh radiation seen by the orbiting muon can push on it, and is being asymmetrically blocked by the proton.

1 Introduction

The proton radius has been measured for many years to be 0.88 fm, with experiments using electron-proton scattering and by using atomic spectoscopy to look at the Lamb shift seen by an orbiting electron, a shift which depends on the proton radius [1].

More recently, it was realised that a more accurate proton radius could be obtained by replacing the electron in the atom with its heavier twin: the muon, but when this was done, the, more accurate, proton radius was found to be 0.84 fm, 4% smaller and a difference seven times larger than the uncertainty in the original measurement [2]. This was confirmed in 2013 [3] and has also been confirmed using a muon orbiting a deuterium nucleus [4].

The standard model has no mechanism that allows the proton to change size in the proximity of a muon as opposed to an electron, so this is a crucial finding. Another possibility however, is that the proton size is not changing but that a new binding energy equal to 320 μeV is appearing [1]. It is the contention of this paper that this extra binding energy comes from sheltering by the hypothesised Unruh radiation.

[5] suggested that black hole event horizons can separate pairs of particles in the zero point field, swallowing one and allowing the other to escape as a real particle, thus allowing black holes to radiate. [6], [7] and [8] then suggested that the same thing may occur when objects accelerate since then a horizon appears, and may similarly seperate paired virtual particles making half of them real. This is now called Unruh radiation.

[9] and [10] suggested that inertia is caused by Unruh radiation: the acceleration of an object causes a Rindler horizon to form on the side opposite to the acceleration vector and this damps Unruh radiation on that side of the object, causing a net imblance in Unruh radiation pressure that pushes it back against the original acceleration. This new process predicts inertial mass [10] and [11] and also predicts deviations from the standard inertial mass that explains the galaxy rotation problem without the need for dark matter [12] and also cosmic acceleration [13]. The crucial point here is that Unruh radiation is taken to exist and to be able to push on particles.

In this paper it is argued that the usually isotropic Unruh radiation seen by the orbiting muon is blocked by the central proton, which subtends a much larger solid angle at the close-orbiting muon than at the distantly-orbiting electron. It is shown that this sheltering effect on Unruh radiation can account for about half of the proton radius anomaly in muonic hydrogen.

2 Method and Results

Let us imagine a muon orbiting around a proton as shown in Figure 1.

In quantum mechanics of course it is not possible to specify an exact orbital speed for the muon, but one can estimate the probable speed: $v \sim \alpha c$ where α is the fine structure constant and c is the speed of light. The acceleration of the muon as it orbits at a radius R is then

$$a = \frac{v^2}{R} = \frac{(\alpha c)^2}{R} \tag{1}$$

where $\alpha \sim 1/137$. The wavelength of Unruh radiation seen by the muon while orbiting can be found using Wien's law for the wavelength emitted by a body of temperature T, $\lambda = \beta hc/kT$ where $\beta = 0.2$, h is Planck's constant, c is the speed

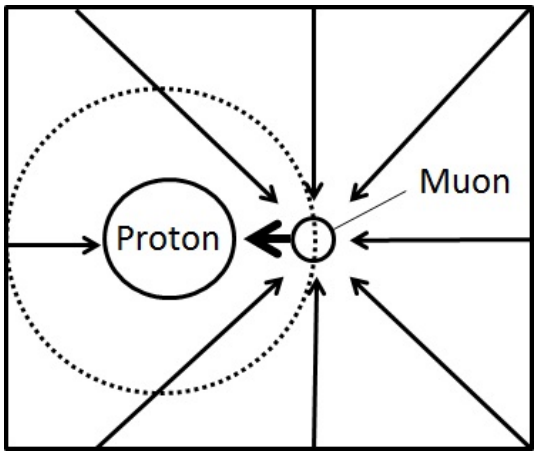

Fig. 1: Schematic showing a muon (the small right hand circle) orbiting close to a proton (the large left hand circle). The muon is pushed by the Unruh radiation associated with its acceleration (the arrows) from all directions except from the direction of the blocking proton (the truncated arrow). So there is a new net force pushing the muon towards the proton. The size of this force produces 55% of the proton radius anomaly.

of light and k is Boltzmann's constant, and combining it with the temperature of Unruh radiation seen at an acceleration a: $T = \hbar a/2\pi ck$, so that

$$\lambda_U \sim \frac{8c^2}{a}. \quad (2)$$

The de Broglie energy associated with this wavelength is

$$E = \frac{hc}{\lambda_U}. \quad (3)$$

Using (2) we get

$$E \sim \frac{ha}{8c} \quad (4)$$

and using (1) we get

$$E \sim \frac{h\alpha^2 c}{8R}. \quad (5)$$

This is the energy in the Unruh radiation field at the muon, which usually strikes the muon isotropically so does not push it in any net direction. However, we shall assume that the proton, as seen from the muon, blocks all the Unruh radiation coming from that direction (Fig. 1). The amount will be proportional to the solid angle of the proton as seen by the muon, which is $\pi r_P^2/2\pi R^2 = 5.7\times10^{-6}$, where r_P is the proton radius and R is the muon-proton distance. Note that we are only looking at one side of the muon, to work out the energy asymmetry that pushes on the muon, so it is the half-sphere we consider.

As energy is being blocked on the side of the muon closer to the proton, this represents a new source of energy pushing the muon towards the proton, and adding to its boundedness. The specific amount of energy is

$$E \sim \frac{h\alpha^2 c}{8R} \times \frac{\pi r_P^2}{2\pi R^2} = 2.8 \times 10^{-23}\text{J}. \quad (6)$$

The extra binding energy required to account for the observed proton radius anomaly is 320μeV or 5.1×10^{-23} J. Therefore a sheltering of Unruh radiation by the proton predicts roughly 55% or 180 μeV of the energy needed to explain the observed proton radius anomaly for muonic hydrogen.

This extra Unruh binding energy is far smaller in the case of the electron. Electrons orbit the proton about 200 times further out than the muon and so the solid angle of the proton at the electron is much smaller. The energy released in the electron case would be

$$E \sim \frac{h\alpha^2 c}{8R} \times \frac{\pi r_P^2}{2\pi R^2} = 7.1 \times 10^{-28}\text{J} \quad (7)$$

or about 5 orders of magnitude smaller than for the muon. So there is no anomaly for normal hydrogen. When the electron is replaced by a muon there is a difference of roughly 180 μeV, or 55% of the observed anomaly.

3 Conclusion

It has been observed that the radius of the proton, as determined by the Lamb shift, is apparently 4% less when measured using an orbiting muon instead of an electron. This can be interpreted as an anomalous increase in the proton-muon binding energy of 320 μeV.

Assuming that Unruh radiation is able to push on particles, and that the proton can block it, predicts an extra proton-muon binding energy of 180 μeV, about 55% of the observed anomaly.

Submitted on January 5, 2017 / Accepted on January 19, 2017

References

1. Carlson C.E. The proton radius puzzle. 2015, arxiv: 1502.05314.
2. Pohl R., et al. *Nature*, 2010, v. 466, 213.
3. Antognini A. et al. *Science*, 2013, v. 339, 417.
4. Pohl R., et al. Laser spectroscopy of muonic deuterium. *Science*, 2016, v. 353, 6300.
5. Hawking S.W. Particle creation by black holes. *Commun. Math. Phys.*, 1975, v. 43, 199.
6. Fulling S.A. *Phys. Rev. D.*, 1973, v. 7(10), 2850.
7. Davies P.C.W. Scalar production in Schwarzschild and Rindler metrics. *J. Physics*, 1975, v. 8(4), 609.
8. Unruh W.G. Notes on black hole explosions. *Phys. Rev. D.*, 1976, v. 14, 870.
9. McCulloch M.E. Modelling the Pioneer anomaly as modified inertia. *MNRAS*, 2007, v. 376, 338–342.
10. McCulloch M.E. Inertia from an asymmetric Casimir effect. *EPL*, 2013, v. 101, 59001.
11. Gine J., McCulloch M.E. Inertial mass from Unruh temperatures. *MPL-A*, 2016, v. 31(17), 1650107.
12. McCulloch M.E. Testing quantised inertia on galactic scales. *ApSS*, 2012, v. 342(2), 575–578.
13. McCulloch M.E. Minimum accelerations from quantised inertia. *EPL*, 2010, v. 90, 29001.

Energy is the Expansion

Jacques Consiglio

52 Chemin de Labarthe, 31600 Labastidette, France
E-mail: Jacques.Consiglio@gmail.com

Here, using Mach's principle we symmetrize the Schwarzschild solution. It enables to compute the universe densities of baryonic matter, dark matter, and dark energy as distinct effects of the same unique source and the time invariance of the theory naturally gives an inflation period (or its illusion). The theory does not change GR equations but its classical limit is a MOND theory which parameter is predicted. Hence we claim the discovery of a natural law.

1 Introduction

In relativity and cosmology, the mystery of the time is the nature of dark matter and dark energy. Dark matter is inferred from the anomalous galaxies rotation curves and dark energy from the universe accelerated expansion. The debate is long open between dark matter particles and modified gravity; the nature of the dark energy field is unknown. On the other hand of physical theories, quantum gravity which cannot be renormalized and gives absurd predictions.

The purpose of this paper is to provide with a natural solution to the first issue without modifying GR, firstly by computing the amount of matter, dark matter and dark energy from elementary symmetry considerations; thus uncovering a fundamental law of nature. It addresses in the most general manner the long expected rule of energy and metric formation — namely space-time and everything therein. We also show that the classical approximation is a MOND-type theory and compute its parameter. Concerning quantum gravity, it shows why a different approach is needed.

Note that all masses, densities and accelerations in this paper are computed using as input the universe age T given by the Planck mission and two natural constants G, and c. The other ΛCDM parameters output of this mission are only used for comparison.

2 Theory

Theoretical physics works by the study of symmetry; for any variation, compensation exists. The universe expands, therefore compensation exists and then symmetry. Take the Einstein field equation:

$$R_{\mu\nu} - \frac{1}{2}\, R\, g_{\mu\nu} = \frac{8\pi G}{c^4}\, T_{\mu\nu} - \Lambda\, g_{\mu\nu}\,, \tag{1}$$

where the term Λ is experimentally justified and is a constant scalar; meaning its density is constant in space. It leads to results which are unique in physics: two kinds of energies do not transform in each other and, as we know from phenomenology, it eventually requires a third kind with the same property, namely dark matter. This is the problem we shall discuss.

On the other hand the ΛCDM model is well verified and it gives no reason to doubt the Friedman-Lemaitre-Robertson-Walker (FRLW) cosmology. Therefore we shall neither modify gravity nor implement ad-hoc fields, but instead discuss energy formation; masses, the scalar Λ, and their relation with G. For this we shall take the problem by the other end and use the standard short distance case with central mass M. The Schwarzschild spherical solution reads:

$$c^2\, d\tau^2 = \left(1 - \frac{R_s}{r}\right) c^2 dt^2 - \left(1 - \frac{R_s}{r}\right)^{-1} dr^2 - r^2\,(d\theta^2 + sin^2\theta\, d\phi^2)\,. \tag{2}$$

This "local" solution does not admit a scalar Λ; it is not appropriate but we shall make direct use of this defect. If we properly instantiate Mach's principle therein we should get a nice correction, because by definition it should includes all effects. The symmetry in (2) is unbalanced since two of the quantities are not geometrical, namely G and M. Then in an attempt to symmetrize the Schwarzschild solution we write:

$$\frac{R_s}{r} = \frac{R_U\, M}{M_S\, r} \rightarrow \frac{2G}{c^2} = \frac{R_U}{M_S}\,, \tag{3}$$

where M_S and R_U represent respectively the scalar field energy and the distance to the event horizon ($R_U = c\,T$). Note that this equation instantiates Mach's principle in the most trivial manner. Now compute:

$$M_S = \frac{R_U\, c^2}{2\, G} = 8.790 \times 10^{52}\,\text{kg}. \tag{4}$$

It looks to the observer like an energy contained in a 3-sphere, but it is actually a conic 4-dimensional structure intersecting the present, the surface of the 4-sphere. Then consider the constancy of Λ: with respect to the 4-sphere volume, and in order to reduce to its surface, we divide M_S by the 4-sphere surface coefficient, namely $2\,\pi^2$; we get:

$$M_V = \frac{M_S}{2\,\pi^2} = 4.453 \times 10^{51}\,\text{kg}, \tag{5}$$

which corresponds to 4.82% of the total mass and density:

$$M_{total} = M_S + M_V = 9.236 \times 10^{52}\,\text{kg}, \tag{6}$$

$$D_{total} = \frac{3\,(M_S + M_V)}{4\,\pi\, R_U^3} = 9.91 \times 10^{-27}\,\text{kg/m}^3. \tag{7}$$

All numerical results above are in great agreement with the Planck mission outputs [1] even though we get a single dark field M_S summing dark energy and dark matter.

The Planck mission also gave $H_0 = 67.74\,(46)$ km/s/Mpc and we use $H = 1/T = 71.10$ km/s/Mpc to compute the distance to the event horizon. Then compare:

$$\frac{M_S + M_V}{M_S} = 1 + \frac{1}{2\pi^2} = 1.0507\,, \tag{8}$$

with:

$$\frac{1}{H_0\,T} = 1.0496\,. \tag{9}$$

This utterly stunning not only for the right orders of magnitude, but for getting also the first two or three decimals right and multiple coincidences — seemingly coherent — which, in principle, address independent quantities. Considering also that from (3) M_S is the critical density, it suggests that the mass terms are linked to G by geometry in a manner that is consistent with GR; possibly a fundamental law of nature ruling the universe formation. Now the equation (4) also reads:

$$2M_S\,c^2 = P_p\,T = \frac{P_p\,R_U}{c}, \tag{10}$$

where $P_p = c^5/G$ is the Planck power. It looks as though a 4-sphere at the surface of which observable energy lies is either inflated or heated by a constant feed; in other words, it replaces the big bang singularity by a constant power and the correlation is such that we must conjecture the following identification: *energy is the expansion*; meaning that M_S and M_V increase linearly in time. Expansion is observed, and then we shall discuss the conjecture as a new theory which is embodied by the equation (3) and the following premises:

P1: The scalar Λ is a constant of nature.

P2: The matter field (all particles) is the surface of a 4-sphere.

P3: A feed mechanism exists inflating the sphere and expanding its inner metric; both effects are simultaneous.

P4: The inner metric expansion is the product of inflation of the sphere radius by the reduction of particles wavelengths; both effects have identical coefficients.

Essentially, we states that M_S is the critical density, that the matter field M_V has no effect on the course of the universe expansion, and that the source terms of the Einstein field equation (1) are not identified for what they are. In the following sections we analyze what the new theory predicts.

3 Predictions

3.1 Inflation

Considering P3 and P4 the wavelength of massive particles reduce in time while the 4-sphere expands, the product of this reduction by this expansion gives a linear increase of the universe radius.

But this is considering constant energy; since the wavelengths reduce the relative rate of time is not constant between distinct epochs and reaches zero at the origin. Therefore the theory requires an inflation period; the global curve is a straight line if expressed in "constant" time T, but a logarithmic law if expressed in proper time.

3.2 The dark matter effect

Let us study the effects at different heights in the gravitational pit of a central mass M (the basic test case) and assume the system far away from other gravitational sources. With respect to (2), M_S is variable in time but constant in space ($M_S \sim T$). At the opposite since gravitation is a retarded interaction, the metric in r is retarded and the equation (3) must be modified accordingly. Hence, using P3-P4, since r and M (or R_s) expand, we write:

$$\frac{R_s}{r} \to \frac{R_s}{r} \times \sqrt{\frac{1 - Hr/c}{1 + Hr/c}}\,, \tag{11}$$

which second order limited development yields:

$$\frac{2\,G\,M}{r\,c^2} \to \frac{2\,G\,M}{r\,c^2} - \frac{M}{M_S} + \frac{M\,r}{M_S\,R_U}. \tag{12}$$

Now examine this expression:

- The first term is nominal.
- The middle term cannot be seen negligible since it addresses identically all masses of the universe. Hence it must be identified to the contribution of M_S to the mass M, and then integrated to M_S, giving -1 *which is the flat metric*. Finding the flat metric here may look stunning but it is coherent with its production.
- Therefore the right hand term must also be integrated to M_S giving $H\,r\,c$ of unit squared velocity, and a cosmological term $H\,c$ with unit of acceleration; it comes from the expansion but its effect in the gravitational field is not trivial.

Still, we know that this value is in the range of the anomalous acceleration at galaxies borders. Then let us discuss angular momentum.

Quantum gravity is usually expected to work from the same principles as any other field. But this assumption holds a fundamental contradiction with the spirit of GR and even more with the theory we discuss, because here gravitation defines *entirely* the context in which the rest of physics lives. In this way, the position of M_S at the denominator of (3) is quite evident since like GR it scales the matter field — but globally. Still, the theory is compatible with the SM fields. The bottom line is scale-independence and all SM couplings constants are unitless including mass ratios.

Now on angular momentum, consider simply the Bohr radius for the simplest but most general case:

$$a_0 = \frac{\hbar}{m_e\,c\,\alpha} = \frac{1}{2\,\pi} \times \frac{\lambda_e}{\alpha}\,. \tag{13}$$

We know that the fine structure constant α did not change during many billion years; then with a linear increase of m_e, the electron wavelength and the Bohr radius decrease together and coherently; but when considering only lengths like in (13) the orbit radius scaling factor is $1/2\,\pi$.

Expressing this simply, when the electron mass increases in time, the Bohr radius and the first Bohr orbit reduce like:

$$\frac{da_0}{dt} = \frac{d\lambda_e}{\alpha\, dt} \times \frac{1}{2\pi} \to \frac{\alpha\, da_0}{d\lambda_e} = \frac{1}{2\pi}\,. \tag{14}$$

But this contraction is universal. It addresses all phenomena ruled by quantum physics (rulers, clocks, etc...); *it is not measurable where only quantum physics rules*.

But there is a neat difference with gravitation: with quantum fields, angular momentum quantizes distances as the inverse of mass, but gravity cannot since its classical force is a product of masses. With the product of two masses increasing simultaneously, we get a square and only half the effect is non-measurable. *Hence in the gravitational field a residual term $H\,c/2\pi$ gives measurable effects*.

3.3 Dark matter and dark energy

In the spirit of the coincidence in (4), GR (or the ΛCDM model) splits the scalar energy M_S into a massive dark matter field and the scalar field Λ, and we have a compression factor which derivative is $H\,c$ applied on any piece of the matter field M_V. But for *any* scalar field X having this double effect, and for any R and $H_R = c/R$, its compression energy M_{Co} (dark matter) at any place is given by:

$$\frac{M_{Co}}{M_X} = \frac{1}{2}\int_0^R \frac{4\pi\rho_X\, r^2}{M_X\, c^2}\,(H_R\, c\, r)\, dr = \frac{3}{8} = 0.375\,, \tag{15}$$

where in the integral energy is given by acceleration, then kinetic energy $p^2/2m$; thus the factor $1/2$. The kinetic impact of X has effect of pressure and its energy is calculable. Obviously, the Planck mission gave the same result:

$$\frac{\Omega_C}{\Omega_{DE}} = \frac{0.2589}{0.6911} = 0.3746. \tag{16}$$

From this equation the sum $\Omega_C + \Omega_{DE} = \Omega_S$ is not a split but a unique field giving distinct effects ruled by geometry, a consequence of which is M_S:

$$\Omega_S = 2\pi^2\,\Omega_V = \frac{11}{8}\,\Omega_{DE} = \frac{11}{3}\,\Omega_C\,. \tag{17}$$

This is not unification of distinct fields, this is unity. In GR:

- Ω_{DE} provides with negative pressure, a repelling force;
- Ω_C is seen as mass but here it must be seen as counterpart, an isotropic stress *and* a positive pressure applied to massive particles by the same repelling force; in the equation (1), stress is part of the stress-energy tensor.
- Ω_V the matter density is the proportion of their sum at the 4-sphere surface.

Here there is no contradiction with (1) nor with the FLRW universe; but the concept appears to imply that dark matter is pressure and that mass is compression work.

3.4 The Hubble paramater

Let a photon be emitted in A at date t_1 with observable energy m, the transit time to the receptor in B is t, and then $t_1 + t = T$. It has no mass, but it takes away a part of the emitter mass m, and then the full energy it transfers includes its share of M_S and corresponds to $m\,(2\pi^2 + 1)$.

During the transfer, its wavelength increases of a factor $\sqrt{(t_1 + t)/t_1}$. Hence:

$$m_{\text{transfer}} = \frac{(2\pi^2 + 1)\,\sqrt{t_1}}{\sqrt{t_1 + t}}\, m\,.$$

But during the time t, the mass of the receptor evolved by a factor $\sqrt{t_1} \to \sqrt{t_1 + t}$. Therefore the energy transferred by the photon to the receptor, before it reconstitutes mass in B evolves like:

$$\frac{m_{\text{transfer}}}{m_{\text{receptor}}} \sim (2\pi^2 + 1)\,\frac{t_1}{t_1 + t}\,.$$

Once the photon is absorbed, it gives:

$$\frac{m_{\text{absorbed}}}{m_{\text{receptor}}} \sim 1 - Ht\,, \tag{18}$$

which is standard red-shift for a universe of age T expanding at constant rate c for which $H\,T = 1$. It fits with observation of type 1A supernova with accelerated expansion due to the scalar field Λ. On the other hand, consider a field of photons created at the origin (not emitted by mass); the term $(2\pi^2 + 1)$ is not present at emission, meaning in facts that the field M_S has decayed of a factor $(1 + 1/2\pi^2)^{-1}$ with mass creation; hence the equation (9). So the theory predicts a discrepancy between measurements of the Hubble parameter from the CMB and type 1A supernovas:

$$H^0_{1A} = \frac{1}{T} = H^0_{CMB}\left(1 + \frac{1}{2\pi^2}\right). \tag{19}$$

This equation is in range of the discrepancy given by the Hubble space telescope measurements in [5], which is currently valid at $\sim 3\sigma$, as compared to the Planck mission. Older data is also compatible with the prediction.

3.5 The classical limit

The limited development in (12) also applies in the classical theory provided a retarded field. (Even though we would obtain $M_S \to 2\,M_S$ with a classical equation in place of (3) and the same reasoning.) According to (14), the cosmological term to apply is is:

$$S_{HC} = \frac{H\,c}{2\,\pi} = 1.10 \times 10^{-10}\text{m/s}^2, \tag{20}$$

where Milgrom's limit is $a_0 = 1.20\,(\pm 0.2) \times 10^{-10}\text{m/s}^2$; so we shall compare with MOND.

But here S_{HC} is a derivative that scales the gravitational field and it cannot be independent of the "normal" acceleration. In a classical manner we need to discuss forces with the following substitution:

$$\frac{G\,m\,M}{r^2} \to \frac{G\,m\,M}{r^2} + m\,S_{HC}\,,$$

which, on circular orbit, corresponds to the Newton acceleration at a distance R such that:

$$\frac{G\,M}{R^2} = \frac{G\,M}{r^2} + S_{HC}\,.$$

Then multiplying this expression by $R^2\,r^2$, using $A = G\,M/r^2$ we get:

$$R^2 = r^2\Big(1 + \frac{S_{HC}}{A}\Big)^{-1}\,.$$

Now this result is the exact opposite of MOND interpolation. This is perfect since we work in forces while MOND modifies the dynamics, namely the effective acceleration a but preserves the Newton force. Then reversing the correction, that is conserving the Newton force in r, using MOND concept that is an anomalous acceleration a and notations with $a_0 = S_{HC}$, we get:

$$\mathbf{F} = m\,\mathbf{a}\Big(1 + \frac{a_0}{a}\Big)^{-1}\,, \tag{21}$$

which is the so called "simple" MOND interpolation function. Hence the classical approximation is MOND [4], which is important considering the wide range of effects it predicts that agree with observation.

It shows, rather stunningly, that MOND and GR as it is are not incompatible, but that the former comes naturally as the classical approximation of the latter if we replace the big bang energy emission by a constant feed. Here again there is no need to choose between modified gravity and dark matter particles; we find that both are irrelevant.

3.6 Other consequences

Firstly the theory does not need dark matter particles nor does it accept any. Considering the "energy feed" a good candidate is a continuous scalar field propagating at light speed — and quantum physics live therein; importantly, the existence of such a field is opposite to the very notion of isolated particle. Secondly, all fields known to particles physics take energy at the same source and they do so permanently; unity is there but theories are not unified. Hence, even though it requires an intuitive leap, the consequence is that all parameters of the SM of particle physics reduce to geometry; a geometry which is scale-independent and fits locally and globally with the new theory. Those parameters need to be natural.

4 Conclusions

It is well known that Einstein was influenced by Mach's principle when designing general relativity. In this article, the principle is expressed in the most trivial manner and leads to an extended theory enabling to compute the densities of the matter, dark matter, and dark energy fields of the ΛCDM model. Its classical approximation is MOND which parameter and equation are predicted; it shows that the ΛCDM and MOND are discussing the same physics. This is an enlightening surprise for it shows the irrelevance of discussing modified gravity and dark matter particles. The theory is also instructive as to the structure of space-time and imposes constraints to its evolution, but also to its nature and origin. It refutes the existence of a big bang as a huge and final energy emission — the very first issue in cosmology; instead it provides with a first step toward unity.

Hence, considering those results, we claim the discovery of law of nature that rules gravity and the universe formation, including metric and energy.

A first note [6] on this theory was previously published by the same author. With respect to this note the present paper was written based on minimal hypothesis.

5 Addendum

The new theory implies that an almost empty galaxy will be understood as made of close to 100% dark matter. Here, with an estimate of 98% dark matter, the observations of Dragonfly 44 recently reported by Van Dokkum & al. [2] is an important test because it will be systematic. A similar ratio will be found in any galaxy of this type; in a general manner, the lesser the baryonic mass the higher the ratio of dark matter given by the standard theory.

Submitted on January 24, 2017 / Accepted on January 26, 2017

References

1. The Plank Collaboration. Planck 2015 results. I. Overview of products and scientific results. arXiv: 1502.01582.
2. Van Dokkum, Pieter et al. A High Stellar Velocity Dispersion and ~100 Globular Clusters For The Ultra-Diffuse Galaxy Dragonfly 44. *The Astrophysical Journal Letters*, 2016, v. 828, no. 1.
3. Milgrom M. A modification of the Newtonian dynamics as a possible alternative to the hidden mass hypothesis. *Astrophysical Journal*, 1983, v. 270, 365–370.
4. Milgrom M. MOND theory. (2014), arXiv: 1404.7661v2.
5. Riess A.G., Macri L.M., Hoffmann S.L., Scolnic D., Casertano S., Filippenko A.V., Tucker B.E., Reid M.J., Jones D.O. A 2.4% Determination of the Local Value of the Hubble Constant. (2016), arXiv: 1604.01424.
6. Consiglio J. On the Absorber in Gravitation. *Progress in Physics*, 2016, v. 12(1), 20–25.

On a 4th Rank Tensor Gravitational Field Theory

Patrick Marquet

18 avenue du Président Wilson, 62100 Calais, France
E-mail: patrick.marquet6@wanadoo.fr

In an earlier publication, we showed that a slightly varying cosmological term is a necessary ingredient to restore the true tensor nature of the gravitational field produced by neutral matter. As a result, this term induces a background field filling the entire vacuum. The global energy-momentum tensor of matter and its gravity field is proved to be intrinsically conserved like the Einstein tensor, once it has been identified with the Rosenfeld-Belinfante symmetric tensor. Within the GR representation in the absence of matter, the remnant field never vanishes and we showed that it represents the lower horizon state of the Lorentzian space-time vacuum. In what follows, we work out a 4th rank tensor theory of gravity which formally leads to have the background field superimposed onto the large scale structure of space-time classically described by the de Sitter Universe with a cosmological constant. Our 4th rank tensor theory thus substantiates the recent investigations which would adopt the de Sitter Space-time as a mathematical frame more general that the Minkowski space.

Introduction

By introducing a space-time variable term Ξ that supersedes the so-called cosmological constant Λ in Einstein's field equations, we formally showed that the gravity field of a (neutral) massive source is no longer described by an *ill-defined pseudo-tensor*, but it is represented by a *true canonical tensor* [1]. As a result, the physical space should be always filled with a *homogeneous vacuum background field* [2] which is described by a tensor on the r.h.s. of the Einstein's "source free" equations. Inspection shows that the matter-gravity tensor must be identified with the *Rosenfeld-Belinfante symmetric tensor* [3, 4], thus complying with the intrinsic conservation property of the *Einstein tensor* as it should be. Regarding the *vacuum background field*, it was shown to be a *space-time contraction* unveiling a low horizon state, arising from the geodesics incompleteness postulate [5]. Conversely, it is desirable to analyze the background field nature in the larger scale. To this effect, we suggest here a 4th rank tensor theory based on the full Riemann curvature, and which suitably generalizes the Einstein-Ricci 2nd rank tensor formulation. Unlike many attempts of the kind, our mathematical approach does not trivially entail Einstein GR theory. In fact, due to its peculiar formulation, it leads to view the usual Einstein equations as merely initial conditions following the Cauchy problem.

As will turn out, such a broader theory clearly grants the background field a sound macroscopic meaning. When matter is absent, it closely follows the pattern of the *constant curvature space-time* described by the de Sitter metric when the term Ξ is reduced to the cosmological constant Λ.

In this way, the vacuum background field may be regarded as an intrinsic property of the basic physical structure of our Universe.

Notations

Space-time Greek indices run from $\alpha = \beta$: 0, 1, 2, 3, while spatial Latin indices run from $a = b$: 1, 2, 3. The space-time signature is -2. In the present text, $\varkappa$ is Einstein's constant $8\pi G/c^4 = 8\pi G$ with $c = 1$.

1 The background field and the gravitational field tensor (reminder)

In a pseudo-Riemannian manifold V_4, let us first set the following tensor densities

$$\mathfrak{g}^{\alpha\beta} = \sqrt{-g}\, g^{\alpha\beta}\,, \tag{1.1}$$

$$\mathfrak{G}^{\alpha\beta} = \sqrt{-g}\, G^{\alpha\beta} \ \text{(Einstein tensor density)}, \tag{1.2}$$

$$\mathfrak{G}^{\alpha}_{\beta} = \sqrt{-g}\, G^{\alpha}_{\beta}\,, \tag{1.2bis}$$

$$\mathfrak{R}^{\alpha\beta} = \sqrt{-g}\, R^{\alpha\beta} \ \text{(Ricci tensor density)}. \tag{1.2ter}$$

In density notations, the usual field equations with a massive source then read

$$\mathfrak{G}^{\alpha\beta} = \mathfrak{R}^{\alpha\beta} - \frac{1}{2}\, g^{\alpha\beta}\mathfrak{R} - g^{\alpha\beta}\Lambda\sqrt{-g} = \varkappa\, \mathfrak{T}^{\alpha\beta}, \tag{1.3}$$

where

$$\mathfrak{T}^{\alpha\beta} = \sqrt{-g}\, T^{\alpha\beta}$$

while Λ is the so-called cosmological constant.

However, unlike the Einstein tensor $G^{\alpha\beta}$ which is *conceptually conserved*, the conditions

$$\partial_\alpha \mathfrak{T}^{\alpha}_{\beta} = 0 \tag{1.4}$$

are never satisfied in a general coordinates system [6]. To cure this problem, we have demonstrated once more the conservation condition

$$\partial_\alpha \left[(\mathfrak{T}^{\alpha}_{\beta})_{\text{matter}} + (\mathfrak{t}^{\beta}_{\alpha})_{\text{gravity}} \right] = 0\,, \tag{1.5}$$

but where $(\mathfrak{t}_\alpha^\beta)_{\text{gravity}}$ is no longer a pseudo-tensor density.

To achieve this, we introduced a space-time varying term Ξ in place of the cosmological constant Λ, and whose scalar density is denoted by

$$\zeta = \Xi\sqrt{-g}\,. \tag{1.6}$$

Its variation is given by

$$\zeta = \sqrt{-g}\,\nabla_a\kappa^a = \partial_a\left(\sqrt{-g}\,\kappa^a\right) \tag{1.7}$$

and the term

$$\zeta = \sqrt{-g}\,\nabla_a\kappa^a \tag{1.8}$$

is related to the *vacuum volume expansion scalar* $\theta = \nabla_a\theta^a$ (see [7] for detail).

Such a form allows to maintain the original *Einstein Lagrangian density* as

$$\mathfrak{L}_E = \sqrt{-g}\,g^{\alpha\beta}\left[\left\{{}^{\nu}_{\alpha\beta}\right\}\left\{{}^{\lambda}_{\lambda\nu}\right\} - \left\{{}^{\lambda}_{\alpha\nu}\right\}\left\{{}^{\nu}_{\beta\lambda}\right\}\right], \tag{1.9}$$

the latter expression being used to derive the new canonical gravity tensor attached to a mass:

$$(\mathfrak{t}_\beta^\alpha)_{\text{gravity}} = \frac{1}{2\varkappa}\Big[\left\{{}^{\alpha}_{\gamma\mu}\right\}\partial_\beta\mathfrak{g}^{\gamma\mu} - \\ - \left\{{}^{\gamma}_{\gamma\mu}\right\}\partial_\beta\mathfrak{g}^{\mu\alpha} - \delta^\alpha_\beta(\mathfrak{L}_E - \zeta)\Big], \tag{1.10}$$

ζ can be regarded as a *Lagrangian density* characterizing a specific *vacuum background field* which pre-exists in the absence of matter. Close inspection of equation (1.10) shows that local gravitational field of matter is just a mere "excited state" of the background field. Sufficiently far from the massive source, $(\mathfrak{t}_\beta^\alpha)_{\text{gravity}} \to (\mathfrak{t}_\beta^\alpha)_{\text{background}}$.

2 Symmetrization of the gravity tensor

The tensor density (1.10) includes the *Einstein-Dirac pseudo-tensor density* [8] which is not symmetric.

Symmetrizing the canonical tensor $(\Theta_\beta^\alpha)_{\text{gravity}}$ extracted from $(\mathfrak{t}_\beta^\alpha)_{\text{gravity}} = \sqrt{-g}\,(\Theta_\beta^\alpha)_{\text{gravity}}$ is equivalent to identifying it with the *Belinfante-Rosenfeld tensor*:

$$(t^{\gamma\beta})_{\text{gravity}} = (\Theta^{\gamma\beta})_{\text{gravity}} + \nabla_\alpha\,\Upsilon^{\gamma\beta\alpha} \tag{2.1}$$

with

$$\Upsilon^{\gamma\beta\alpha} = \frac{1}{2}\left(S^{\gamma\beta\alpha} + S^{\beta\gamma\alpha} - S^{\alpha\beta\gamma}\right), \tag{2.2}$$

where the antisymmetric tensor $S^{\alpha\beta\gamma}$ is the contribution of the *intrinsic angular momentum*. Now, we check that:

$$\nabla_\alpha(\Theta_\beta^\alpha)_{\text{gravity}} = \nabla_\alpha(t_\beta^\alpha)_{\text{gravity}} = 0\,. \tag{2.3}$$

Far from matter $(t^{\alpha\beta})_{\text{gravity}} \to (t^{\alpha\beta})_{\text{background}}$ and $\Upsilon^{\alpha\beta\gamma} = 0$. By essence, $(t^{\alpha\beta})_{\text{background}}$ is thus symmetric.

The field equations with a (neutral) massive source together with its gravity tensor can now be explicitly written down

$$G^{\alpha\beta} = R^{\alpha\beta} - \frac{1}{2}\,g^{\alpha\beta}R = \varkappa(T^{\alpha\beta})_{\text{global}}\,, \tag{2.4}$$

where

$$(T^{\alpha\beta})_{\text{global}} = (T^{\alpha\beta})_{\text{matter}} + (t^{\alpha\beta})_{\text{gravity}} \tag{2.5}$$

with, for example $(T^{\alpha\beta})_{\text{matter}} = \rho u^\alpha u^\beta$ (here ρ is the homogeneous mass density).

3 The 4th rank theory of the gravitational field

3.1 The new field equations

We now state that the *true gravitational field equations with a source* are the 4th rank tensor equations

$$G_{\beta\gamma\ \mu}^{\ \alpha} = \varkappa\,T_{\beta\gamma\ \mu}^{\ \alpha}\,, \tag{3.1}$$

where

$$G_{\beta\gamma\ \mu}^{\ \alpha} = R_{\beta\gamma\ \mu}^{\ \alpha} - \frac{1}{2}\,R\left(\delta^\alpha_\gamma g_{\beta\mu} - \delta^\alpha_\mu g_{\beta\gamma}\right) \tag{3.1bis}$$

and

$$T_{\beta\gamma\ \mu}^{\ \alpha} = \delta^\alpha_\gamma(T_{\beta\mu})_{\text{global}} - \delta^\alpha_\mu(T_{\beta\gamma})_{\text{global}} \tag{3.2}$$

is the generalized energy-momentum tensor.

Our assumption can be legitimized by the following considerations. From Bianchi's second identities [9]

$$(s)_{\alpha\beta\gamma}\nabla_\alpha R_{\beta\gamma\lambda\mu} = 0\,, \tag{3.3}$$

where (s) denotes the cyclic sum, we easily infer [10]

$$\nabla_\alpha R_{\beta\gamma\ \mu}^{\ \alpha} = \nabla_\gamma R_{\beta\mu} - \nabla_\mu R_{\beta\gamma}\,, \tag{3.4}$$

hence

$$\nabla_\alpha G_{\beta\gamma\ \mu}^{\ \alpha} = \nabla_\gamma R_{\beta\mu} - \nabla_\mu R_{\beta\gamma} - \frac{1}{2}\,\nabla_\alpha R\left(\delta^\alpha_\gamma g_{\beta\mu} - \delta^\alpha_\mu g_{\beta\gamma}\right) \tag{3.5}$$

i.e.

$$\nabla_\alpha G_{\beta\gamma\ \mu}^{\ \alpha} = \nabla_\gamma R_{\beta\mu} - \nabla_\mu R_{\beta\gamma} - \frac{1}{2}\,\nabla_\gamma R g_{\beta\mu} + \frac{1}{2}\,\nabla_\mu R g_{\beta\gamma}\,. \tag{3.5bis}$$

The right hand side equation is obviously zero, therefore:

$$\nabla_\alpha G_{\beta\gamma\ \mu}^{\ \alpha} = 0\,. \tag{3.6}$$

The tensor

$$G_{\beta\gamma\ \mu}^{\ \alpha} = \delta^\alpha_\gamma R_{\beta\mu} - \delta^\alpha_\mu R_{\beta\gamma} - \frac{1}{2}\,R\left(\delta^\alpha_\gamma g_{\beta\mu} - \delta^\alpha_\mu g_{\beta\gamma}\right) \tag{3.6bis}$$

is thus intrinsically conserved as is the case for the Einstein-Ricci tensor $G_{\beta\mu}$, and we call it the *Einstein 4th rank tensor*.

In addition, we also have:

$$\nabla_\alpha\,T_{\beta\gamma\ \mu}^{\ \alpha} = \nabla_\alpha\left[\delta^\alpha_\gamma(T_{\beta\mu})_{\text{global}} - \delta^\alpha_\mu(T_{\beta\gamma})_{\text{global}}\right] = 0\,. \tag{3.7}$$

Proof:

$$\delta^\alpha_\gamma(T_{\beta\mu})_{\text{global}} = \delta^\nu_\gamma g_{\beta\nu}(T^\alpha_\mu)_{\text{global}} = g_{\beta\gamma}(T^\alpha_\mu)_{\text{global}} \tag{3.8}$$

and since $\nabla_\alpha\,(T^\alpha_\mu)_{\text{global}} = 0$ according to our initial demonstration, then $\nabla_\alpha\left[\delta^\alpha_\gamma(T_{\beta\mu})_{\text{global}}\right] = 0$. The same reasoning holds for $\delta^\alpha_\mu(T_{\beta\gamma})_{\text{global}}$

$$\delta^\alpha_\mu(T_{\beta\gamma})_{\text{global}} = \delta^\nu_\mu g_{\beta\nu}(T^\alpha_\gamma)_{\text{global}} = g_{\beta\mu}(T^\alpha_\gamma)_{\text{global}} \tag{3.8bis}$$

which finally yields (3.7).

Equations (3.6) and (3.7) tell us that the conservation conditions are fully satisfied by the system:

$$G_{\beta\gamma\ \mu}^{\ \ \alpha} = \varkappa\, T_{\beta\gamma\ \mu}^{\ \ \alpha}\,. \tag{3.9}$$

Hence, $T_{\beta\gamma\ \mu}^{\ \ \alpha}$ is confirmed to be the appropriate generalization of the energy-momentum 2nd rank tensor $(T_{\gamma\mu})_{\text{global}}$.

How do the Einstein second rank tensor equations fit in the theory?

3.2 Some hypothesis on the Cauchy problem

Let us consider again (3.1bis) and (3.2)

$$G_{\beta\gamma\ \mu}^{\ \ \alpha} = \delta^\alpha_\gamma R_{\beta\mu} - \delta^\alpha_\mu R_{\beta\gamma} - \frac{1}{2}\, R\left(\delta^\alpha_\gamma g_{\beta\mu} - \delta^\alpha_\mu g_{\beta\gamma}\right),$$

$$T_{\beta\gamma\ \mu}^{\ \ \alpha} = \delta^\alpha_\gamma (T_{\beta\mu})_{\text{global}} - \delta^\alpha_\mu (T_{\beta\gamma})_{\text{global}}\,,$$

and by subtraction we have:

$$\delta^\alpha_\gamma \left[G_{\beta\mu} - \varkappa (T_{\beta\mu})_{\text{global}}\right] - \delta^\alpha_\mu \left[G_{\beta\gamma} - \varkappa (T_{\beta\gamma})_{\text{global}}\right] = 0 \tag{3.10}$$

i.e.

$$P_{\beta\mu} - P_{\beta\gamma} = 0\,. \tag{3.10bis}$$

where $\boldsymbol{P} = \boldsymbol{G} - \varkappa \boldsymbol{T} = 0$ are the Einstein equations with a source which read in mixed indices as:

$$P^\alpha_\beta = 0\,. \tag{3.11}$$

Both relations (3.10bis) and (3.11) then strongly suggest that the Einstein equations $\boldsymbol{P} = 0$ can be regarded as mere initial conditions on a spacelike hypersurface Σ defined on V_4. To see this, consider Σ on which is given $P^\alpha_\beta = 0$, we must show that upon the above conditions, $\boldsymbol{P} = 0$ also holds beyond Σ [11].

For $\beta = 0$ and α reduced to spatial indices $i, k = 1, 2, 3$, equation (3.10bis) can be expressed by

$$P_{0\mu} = P_{0\gamma} \tag{3.12}$$

and (3.11) becomes:

$$g_{00} P^{i0} = -2 g^{i0} P_{00} - g^{ik} P_{k0} \tag{3.12bis}$$

Now, if the hypersurface Σ admits the local equation $x^0 = 0$, we have $g_{00} \neq 0$ which means that $\boldsymbol{P} = 0$ would also hold beyond Σ.

On the hypersurface Σ, the zero initial data require that the system (3.12)–(3.12bis) admits nothing but the zero solution leading to $\boldsymbol{P} = 0$ as well. This is what we wanted to show.

In relation with (3.12), one may regard the equations

$$G_{\beta 0\ \mu}^{\ \ \alpha} - \varkappa \left[\delta^\alpha_0 (T_{\beta\mu})_{\text{global}} - \delta^\alpha_\mu (T_{\beta 0})_{\text{global}}\right] = 0 \tag{3.13}$$

as *constraint equations for the initial data at the time* $x^0 = 0$ which are usually set in the Cauchy problem. For a particular example see [12].

3.3 Newton's law

Let us consider the massive tensor classically expressed by

$$(T^{\alpha\beta})_{\text{global}} = \rho u^\alpha u^\beta + (t^{\alpha\beta})_{\text{gravity}} \tag{3.14}$$

which becomes here

$$T_{\beta\gamma\ \mu}^{\ \ \alpha} = \delta^\alpha_\gamma \left[\rho u_\beta u_\mu + (t_{\beta\mu})_{\text{gravity}}\right] - \\ - \delta^\alpha_\mu \left[\rho u_\beta u_\gamma + (t_{\beta\gamma})_{\text{gravity}}\right]. \tag{3.15}$$

When the spatial 3-velocities are low and the gravitational field is weak, the static case corresponds to the Newton's law for which $u_0 = 1$ in an orthonormal basis. In the framework of our theory, this translates to:

$$G_{0i\ 0}^{\ \ i} = \varkappa\, T_{0i\ 0}^{\ \ i} \tag{3.16}$$

Explicitly: the left hand side is easily shown to reduce to:

$$G_{0i\ 0}^{\ \ i} = R_{00} - \frac{1}{2}\, R g_{00}\,. \tag{3.17}$$

In the same way, the right hand side of (3.16) reduces to:

$$T_{0i\ 0}^{\ \ i} = (\rho + t_{\text{gravity}}). \tag{3.17bis}$$

As usual, we can re-write the field equations as

$$R^0_0 = \varkappa \left[(\rho + t_{\text{gravity}}) - \frac{1}{2}\, \delta^0_0 (\rho + t_{\text{gravity}})\right] \tag{3.18}$$

which eventually yields with the explicit value of the Einstein's constant

$$R^0_0 = 4\pi G (\rho + t_{\text{gravity}})\,, \tag{3.19}$$

where G is Newton's constant.

We then retrieve the *Poisson equation* which is also expressed by:

$$\Delta\psi = 4\pi G \rho'. \tag{3.19bis}$$

We have set: $\rho' = \rho + t_{\text{gravity}}$ because we consider a stationary gravity field (in a general case, the gravity field is "dragged" along with the mass and $\rho' = \rho + t_{\text{gravity}}$ no longer holds). With the metric approximation:

$$g_{00} = 1 + 2\psi\,, \tag{3.20}$$

where ψ is the Newton's gravitational potential

$$\psi = -G \int \frac{\rho'}{R}\, dV\,, \tag{3.21}$$

while R is here the distance from the observer to the volume element dV. Integration is performed over a volume V which comprises both the bare mass and its (stationary) gravitational field.

4 The background field in our Universe

We now come to the persistent field appearing in the 2nd rank tensor field equations when matter is absent. These are

$$G^{\beta\gamma} = R^{\beta\gamma} - \frac{1}{2}\, g^{\beta\gamma} R = \varkappa (t^{\beta\gamma})_{\text{background}} \tag{4.1}$$

with

$$(t_{\alpha\beta})_{\text{background}} = \frac{\Xi}{2\varkappa}\, g_{\alpha\beta}\,. \tag{4.2}$$

Expressed in the framework of the 4th rank tensor theory, this yields:

$$G_{\beta\gamma\ \mu}^{\ \ \alpha} = R_{\beta\gamma\ \mu}^{\ \ \alpha} - \frac{1}{2}\, R\left(\delta^\alpha_\gamma g_{\beta\mu} - \delta^\alpha_\mu g_{\beta\gamma}\right) = \\ = \frac{\Xi}{2}\left(\delta^\alpha_\gamma g_{\beta\mu} - \delta^\alpha_\mu g_{\beta\gamma}\right). \tag{4.3}$$

In virtue of $\nabla_\alpha G_{\beta\gamma\ \mu}^{\ \ \alpha} = 0$, the r.h.s. is conserved:

$$\nabla_\alpha \left[\frac{\Xi}{2}\left(\delta^\alpha_\gamma g_{\beta\mu} - \delta^\alpha_\mu g_{\beta\gamma}\right)\right] = 0\,. \tag{4.3bis}$$

The latter equation is worthy of attention, for the term Ξ never happens to be a constant as could be (ambiguously) the case for $\nabla_\alpha G^{\alpha\beta} = \nabla_\alpha \frac{\Xi}{2} g^{\alpha\beta}$.

This lends support to the fact that only a 4th rank tensor theory can strictly describe a metric with a variable cosmological term. Therefore, after interchanging α with β, we find:

$$G_{\alpha\beta\gamma\mu} = \frac{\Xi}{2}\left(g_{\alpha\gamma} g_{\beta\mu} - g_{\alpha\mu} g_{\beta\gamma}\right). \tag{4.4}$$

The latter equations constitute here the *4th rank tensor background field equations* which characterize the *fundamental structure of physical space-time*.

They adequately generalize the Einstein space endowed with the cosmological constant Λ defined as:

$$G_{\beta\gamma} = R_{\beta\gamma} = \Lambda\, g_{\beta\gamma}\,. \tag{4.5}$$

For a specific value of Ξ, we retrieve the space-time of constant curvature [13], which characterizes the de Sitter Universe when $3\Lambda = R$ [14]:

$$R_{\alpha\beta\gamma\mu} = \frac{R}{12}\left(g_{\alpha\gamma} g_{\beta\mu} - g_{\alpha\mu} g_{\beta\gamma}\right). \tag{4.6}$$

Finally, let us emphasize a major point. In a Universe devoid of matter described by equations (4.4), the Weyl conformal trace-free tensor $C_{\alpha\beta\gamma\mu}$ never vanishes, in contrast to the de Sitter model equipped with curvature (4.6). However, the Weyl tensor being that part of the curvature which is not determined locally by the matter distribution, there is no reason why it should disappear in an "empty" model of space-time. Hence, our approach of a Universe with a pervasive background field proves to be physically consistent for it preserves the Weyl tensor, whatever its content.

So, as expected from our 2nd rank tensor field equations (4.1), the case $G^\alpha_{\beta\gamma\ \mu} = 0$ will never occur.

Conclusion

Our 4 th rank tensor gravitational field theory appears to be the appropriate extension of the 2nd order Einstein-Ricci formulation.

However, it should be noted that the presented theory does not use the well-known *Bel-Robinson tensor* [15] which gave birth to the very thorough paper of *R. Debever* on *Super Energy* [16].

The presented remarkably simple theory is partly inspired from a lecture given by *A. Lichnérowicz* in a Paris seminar dedicated to linearized field quantization solutions prior to their global formulation [17]. We have however substantially modified this theory allowing for a clearer physical significance of the vacuum background field on the very large scale structure of space-time.

Indeed, when matter is absent, the intrinsic curvature of space-time is modeled by the background field through its variable term Ξ, just as de Sitter's empty Universe does with its cosmological constant Λ arbitrarily introduced.

Such a close similarity with the de Sitter curvature should not come as a surprise. The de Sitter metric recently saw some revived interest among several physicists [18–20]. They conjectured that the laws of physics are invariant under the symmetry group of de Sitter space (*maximally symmetric* space-time), rather than the Poincaré group of special relativity. The full Poincare group is the semi-direct product of translations $\mathbf{T}$ with the Lorentz group $\mathbf{L} = \mathrm{SO}(3,1)$: $\mathbf{P} = \mathbf{L} \otimes \mathbf{T}$. The latter acts transitively on the *Minkowski space* $\mathbf{M}$ which is homogeneous under $\mathbf{P}$.

In the framework of a generalized group where translations mix up non trivially with rotations, the requirements of homogeneity and isotropy lead ipso facto to the de Sitter Universe with a uniform scalar curvature. More specifically, the de Sitter space whose metric is induced from the pseudo-Euclidean metric $(+1,-1,-1,-1,-1)$ has a specific group of motion which is the pseudo-orthogonal group SO(4, 1) [21]. Then, de Sitter group obviously involves an additional length parameter l which is related to the (positive) cosmological term by:

$$\Lambda = \frac{3}{l^2}\,.$$

The *Poincaré group* "contracts" to the *Galilean group* for low velocities.

Analogously the *de Sitter group* "contracts" to the *Poincaré group* for short distance kinematics, when the order of magnitude of all translations are small compared to the de Sitter radius. (See: Wigner and Inönü, for the group contraction concept [22]). These distances are probed by high energies meaning that quantum effects must be taken into account. In that case, when we have $\Lambda \to \infty$, this would correspond to $\Lambda_P = 3/l_P^2$, where l_P is the Planck length. If $\Lambda \to 0$, however, the underlying space-time would reduce to the Minkowski space.

From the fundamental vacuum field equations (4.4), the variable term Ξ would represent a fluctuation between two appropriate values of Λ wherein the de Sitter space-time can be fully represented. In this view, the 4th rank tensor field equations are to the de Sitter space-time, what the 2nd rank tensor field equations are to the Minkowski space.

Submitted on January 20, 2017 / Accepted on January 25, 2017

References

1. Marquet P. The gravitational field: a new approach. *Progress in Physics*, 2013, v. 9, issue 3, 62–66.
2. Marquet P. Vacuum background field in General Relativity. *Progress in Physics*, 2016, v. 12, issue 4, 314–316.
3. Belinfante J. *Physica*, 1939, v. 6, 887.
4. Rosenfeld L. Sur le tenseur d'Impulsion-Energie. *Acad. Roy. de Belgique* (*Mémoires de Classes de Sciences* 18), 1940.
5. Marquet P. Some insights on the nature of the vacuum background field in General Relativity. *Progress in Physics*, v. 12, issue 4, 366–367.
6. Landau L. and Lifshitz E. The Classical Theory of Fields. Addison-Wesley, Reading (Massachusetts), 1962, p. 402 (French translation).
7. Straumann N. General Relativity and Relativistic Astrophysics. Springer-Verlag (Berlin), 1984, p. 159.
8. Dirac P.A.M. General Theory of Relativity. Princeton University Press, 2nd edition, 1975, p. 61.
9. Hawking S.W., Ellis G.F.R. The Large Scale Structure of Space time. Cambridge University Press, 1987, p. 62.
10. Lapiedra R. Sur les équations d'ordre supérieur du champ gravitationnel. *Annales de l'IHP*, section A, 1969, t. 11, 277–307.
11. Lichnérowicz A. Propagateurs. Quantification du Champ. *Séminaire Janet*, 1960, no. 4, 3ème année.
12. Choquet-Bruhat Y., York J.W. Jr. Well posed reduced systems for the Einstein equations. arXiv: gr-qc/9606001.
13. Kramer D., Stephani H., Hertl E., MacCallum M. Exact Solutions of Einstein's Field Equations. Cambridge University Press, 1979, p.101.
14. de Sitter W. On the curvature of space. *Proc. Roy. Acad. Sci. Amsterd.*, 1917, v. 20, 229–243.
15. Bel L. Introduction d'un tenseur du 4ème ordre. *Comptes rendus hebdomadaires des Séances de l'Académie des Sciences*, 1956, t. 248, 1297.
16. Debever R. Super-energy in General Relativity. *Bull. Soc. Math. Belg.*, 1958, v. 10, 112–147.
17. Lichnérowicz A. Propagateurs et commutateurs en Relativité Générale. *Institut des Hautes Etudes Scientifiques*, *Publications mathématiques*, 1961, no. 10.
18. Aldrovani R., Beltran Almeida J.P., Pereira J.G. Some implications of the cosmological constant to fundamental physics. arXiv: gr-gc/0702065.
19. Bacry H., Levy-Leblond J.M. *Journal of Mathematical Physics*, 1968, v. 9(10), 1605.
20. Lev F.M. de Sitter symmetry and quantum theory. arXiv: 1110.0240.
21. Aldrovani R., Beltran Almeida J.P., Pereira J.G. de Sitter special relativity. arXiv: gr-gc/0606122.
22. Inönü E., Wigner E.P. *Proc. Natl. Acad. Scien.*, 1953, v. 39, 510.

Optimizing the Teflon Thickness for Fast Neutron Detection Using a Ge Detector

Sylvian Kahane[1] and Raymond Moreh[2]

[1]P.O. Box 1630, 84965, Omer, Israel. E-mail: sylviankahane@gmail.com
[2]Department of Physics, Ben-Gurion University, 84120, Beer-Sheva, Israel. E-mail: moreh@bgu.ac.il

The optimum Teflon $(C_2F_4)_n$ thickness for fast neutron detection through the ^{19}F(n,α)^{16}N reaction was calculated and found to be $\approx$ 5.0 cm. Here, the 6.13 MeV γ ray emitted by ^{16}N is assumed to be detected by a Ge diode. The geometry of the system is discussed and the γ line intensity was found to vary weakly with Teflon thickness.

1 Introduction

Several methods are used in the literature for fast neutron detection. Among those methods are: (1) the detection of protons recoiling from the impinging neutrons [1], (2) the use of plastic and liquid scintillators [2], (3) the use of Gd-loaded liquid scintillators [3], (4) ^{3}He gas-filled detectors can be used for both neutron detection and spectroscopy measurements [4], (5) Semiconductor-based neutron detectors [5]. In other methods the neutrons are first moderated to thermal velocities then captured using BF_3 detectors via the ^{10}B(n,α)^{7}Li reaction [6]. In addition, fast neutron detection often relies on neutron induced nuclear reaction.

The topic of the present work is the use the ^{19}F(n,α)^{16}N reaction [7] to detect fast neutrons with energies $E_n > 3$ MeV. This may be done by holding Teflon $(C_2F_4)_n$ in close vicinity to a Ge gamma detector. When the Teflon is hit by fast neutrons it forms ^{16}N; it is a β emitter (τ = 7.2 s) proceeding to an excited state in ^{16}O (68%) which emits a 6.13 MeV photon. This can readily be measured using a Ge detector. Teflon is a combination of 24.0% C and 76.0% F (by weight), with a density of 2.2 g/cc [8]. Note that because of the high gamma energy emitted by ^{16}O, it is easily visible above background and may be viewed as an excellent finger print of fast neutrons. The ^{19}F(n,α)^{16}N reaction is endothermic with $Q = -1.52$ MeV and because of the Coulomb barrier viewed by the emitted α–particles, a non-zero yield is obtained only for $E_n > 3$ MeV.

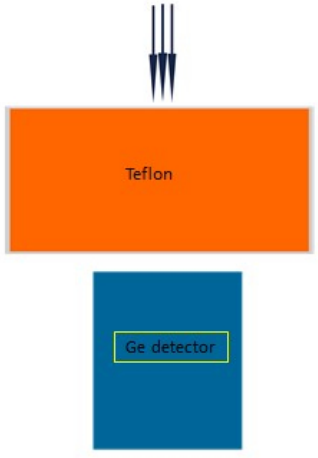

Fig. 1: A pencil neutron beam is hitting few cm thick Teflon absorber, at 5.0 mm above a ϕ 64×90 mm Ge coaxial detector, placed in a 1 mm thick Aluminum case (not shown).

In the past, this reaction was discussed in some detail for the detection of fast neutrons [7] where a Teflon cup covering a 30 cc Ge(Li) diode was used to detect the 6.13 MeV photon. Our interest here is to calculate the optimum thickness of the Teflon covering a pure Ge detector.

We use the simple geometry described in Fig. 1. The present calculation includes two representative Ge detector volumes: 100 cc, and 300 cc. In Fig. 1 the neutron beam is assumed to be mono-energetic with E_n = 5 to 11 MeV, hitting the Teflon in a normal direction (shown by the arrows), or embedded in a neutron field of uniform flux. Results were obtained also for a fission neutron spectrum having a Watt shape.

2 Simulations

The goal of the simulations is to "measure" the response of a Ge detector to the gamma rays induced by incoming neutrons on a Teflon shield, 5 mm above the detector, placed in an Aluminum cover, Fig. 1. This is calculated as a function of the Teflon thickness. We are especially interested in the β decaying ^{16}N nuclei proceeding to the excited level in ^{16}O emitting the 6.13 MeV γ line. The incoming neutron undergoes nuclear reactions with the Fluorine nuclei producing ^{16}N by ^{19}F(n,α) and ^{15}N by ^{19}F(n,α+n) respectively. ^{15}N is stable with no further decays or γ rays. The respective cross sections, from Janis [9], are shown in Fig. 2.

It can be seen that the first reaction has a non-zero cross section at a threshold of 3 MeV while the threshold of the second is 5 MeV. The simulations proceed in two steps, one for neutrons and one for gammas. The neutron simulation "measures" the production yield of the ^{16}N nuclei in Teflon cylinders of different thicknesses. The gamma simulations "measure" the actual detector response to the 6.13 MeV γ produced in the same Teflon cylinders. A convolution of the two results produces the response of the detector, per neutron, as a function of the Teflon thickness.

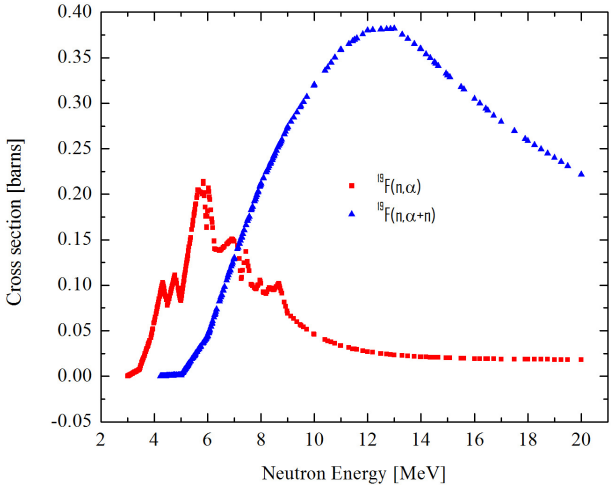

Fig. 2: The cross sections of the ^{19}F(n,α) and ^{19}F(n,α+n) reactions taken from the Japanese cross sections library JENDL-4.0.

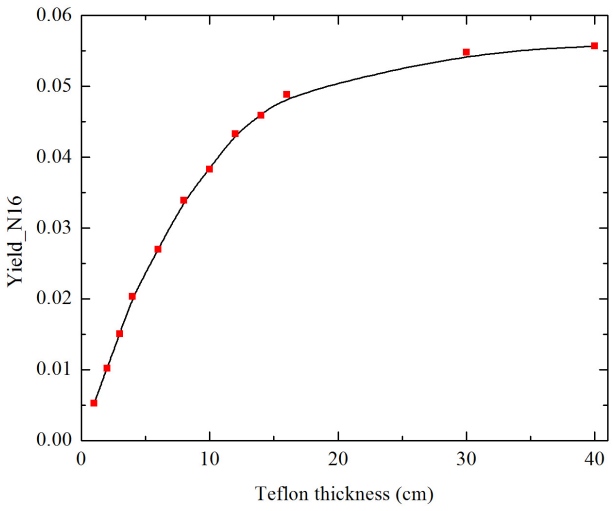

Fig. 3: Calculated yield of ^{16}N nuclei as a function of Teflon thickness obtained by assuming a neutron pencil beam of E_n = 5 MeV. The line is only a guide to the eye.

2.1 Neutrons

Two different geometries were employed: in one a monoenergetic and monodirectional pencil beam of neutrons impinges on a cylindrical Teflon sheet placed above the Ge detector, Fig. 1; in the second, the same Teflon cylinder, is placed in a "bath" of monoenergetic neutrons, simulating a uniform neutron field. The number of ^{16}N nuclei produced is counted and normalized to the number of neutrons used in the simulation. For the present purpose this quantity is called *Yield–^{16}N* which is the γ–source of interest. It increases with Teflon thickness reaching a saturation which depends on the extent of neutron absorption (Fig. 3). The statistical error in this Monte Carlo calculations is less than 1%, using 10^6 neutrons

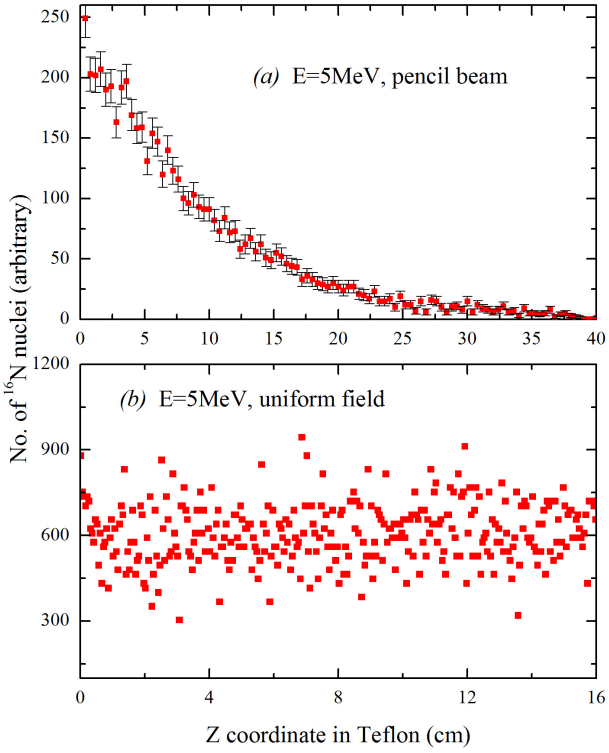

Fig. 4: The distribution of the ^{16}N nuclei along the z axis of the Teflon cylinder for two cases: (a) pencil beam and (b) uniform flux. In the second case the standard deviation is larger (17%) but the distribution is undoubtedly uniform.

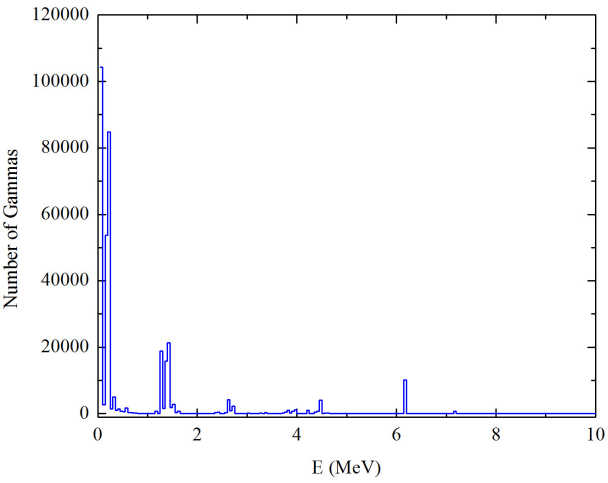

Fig. 5: Energies of the gammas produced in Teflon by 5 MeV neutrons. The gammas at 6.13 MeV are free of any interference.

for the case of a pencil beam and 4×10^6 for an uniform flux of neutrons.

Additionally, we calculated the distribution of the ^{16}N nuclei along the z axis of the Teflon cylinders (taken to be along the direction of the normal). Obviously, in the case of a uni-

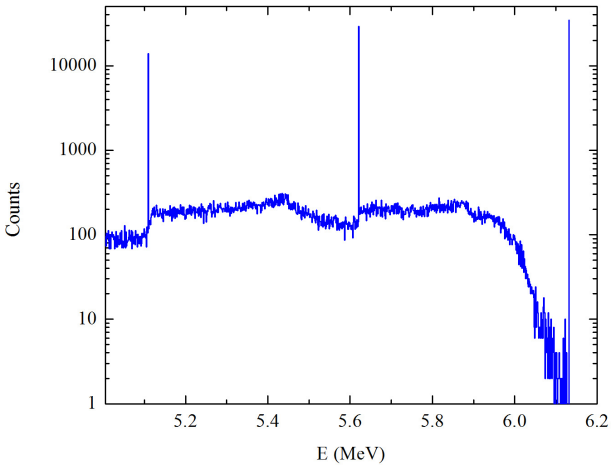

Fig. 6: Calculated spectrum in the 300 cc detector from a Teflon shield of 5cm.

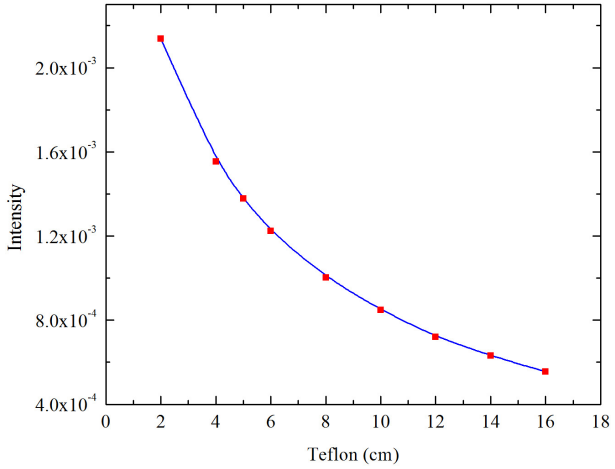

Fig. 7: Photopeak (6.13 MeV) intensity as a function of the Teflon thickness, calculated for the 100 cc detector.

form neutron field this distribution is also uniform, but in the case of a pencil beam the nuclei density is highest at the beam entrance, Fig. 4.

2.2 Technical details

The neutron simulations were performed with Geant4 [10]. This platform was chosen because it produces a plethora of ions in Teflon, both by nuclear reactions and by radioactive decay. An example is given in Tab. 1.

The kinetic energies of the *C*- and *F*–ions appearing in the table are acquired via elastic and inelastic neutron scattering. The number of α's is equal to the sum of ^{15}N and ^{16}N ions. The total number of gammas (1.4×10^6) is far larger than the ones at 6.13 MeV (4×10^4), but most of the gammas have low energies < 0.3 MeV (Fig. 5) and do not interfere with the measurements. The Geant4 system offers many options concerning the exact physics to be used in the simulations. We borrowed the detailed physics which appears in the example Hadr06 (/examples/extended/hadronic) found in its distribution. It employs high precision (HP) neutron physics i.e. uses actual neutron cross sections, for neutrons under 20 MeV, and not models, standard electromagnetic physics, radioactive decay and ion physics based on the internal models used by Geant4. Furthermore, the new neutron cross sections, developed by Mendoza and Cano-Ott [11], based on ENDF-VII, were adopted.

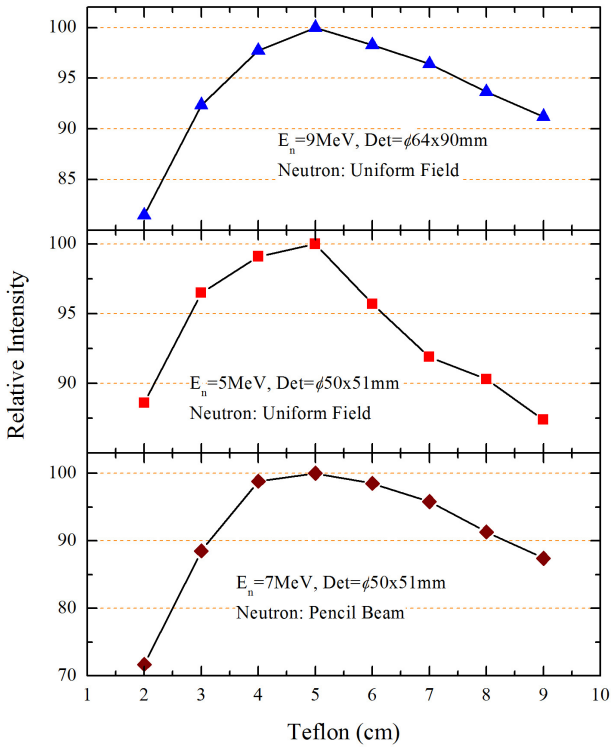

Fig. 8: Relative intensities versus Teflon thickness for various neutron energies and different Ge volumes. Some input data are listed in the figures.

2.3 Gammas

Here, the Teflon cylinder acts as a volume source. The exact departing point of each gamma is sampled in this volume, uniformly in the radial direction, and according to the distributions of Fig. 4 in the z direction. The statistical error is negligible. The simulations were carried out for two detector volumes: 100 cc (ϕ 50×51 mm), and 300 cc (ϕ 64×90 mm). These dimensions correspond to one of our detectors (100 cc) or taken from the ORTEC catalog (300 cc). The spectrum of the energy deposition is calculated by assuming no broadening, i.e. with zero energy resolution, in 1 keV bins (Fig. 6). This is because we did not compare to an actual measured spectrum but are interested only in the relative peak intensities.

Table 1: Number of ions produced in Teflon by a uniform neutron field of 5 MeV (4×10^6 neutrons). The numbers in square brackets are the energies of excited levels in keV, i.e. ^{19}F [1554.0] stands for the 1554.0 keV level of ^{19}F.

Ion	Numbers produced	Mean Energy
^{12}C	559603	436.0 keV
^{13}C	5907	404.1 keV
^{19}F	1414198	267.8 keV
^{19}F [109.9]	46	60.9 eV
^{19}F [1554.0]	1033	217.1 eV
^{19}F [197.1]	1884	224.2 eV
^{19}F [2779.9]	1	72.1 eV
^{19}F [4377.7]	1	11.2 eV
^{20}F	77	188.3 keV
^{15}N	294	535.9 keV
^{16}N	60366	891.2 keV
^{20}Ne	77	71.7 eV
^{20}Ne [1633.7]	77	487.1 eV
^{16}O	60364	1.6 keV
^{16}O [6049.4]	9	387.2 eV
^{16}O [6129.9]	40378	427.6 eV
^{16}O [6917.1]	22	128.20 eV
^{16}O [7116.9]	3037	260.8 eV
^{16}O [8871.9]	614	70.9 eV
^{19}O	2025	294.2 keV
α	60660	2.38 MeV
anti-ν_e	62466	3.14 MeV
e+	2786	2.00 MeV
e-	2030049	186.6 keV
γ	1416604	707.0 keV
Neutron	564213	2.72 MeV
Proton	2025	673.2 keV

The peak intensities are normalized per one gamma at source. As a function of the Teflon thickness it is a descending plot (less Teflon, less absorption) – Fig. 7. In order to obtain the intensities per neutron one has to multiply by the number of gammas found at a given Teflon thickness, this is what we called *Yield-*^{16}N, in Fig. 3. One of the graphs is going up (Fig. 3) and one is going down (Fig. 7), hence a maximum appears at a point corresponding to the optimum thickness – Fig. 8.

We sought the optimum with a resolution of 1 cm. We obtained a thickness of 5 cm for this optimum, for both detectors, for both neutron fields and for all the energies studied (between 5 to 11 MeV).

Fig. 8 presents the obtained intensities as percentage points where the optimum is 100%. Data come from the first escape (FE) peak in the case of the 100 cc detector and from the photopeak in the case of the 300 cc detector. While the optimum is well defined it is not very sharp, Fig. 8 shows that there are additional values, for the Teflon thickness, which differ from the optimum by only few percent. An interesting point in the results of the calculations is that the optimum thickness is sensitive neither to the incident neutron energy (in the energy range of our calculations) nor to the size of the detector. It may be seen that by varying the Teflon thickness between 4 to 6 cm, the counting rate of the detector varies by few percent only. In general, it can be said that the range 4–6 cm for Teflon will provide equally good counting results in an actual measurement. Even when using a much thinner Teflon of 2 cm we are within 15% from the optimum (in the uniform field case).

2.4 Fission like neutron spectrum

In the vicinity of nuclear reactors or a ccelerators there are non monoenergetic neutron fields. For nuclear reactors one can assume a fission like uniform Watt spectrum:

$$f(E) = \exp(-E/0.965) \times \sinh(2.29 \times E). \quad (1)$$

With the parameters taken from the defaults given in the MCNP manual [12] (the units are MeV for the first parameter and MeV^{-1} for the second). Obviously, because we obtained a flat value of 5 cm for all the energies of interest in the Watt spectrum, the optimum value for a reactor spectrum will be also 5 cm.

2.5 Other details

The simulations for the gammas were done with the MCNP program [12]. In principle, they can be done also by using Geant4 but with greater effort. Geant4 is a library and the user has to possess considerable programming skills in order to build a running program. MCNP is a closed, tested program and the user has to provide only the input data.

3 Conclusions

As may be seen from the above, the Teflon thickness yielding the optimum intensity of the 6.13 MeV γ line is $\approx$ 5.0 cm. It is surprising to see that this thickness is almost independent on the volume of the Ge detector, on the incident neutron energy (in the range studied) and on the direction of incidence of the neutrons.

Acknowledgements

One of us (R.M.) would like to thank Y. Ben-Galim for help in the initial stages of this work.

Submitted on February 11, 2017 / A ccepted on February 17, 2017

References

1. Shultis J. K., McGregor D. S. Efficiencies of coated and perforated semiconductor neutron detectors. *IEEE Trans. Nucl. Sci.*, 2006, v. 53, 1659.
2. Knoll G. F. Radiation Detection and Measurement. John Wiley & Sons, New York, 2010.

3. Kapoor S. S., Ramamurthy V. S. Nuclear Radiation Detectors. New Age International, New Delhi, 1986.
4. Tsoulfanidis N., Landsberger S. Measurement and Detection of Radiation, 4th Edition. CRC Press, Boca Raton, 2015.
5. Hussein E. M. Handbook on Radiation Probing, Gauging, Imaging and Analysis: Volume I. Kluwer Academic Publishers, New York, 2004.
6. Ben-Galim Y., Wengrowicz U., Moreh R., Orion I., Raveh A., Using the Doppler broadened γ line of the ^{10}B(n,$\alpha\gamma$)^{7}Li reaction for thermal neutron detection. *Nucl. Inst. Meth. Phys. Res. A*, 2016, v. 810, 140–143.
7. Wolf A., Moreh R., Utilization of Teflon covered Ge(Li) diodes for fast neutrons detection. *Nucl. Inst. Meth.*, 1978, v. 148, 195–197.
8. http://physics.nist.gov/cgi-bin/Star/compos.pl?matno=227.
9. https://www.oecd-nea.org/janis.
10. Agostinelli S. *et al*. Geant4 — a simulation toolkit. *Nuc. Inst. Meth. Phys. Res. A*, 2003, v. 506, 250–303.
11. https://www-nds.iaea.org/geant4.
12. Briesmeister J. F. MCNP-A General Monte Carlo N-Particle Transport Code. Technical Report LA-13 709-M, Los Alamos National Laboratory, NM, USA, 2001.

The Newtonian Constant G and the Einstein Equations

Bernard G. Colenbrander and Willem S. Hulscher

E-mail: b.g.colenbrander@gmail.com

The measurement of the Newtonian constant of gravitation G is in an impasse because most results deviate from the average value more than 10 times their estimated measurements uncertainties. Via the Einstein field equations G is related to the cosmological constant Λ and because normal matter, dark matter and dark energy must add up to 100%, Λ is a measure for dark energy. So it follows that G is related to dark matter. The density of the dark matter halo around the earth is influenced by the gravitational attraction of the earth and because the earth is not a perfect sphere, the halo varies along the surface. So we expect a variation of dark matter density with the gravitational acceleration g. These variations in dark matter affect G and indeed we have found a correlation between the constant G and the local value of the gravitational acceleration g.

1 Introduction

The gravitational constant G is commonly measured by using a torsion balance suspended by a wire as has been introduced by Cavendish. The plane of the rotating masses is positioned exactly horizontal and therefore the influence of local gravity variations is supposed to be negligible. However, the horizontal attraction force between the test masses in the apparatus is not only governed by these masses and their distance, but also by the local density of dark matter. We accept that gravitational attraction forces are influenced by dark matter and the local density of dark matter will vary with the local mass variations of the earth. So we expect a correlation between G and the gravitational acceleration g.

2 The correlation between G and g

In the following analyses 16 values of G recommended by CODATA in the period 1999-2014 [1, 2, 3] are represented, as they were measured by 9 institutes. The values of the gravitational acceleration g at 8 different locations are calculated by the website Wolfram Alpha. This calculation method is based on the Earth Gravitational Model, EGM 2008. It is noted that Uci-14 has not been measured at Irvine, California but near Handford, Washington [4].Therefore the value of g is calculated for the nearby city Richland.

Furthermore, the g value of Florence was measured in situ with the Atom Interferometer by the group of Tino [5, 6].

The analysis results in the following table and Figure 1.

G is the gravitational constant in 10^{-11} $m^3kg^{-1}s^{-2}$ and the last column in the table shows the standard uncertainty u of the measured value of G.

The graph shows a correlation of the gravitational constant G with the gravitational acceleration g according to the best-fit linear regression line, having a slope of 0.1371 and the coefficient of determination $R^2 = 0.6323$.

Obviously this effect also results in a dependency of G on the geographical latitude on the earth, as shown in Figure 2.

From 1999 onwards the measured values of G seem to be more reliable than before, so we have included only the values from the year 1999 and after. Where CODATA replaces old measured values by later measurements from the same institute, we have included all values measured in the named

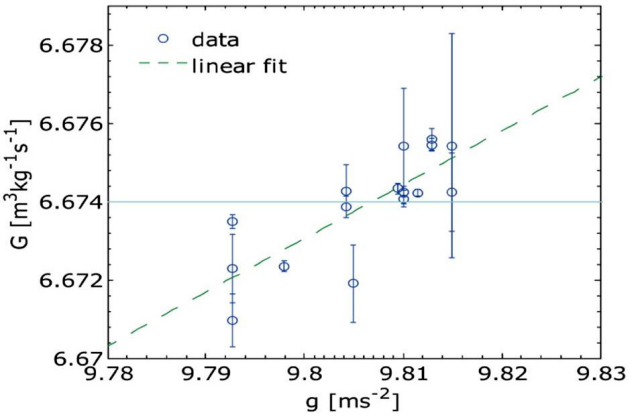

Fig. 1: Correlation of the gravitational constant G with the gravitational acceleration g. G = 0.1371 g + 5.328; R^2=0.6323.

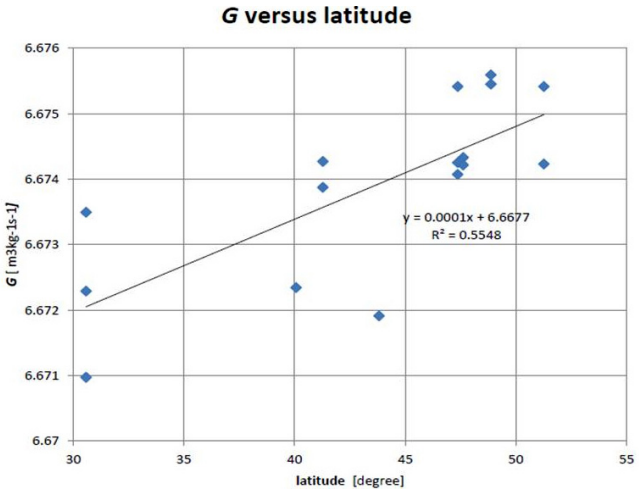

Fig. 2: Dependency of G on the geographical latitude.

Table 1: The 16 values of G recommended by CODATA in the period 1999-2014.

g -	G $\times 10^{-11}$	Institute -	Location -	Latitude Degree	std $\times 10^{-11}$
9.7927	6.67097	hust 99	Wuhan	30.58	0.00067
9.7927	6.67229	hust 05	Wuhan	30.58	0.00087
9.7927	6.67349	hust 09	Wuhan	30.58	0.00018
9.79795	6.67234	jila 010	Boulder	40.07	0.00014
9.80422	6.67427	msl 99	New Zeland	41.28	0.00067
9.80422	6.67387	msl 03	New Zeland	41.28	0.00027
9.80492	6.67191	lens 14	Florence	43.82	0.00099
9.80943	6.67433	uci 14	Richland	47.62	0.00013
9.81007	6.67542	uzur 99	Zurich	47.37	0.00147
9.81007	6.67407	uzur 02	Zurich	47.37	0.00022
9.81007	6.67425	uzur 06	Zurich	47.37	0.00013
9.81145	6.67422	uwash 00	Seattle	47.62	0.00009
9.81289	6.67559	bipm 01	Paris	48.87	0.00027
9.81289	6.67545	bipm 13	Paris	48.87	0.00016
9.81498	6.67542	uwup 99	Wuppertal	51.26	0.00287
9.81498	6.67423	uwup 02	Wuppertal	51.26	0.00100

period. The horizontal line in the graph at G = 6.674×10^{-11} $m^3kg^{-1}s^{-1}$ represents the average value calculated by CODATA in the year 2010. However, the correlation between G and g as we have found, renders it not useful to calculate an average value for G.

3 Further measurements

It has been raised by Quinn [7] that the Newtonian constant may be too difficult to measure, as the measured values spread 10 times more than the uncertainties of most measurements. However, we maintain that the problem is not the difficulty of the measurement but ignorance about the correlation of G and g.

Further compelling evidence for the named correlation can be obtained by doing several measurements with one and the same apparatus at different locations. Then the measured values can be compared better, because their accuracy is the same and no differences occur due to different measuring methods and different devices. It is also necessary to measure g in situ instead of calculating that value. More clarity can be obtained by taking additional measurements at places where g has an extreme value, for instance far away from the equator (e.g. at Helsinki) and nearby (e.g. at Quito). The group of Tino [5, 6] has developed a small apparatus based on atom interferometry. Such apparatus would be quite suitable for measuring both G and g.

4 Conclusion

Our analysis shows a correlation between G and g. This correlation suggests that the value of G depends on the place where it is measured, and thus G is not a universal constant of nature.

5 Appendix

The original Einstein field equations are:

$$R_{\mu\nu} - \frac{1}{2}Rg_{\mu\nu} = \frac{8\pi G}{c^4}T_{\mu\nu}.$$

The right hand part of the equation is the energy/momentum tensor and governs the curvature of space-time. The left hand part describes the measure of this curvature.

This set of equations generates no stationary solution, and therefore Einstein made a correction by adding an extra term with the cosmological constant Λ. The corrected field equations are:

$$R_{\mu\nu} - \frac{1}{2}Rg_{\mu\nu} + \Lambda g_{\mu\nu} = \frac{8\pi G}{c^4}T_{\mu\nu}$$

which can generate a stationary solution by inserting a suitable value for Λ.

At the end of the 20th century dark matter and dark energy were introduced in order to understand the uneven expansion of the universe and since then Λ is considered to be a measure of dark energy. When dark energy dominates dark matter, there is an accelerated expansion of the universe, and when dark matter dominates, the expansion is decelerated.

The cosmological constant Λ is linked to the gravitational constant G by the corrected field equations of Einstein. At the same time dark energy, dark matter and normal matter must add up to 100%. So dark energy and dark matter are dependent. In the field equations Λ and G are dependent as well. This means that we can rewrite the corrected field equations in the original form, without Λ, realizing that G depends on place and time. The field equations then become:

$$R_{\mu\nu} - \frac{1}{2}Rg_{\mu\nu} = \frac{8\pi G(r,t)}{c^4}T_{\mu\nu}.$$

Submitted on January 27, 2017 / Accepted on January 27, 2017

References

1. Mohr P.J. and Taylor B.N. CODATA recommended values of the fundamental physical constants: 2002.
2. Mohr P.J., Taylor B.N. and Newell D.B. CODATA recommended values of the fundamental physical constants: 2006.
3. Mohr P.J., Taylor B.N. and Newell D.B. CODATA Recommended Values of the Fundamental Physical Constants. arXiv: 1203.5425v1 [physics, atom-ph] 24 Mar 2012.
4. Schlamminger S., Gundlach J.H. and Newman R.D. Recent measurements of the gravitational constant as a function of time. *Phys. Rev. D*, 2015, v. 91, 121101(R).
5. Rosi G., Sorrentino F., Cacciapuoti L., Prevedelli M. and Tino G.M. *Nature*, 2014, v. 510, 518–521.
6. De Angelis M., Greco F., Pistorio A., Poli N., Prevedelli M., Saccorotti G., Sorrentino F. and Tino G.M. *Eur. Phys. J. Plus*, 2012, v. 127, 27.
7. Quin T. and Speake C. The Newtonian constant of gravitation - a constant too difficult to measure? An introduction. *Phil. Trans. R. Soc. A*, 2014, v. 372, 20140253.

Null Result for Cahill's 3-Space Gravitational Wave Experiment with Zener Diode Detectors

Wolfgang Baer[1], Eric Reiter[2], Harry Jabs[3]

[1]Nascent Systems Inc., 380 W Carmel Valley Rd., Carmel Valley, CA 93924 , USA, wolf@NascentInc.com
[2]Unquantum Lab, 251 Nelson Avenue, Pacifica, CA 94044, USA, unquant@yahoo.com
[3]Institute for Frontier Science, 6114 LaSalle Avenue, no. 605, Oakland, CA 94611, USA, harryjabs@yahoo.com

Zener diode detectors have been reported to show correlated current output related to the absolute motion of the earth through space [1–4]. Such reports are of utmost importance since it would contradict the Michelson-Morely experiments, the basis of Special Relativity, and connect the randomness of quantum theory with gravitation. Experiments designed to reproduce the reported effects have not seen the reported wave form output or any correlation between Zener diode detectors. Instead we found no detectable signal could be discerned above the noise floor of the digital storage scopes themselves. This does not mean the Cahill's space flow effect does not exist, however the methods reported in the literature do not describe equipment that reproduced the reported measurements.

1 Introduction

Experimental detection of space inhomogeneities flowing at approximately 500 km/sec in the direction of the constellation Vega has been reported [1–3]. Two Zener Diode detectors were oriented in inertial space so that the flow passing first through one detector and subsequently the second detector would produce correlated current output.

A diagram showing a single detector and its circuit diagram copied from reference [1] is shown in Figure 1. The voltage V across the resistor is used to determine the turbulent space flow driven fluctuating tunneling through the Zener diodes. Two such detectors are placed next to each other as shown in Figure 2.

At the bottom of the detector boxes a coaxial cable is shown which in the original experiment connected to a LeCroy Waverunner 6051A 500 MHz, 2 channel 5 Gs/sec Digital Storage Oscilloscope (DSO), which was used to record and display the two resistor voltage measurements. Correlated voltage from the two collocated detectors reported in reference [1] and [2] are shown in Fig 3.

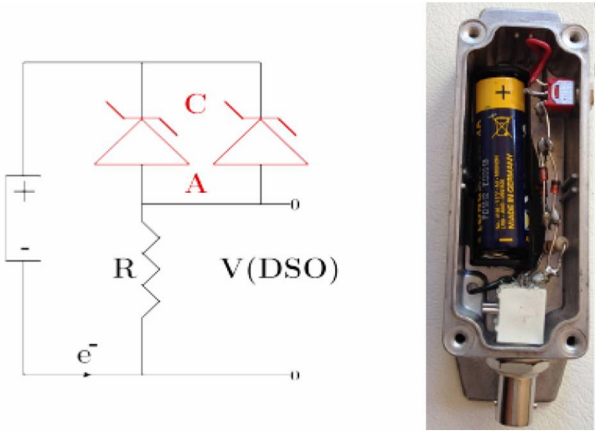

Fig. 1: Left: Circuit of Zener Diode Space Flow Detector, showing a 1.5 V AA battery, two 1N4728A Zener diodes operating in reverse bias mode, having a Zener voltage of 3.3 V, and resistor R=10 kΩ [2].

A clear correlation is indicated by the wave forms of approximately 200 MHz along with some noise. A similar diagram with the two wave forms 180° out of phase was reported when the alignment of the two detectors was reversed so that one coaxial lead came out the top while the second one came out the bottom.

The correlation presumed by R. Cahill is due to structure in the flow which passed through each diode in the detectors. When the detectors were separated by 25 cm and aligned in direction RA=5 h, Dec=-80 deg similar correlation diagrams were shown but required a delay of 0.48 μs to compensate for the flow speed estimated to be 520 km/s from these measurements.

The simplicity of the detectors and the obvious correlated wave forms along with the enormous significance of these

Fig. 2: Two collocated detectors.

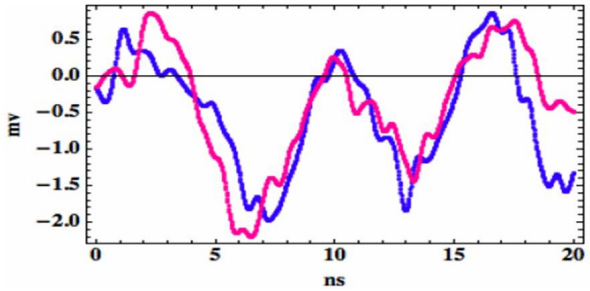

Fig. 3: Correlated current fluctuations as indicated by voltage across resistor R and with DSO operated with 1 MΩ AC input, and no Filters.

reported experiments encouraged us to attempt a verification experiment.

2 Initial verification experiment

The straight forward verification of the Space Flow Detectors was a simple experiment which consisted of building two Space Flow Detectors, connect their two channels to a DSO, move the detectors around a Southerly direction and watch the sum and difference signals on the screen. A qualitative indicator of signal correlation would show a small difference reading for the difference display and relatively large amplitudes in the sum display. Such oscilloscope comparisons are easy to make, and if seen would be the initial indicator that the equipment was functioning properly and the hoped for space flow could be measured.

The initial work was done in E. Reiter's lab. Figure 4 shows the two detectors. Each one has two Zener Diodes closely packed together. The bottom metal square shows the coaxial cable connection. In the left corner the metal shielding tube can be seen. In operation the detectors are completely encased in metal shielding so any external electromagnetic signals would be attenuated all the way to the DSO's two input channels. The initial correlation search experiment was run over many trials, days, orientations, and separation distances.

We also built detectors with more diodes packed in a cluster. A side view of a single detector with 5 z-diodes, in front of the LeCroy Waverunner LT344 500 MHz, 4 channel, 500 Ms/sec DSO, is seen in Figure 5.

No evidence of correlation could be detected. A typical screen shot of the DSO front panel showing Channels 1 and 2, at the first and fourth trace, is shown in Figure 6.

The second and third traces shows an amplified difference and sum trace. These traces show noise without discernible amplitude differences we would expect if correlations were present.

Using the storage facility of the DSO, E. Reiter searched for signals. A typical report reads: "I'm looking at diode noise for 10 div × 20 sec × 1412 sweeps = 282400 s = 3.2

Fig. 4: Two Zener diode detectors.

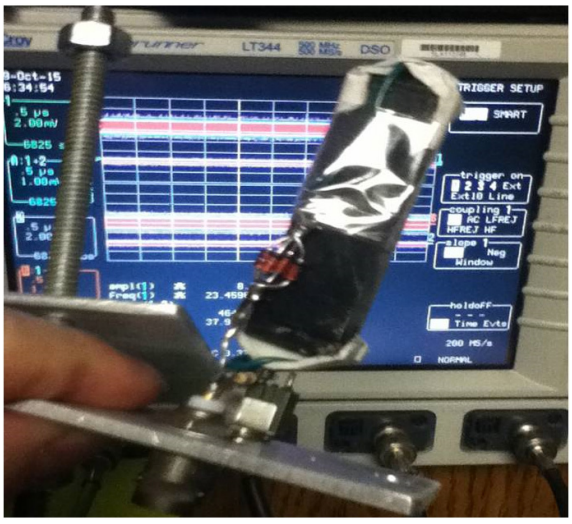

Fig. 5: Detector in front of DSO.

days. It is just non-interesting noise. Trigger is at 0.32 millivolts. I also searched with the trigger at 1 mV to see if there were periodicities; there were none."

We had not seen any indication of either a correlated signal or a periodic wave form as reported in the literature. We must assume something was wrong with our equipment or technique. To get to the bottom of the problem we contacted Prof. Cahill, who helped us diagnose our experimental setup.

3 Configuration refinement

The details of the actual phenomena had to be examined to determine whether any features could be detected. The earth is moving at roughly 500 km/s toward the direction RA=5 h, Dec=-80 deg. Figure 7 shows a space flow coming from the southerly direction. In this orientation the flow past our detectors should be in parallel so that no time delay would be encountered. However if the orientation to the South Sidereal Pole is offset by θ degrees when the spacing between the detector clusters is "d"centimeters then the time delay is

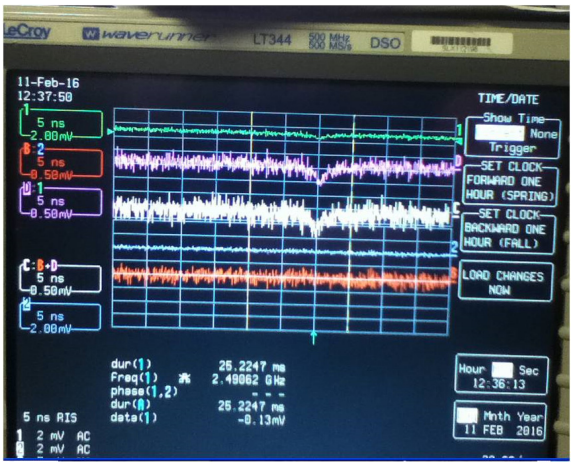

Fig. 6: Typical DSO trace.

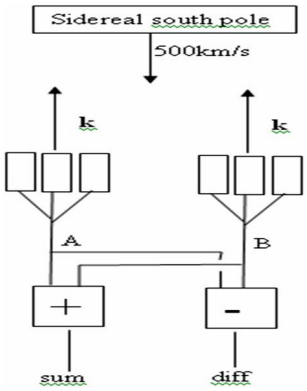

Fig. 7: Detector configuration.

calculated by

$$t = \frac{d\ \sin(\theta)}{500\ \text{km/sec}}. \qquad (1)$$

For a typical spacing of d=5 cm between side by side shielded detectors with an angle of $\theta = 30°$, the delay is 50 ns. The delay time for a 25 cm spacing would be on the order of 250 ns at 30° angle and 500 ns at 90°. This time delay of 0.5 μs corresponds to side by side direction pointing to the Sidereal South Pole and was also calculated in reference [3, Fig. 28].

Wave features similar to those shown in Figure 3 above where published showing wave features with approximate periodicities, of 10 ns in reference [1] Fig. 5, of 100 ns in references [2] Fig. 5, of 6 ns reference [1] Fig. 4, and 200 to 300 ns in reference [3] Fig. 28.

From this analysis it can be concluded that with a 500 Msamples/sec scope all but the highest frequency features reported would be adequately sampled to allow simple correlation. The time delay issue is more critical. Features with a structure on the order of 10 ns can only be convincingly correlated using our sum-difference strategy when the delay between the signals A and B in Fig. 7 is on the order of 1 ns. Using eq. 1 and assuming that the packaging distance "d" is limited to 2 cm the alignment angle must be controlled to,

$$1.4° = \arcsin\left(\frac{1\ \text{ns} \cdot 500\ \text{km/s}}{2\ \text{cm}}\right). \qquad (2)$$

This is not only a difficult orientation tolerance to maintain but the 1.4° angle at 2 cm spacing corresponds to 1.4 mm linear distance by which the diodes must be aligned with each other in a cluster. If the packaging could be reduced to half a centimeter and the time delay restriction relaxed to 2 ns we would get an angular tolerance of 11.5°. This is an orientation tolerance that could be met with fairly primitive equipment.

During our communications with Prof. Cahill many additional possible error sources were discussed. Improper cabling allowing EM radiation from external sources could explain sinusoidal wave forms. This possibility was soundly rejected by Prof. Cahill. Whether additional data processing was used to searched for correlations in oder to achieve the results was also denied. Cherry picking of accidental correlations to show in the reported papers was also denied. Prof. Cahill claimed to have observed consistent and reproducible correlation measurements many times.

We explored the possibility of borrowing the detectors to explore any differences in construction but such an exchange was rejected as time consuming due to the requirements of export regulations. This left some additional theoretical questions. We wondered about the size of the features in both time and space that were predicted. Since correlations were found between well separated detectors after time delay adjustment and time features of between 5 and 200 ns were routinely measured by Prof. Cahill. This could not be a problem.

Could the earth mass between the detector location and the Sidereal South pole attenuate the space flow signals more in the northern hemisphere than the south? A mass shielding effect was not considered likely from Cahills theory and because measurements of the effect were reported involving random number generators in Europe. Therefore the improvement in the three design features discussed above were left to consider when designing a follow on experiment.

4 Follow on experiment design

A repetition of the experiment was planned with the following changes:

1. Collocated detector design with minimum Zener Diode distances
2. careful alignment of the diode cluster to less than 1 mm
3. Less than 10° orientation with the direction of the expected velocity vector.

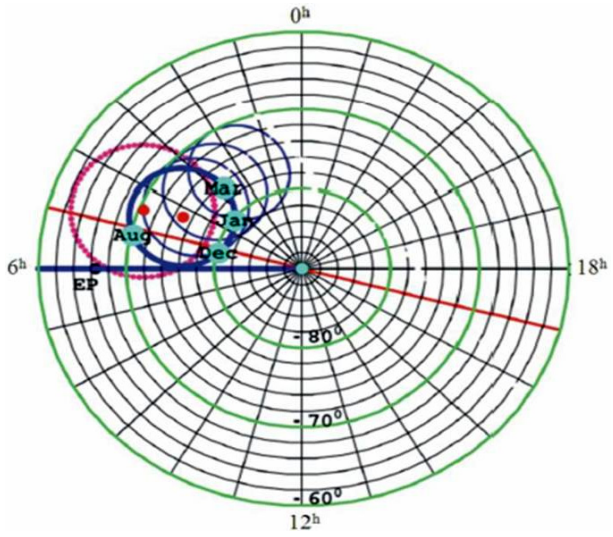

Fig. 8: Earth motion directions [3].

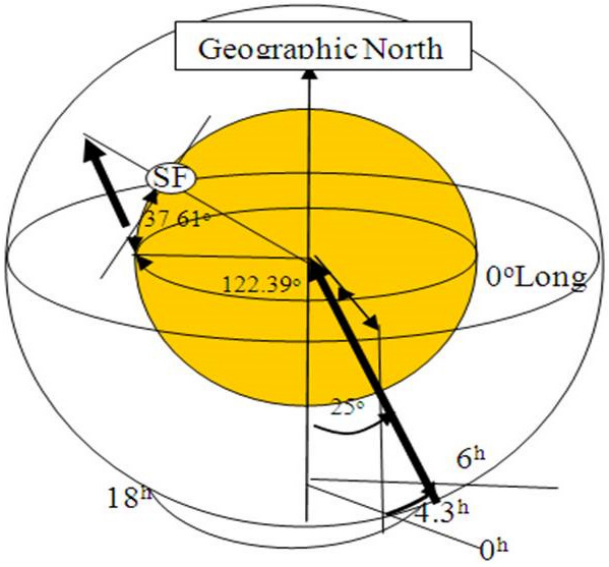

Fig. 9: Sidereal geography.

4.1 Orientation in inertial space

Fig. 8 shows the Sidereal South pole region. The right dot (red) at RA=4.3 h, Dec=75°S is the direction of motion of the solar system through space with a speed of 486 km/s as determined from NASA spacecraft earth-flyby Doppler shifts. The thick circle centered on this direction is the observed velocity direction for different days of the year. Relative to the earth location of the San Francisco Airport is 37.61 latitude and -122.39 longitude.

Figure 9 shows the Earth with San Francisco (SF) on the left edge. The local time in San Fransisco is 3.8 h AM and the Greenwich Meridian 122.39° toward the East is at 0 h. The Sidereal south pole is 4.3 h or 64.5° further east and 75° south latitude. The bold arrow shows the direction of the earth motion pointing toward the center of the earth. The parallel velocity vector at that time will point down toward an elliptic path.

4.2 Detector configuration

A stand placed flat on the ground aligned to geographic North, with a beam pointing down toward the ellipse marked by local time of day shows the direction of the Sidereal South Pole from San Francisco.

A dual detector is aligned so the Zener diodes clusters are correctly aligned to intercept the Flow vector as nearly perpendicular as possible.

The dual detector assembly was constructed with two single Zener diodes, mounted in a sealed metal box to eliminate external noise so that the entire assembly could be oriented perpendicular to the presumed space flow. A variable battery voltage supply was introduced to allow us to adjust the voltage close to the reverse bias breakdown voltage and thereby maximize the expected noise output. Dip switch jumpers

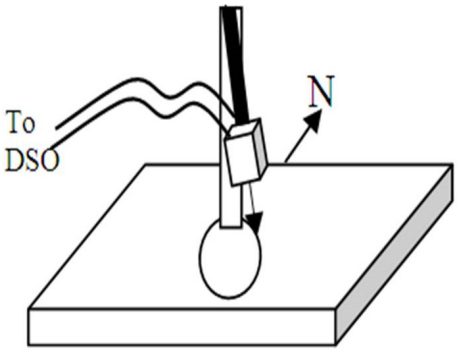

Fig. 10: Detector stand.

were added to allow multiple circuit configurations of the circuit shown in Figure 11.

With this new detector we began calibrating the variable battery voltage to determine the optimum noise output before attempting space flow alignment.

4.3 Experimental result

To our surprise we could not determine any sensitivity of output noise level. The noise level remained the same even when the battery power was completely turned off. In fact after first disconnecting the battery and then disconnecting the Detector from the DSO and replacing the cables with terminators placed directly on the oscilloscope input connector no difference in noise level showed. We had all along been attempting to find correlations between internally generated DSO noise.

Could Dr. Cahill have used a white noise amplifier [5] in his circuit and simply failed to mention the fact? He claimed no amplifier was used but did acknowledge that he had dis-

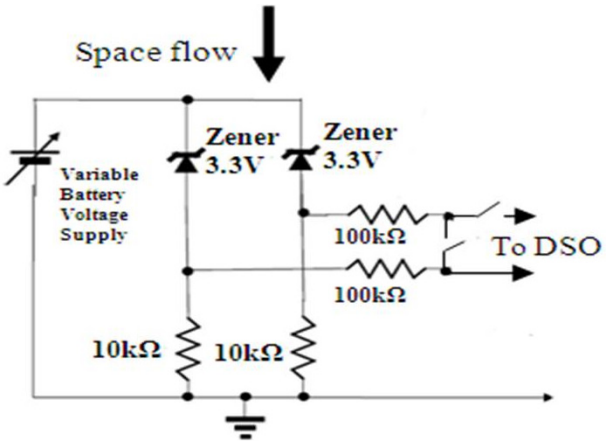

Fig. 11: Dual detector.

covered a space flow correlation simply between DSO devices and sent us the article [6]. We separately tested a second available DSO to verify the noise output when

(a) no detector was attached,

(b) no battery was in the detector, and

(c) everything was connected as described in the literature.

We performed sum and difference signal testing on the two input channels to see if any correlation between the noise sources existed. These experiments also showed nothing. FFT analysis of the signals only showed power at frequencies corresponding to wi-fi routers. Leakage from these high frequency signals were surprisingly difficult to eliminate but clearly not due to Zener diode noise.

5 Conclusion

We have attempted to verify the space flow detector experiment reported by Dr. Cahill which reported an effect that is consistent with the absolute motion of the earth through inertial space. Our conclusions are:

1. Zener Diode circuits without a white noise amplifier could not provide the signal levels reported in the literature as duplicated here in Figure 3.
2. Nothing in any signals produced by Zener diodes in reverse bias mode contains substantial power at frequencies whether of the 7ns periods or any others published by Dr. Cahill.
3. Internal Noise by Zener Diodes or other components in DSO equipment may be the source of the signals reported by Dr. Cahill.
4. There is no indication any signals generated by equipment reported by Dr. Cahill in the literature contains correlations that can support the space flow hypothesis.

No statement is made here regarding the theory of space flow as proposed by R. Cahill. There are other experiments supporting similar theoretical results [7] are also controversial [8]. Only the ability to detect space flow with the Zener diode detector design reported by Cahill in the literature has been tested.

In order to further explore the possibility that a Cahill type space flow disturbance may exist and may have a detectable effect on quantum devices it will be necessary to repeat Dr. Cahill's correlation experiments augmented by white noise amplifiers, statistical correlation software, and adequate shielding tested to eliminate any possibility of local signal corruption.

Submitted on February 4, 2017 / Accepted on February 19, 2017

References

1. Cahill R.T. Quantum Gravity Experiments. *Progress in Physics*, 2015 v. 11, 317–320.
2. Cahill R.T. Gravitational Wave Experiments with Zener Diode Quantum Detecors: Fractal Dynamical Space and Universe Expansion with Inflation Epoch. *Progress in Physics*, 2014 v. 10, 131–138.
3. Cahill R.T. Review of Gravitational Wave Detections: Dynamical Space. *Physics International*, 2014 v. 5(1), 49–86.
4. Cahill R.T. Process Physics: Emergent Unified Dynamical 3-Space, Quantum and Gravity-a Review. *Physics International*, 2015 v. 6(2), 51–67.
5. Application note, Building a Low-Cost White Noise Generator, Electronics Sep-Oct 2004: http://www.maximintegrated.com/en/app-notes/index.mvp/id/3469
6. Cahill R.T. Nanotechnology Quantum Detectors for Gravitational Waves: Adelaide to London Correlations Observed. *Progress in Physics*, 2013, v. 4, 57–62.
7. Silvertooth E.W. and Whitney C.K. A New Michelson-Morley Experiment. *Physics Essays*, 1992, v. 5, 1, 82–88.
8. Marett D. A Replication of the Silvertooth Experiment (2012) http://www.conspiracyoflight.com/Silvertooth/Silvertooth.pdf

LETTERS TO PROGRESS IN PHYSICS

Calculating the Parameters of the Tetraneutron

Anatoly V. Belyakov
E-mail: belyakov.lih@gmail.com

A large international group of theorists, using the high precision nucleon-nucleon interaction between neutrons, issued the theoretical estimates of the four-neutron (4n) system resonance state energy and its lifetime. For this purpose numerous calculations using supercomputers have been made and obtained the values of 0.84 MeV and 5×10^{-22} seconds. The same results were obtained with much less efforts based on the mechanistic interpretation of John Wheeler's geometrodynamic idea.

1 Introduction

In the Japanese RIKEN Institute as a result of experiments by the decay of 8He nuclei (alpha particle and four neutrons) some events managed to allocate, which are interpreted as short-lived resonance state of the tetraneutron. In a recent article, published in Physical Review Letters [1], according to calculations the tetraneutron resonance energy is estimated at 0.84 MeV, and its lifetime is about 5×10^{-22} seconds, which is consistent with the Japanese experimental data.

According to the first author of the article Andrey Shirokov (MSU: Lomonosov Moscow State University), "*... theoretical approach has been carefully designed and numerous calculations using supercomputers were made...*". For the calculation of only a few parameters characterizing tetraneutron scientific forces of the various institutes and organizations were involved in the work process and the expensive computing resources based on international scientific cooperation were expended. As stated in the original, "*Computational resources were provided by NERSC, which is supported by the U.S. Department of Energy under Contract No. DE-AC02-05CH11231 and by Lawrence Livermore National Laboratory (LLNL) institutional Computing Grand Challenge program under Contract No. DEAC52-07NA27344*".

There is a great regret for the efforts and the lack of other physical paradigms that could have given the same result with much less expenses. The same is confirmed by the authors themselves: "*More recent state-of-the-art theoretical calculations have concluded that without altering fundamental characteristics of the nuclear forces, the tetraneutron should not be bound. More theoretical calculations were performed, all of them agreeing that a bound tetraneutron is not supported by theory*".

2 Calculation of the tetraneutron parameters

The basis for one of the alternative theories could be a model based on the use of the elementary *mechanistic interpretation of J. Wheeler's geometrodynamic concept* where the charges are seen as singular points on the three-dimensional surface, connected "wormholes" or current tubes by drain-source type through an extra dimension, forming in general a closed *contour*. It is assumed the existence of common or similar natural laws, which are reproduced at different scale levels of matter. Earlier, on the basis of this model the binding energy of the deuteron, triton and alpha particle have been determined [2], as well as many other parameters for both micro- and macrocosm [3–6].

We now determine the binding energy for the tetraneutron. Let us recall that the contour or vortex thread having a radius r_e and the linear density m_e/r_e, along which some medium with velocity v circulates, a vortex thread with radius r fills a spiral manner. The vortex thread can be regarded as completely "stretched", i.e. elongated proportional to r_e/r or, on the contrary, extremely "compressed", i.e. shortened proportional to r_e/r and filling all the vortex tube of radius r_e.

In papers [3, 4], proceeding from the conditions of conservation of charge and constancy of the linear density when contour's changing, parameters of the vortex thread v, r for an arbitrary plus-minus contour is defined as a proportion of the light speed and electron radius as:

$$v = \frac{c_0^{1/3}}{(an)^2}, \tag{1}$$

$$r = \frac{c_0^{2/3}}{(an)^4}, \tag{2}$$

where n is the own quantum number for the microparticles, a is the inverse fine structure constant, c_0 is the dimensionless velocity of light, $c/[\text{m}/\text{sec}]$. For the proton

$$n = \left(\frac{2c_0}{a^5}\right)^{1/4} = 0.3338, \tag{3}$$

and of the above formulas it follows: $v = 0.320$, $r = 0.102$.

Assume that neutrons, surrounding an alpha particle before decay of 8He, is polarized the same as in the alpha-particle (1, −2/3, and 1/3). Let the four polarized neutrons disposed symmetrically like the nucleons in the alpha particle, as shown in the figure. Charge radius neutrons r_n is assumed to be the radius of the proton, plus 3% (since on this

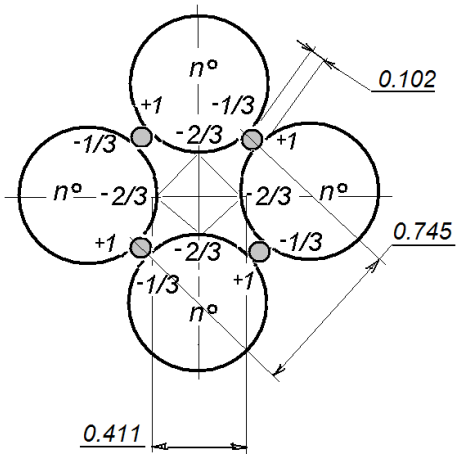

value the radius of the neutron magnetic moment distribution is increased in comparison with that of a proton), then

$$r_n = 0.322\ (\text{or } 9.07) \times 10^{-16}\ \text{m}. \tag{4}$$

There are taken into account four interactions between charges of $+1$ and $-1/3$ (attraction) at a distance $r = 0.102$, and six interactions between charges of $-2/3$ (repulsion), i.e. their projections on the sides of the square and along the diagonals at distances determined from geometrical considerations (0.291 and 0.411). The minimum distance between the charges made equal to the transverse dimension of the nucleon vortex tube (thread) $r = 0.102$. This characteristic size has also been adopted by reason that for the magneto-gravitational equilibrium with given parameter and charges of $+1$ and $-1/3$ the product of the quark masses, involved in the circulation contour, found to be equal to the value of 84.3. Thus, the average mass of the quarks $(84.3)^{1/2} = 9.18$ is nearly the mass of two neutron quarks $(8.6\, m_e)$, defined on the basis of entirely different reasons earlier [4].

The tetraneutron bonds form a closed system, so one can assume that the tetraneutron binding energy is the averaged binding energy of a link, since at destruction of a link the particle splits as a whole (as the alpha particle). Having in mind the accepted scheme of charges arrangement, tetraneutron geometry, and specified dimensions, we can write the final formula for the binding energy as the average energy per bond. For single charges in units of MeV, and in a proportion of r_e we have:

$$E = \frac{0.511}{r}\,. \tag{5}$$

In our case by substituting the data we obtain:

$$E = \frac{0.511}{4} \times \left(\frac{4 \times 1 \times \frac{1}{3}}{0.102} - \frac{4 \times \frac{2}{3} \times \frac{2}{3} \times \cos 45^\circ}{0.291} - \right.$$
$$\left. - \frac{2 \times \frac{2}{3} \times \frac{2}{3}}{0.411} \right) = 0.835. \tag{6}$$

Note, that if the charges of the polarized neutron is $(+2/3, -1/3$, and $1/3)$, and in this case the binding energy is approximately the same amount.

Tetraneutron instability can be explained by the fact that kinetic energy of the tetraneutron quarks (having a total mass m_k and rotating on the same radius r at speed v), is comparable to the binding energy. Let's equate these energies. At the units of MeV we have:

$$m_k\, m_e\, (vc)^2 = 0.835\ \text{MeV}. \tag{7}$$

Since $m_e c^2 = 0.511$ MeV, then from (7), by substituting the values of v, we have $m_k = 16.0$. That is, the value, which is close to the total two neutron quark mass involved in the circulation counter, creates the inertia repulsive forces that can destroy, at least, one bond of the tetraneutron.

The lifetime of the tetraneutron τ is determined from the reason of the duration of existence of four neutrons in a bound state, which should at least be sufficient for one circulation of medium flow along the contour having some diameter d. Suppose that it is equal to the distance between the centers of neutrons, $d = 0.745$.

Then, taking into account the "stretching" (i.e. elongation of the vortex thread is a multiple of $1/r$ and decreasing in the flow velocity is a multiple of v), and substituting the data we obtain:

$$\tau = \frac{\pi\, d\, r_e}{c} \times \frac{1}{vr} = 6.73 \times 10^{-22}\ \text{sec}. \tag{8}$$

3 Conclusion

Thus, the calculated parameters of the tetraneutron are consistent with those obtained in the experiments of RIKEN and coincide to those declared in [1] that once again proves the validity of the proposed model.

Submitted on January 22, 2017 / Accepted on January 25, 2017

References

1. Shirokov A. M., Papadimitriou G., Mazur A. I., Mazur I. A., Roth R., Vary J. P. Prediction for a four-neutron resonance. *Phys. Rev. Lett.*, 2016, v. 117, 182502; arXiv: 1607.05631 [nucl-th].
2. Belyakov A. V. Nuclear power and the structure of a nucleus according to J. Wheeler's geometrodynamic concept. *Progress in Physics*, 2015, v. 11, issue 1, 89–98.
3. Belyakov A. V. Charge of the electron, and the constants of radiation according to J. A. Wheeler's geometrodynamic model. *Progress in Physics*, 2010, v. 4, 90–94.
4. Belyakov A. V. Macro-analogies and gravitation in the micro-world: further elaboration of Wheeler's model of geometrodynamics. *Progress in Physics*, 2012, v. 2, 47–57.
5. Belyakov A. V. Determination of the neutrino mass. *Progress in Physics*, 2016, v. 12, issue 1, 34–38.
6. Belyakov A. V. Evolution of stellar objects according to J. Wheeler's geometrodynamic concept. *Progress in Physics*, 2013, v. 1, 25–40.

Harmonic Orbital Resonances and Orbital Long-Range Order of the TRAPPIST-1 Exoplanetary System

Felix Scholkmann
Research Office for Complex Physical and Biological Systems (ROCoS),
Mutschellenstr. 179, 8038 Zurich, Switzerland. E-mail: felix.scholkmann@gmail.com

Recently, seven exoplanets orbiting the ultra-cool dwarf star TRAPPIST-1 were reported. The present paper explores whether (i) the sequence of semi-major axis values of the planets shows a long-range order, and whether (ii) the values can be described by harmonic orbital resonances. The analysis showed that orbits of the planets follow (i) a long-range order, and (ii) a quantization in accordance with harmonic orbital resonances. The study supports the view that planetary systems are best viewed as self-organizing systems with attractor states of the planet orbits being related to resonance effects.

1 Introduction

A paper [1] was recently published on the discovery and description of an extrasolar planetary system with seven planets (TRAPPIST-1b, c, d, e, f, g and h) orbiting an ultra-cool dwarf star (TRAPPIST-1, 2MASS J23062928-0502285; apparent magnitude: $V = 18.80$) in the constellation Aquarius (RA = $23^{\mathrm{h}}\,06^{\mathrm{m}}\,29.28^{\mathrm{s}}$, dec = $-05^{\circ}\,02'\,28.5''$).

This discovery was the result of an intensive observation program using space- and earth-based telescopes comprising the TRAPPIST (TRansiting Planets and PlanetsIsimals Small Telescope) North system (Chile), the TRAPPIST-North telescope (Morocco), the Himalayan Chandra Telescope (India), the Very Large Telescope (Chile), the UK Infrared Telescope (Hawaii), the Spitzer Space Telescope, the William Herschel and Liverpool telescopes (La Palma, Spain), as well as the South African Astronomical Observatory telescope [1, 2].

The orbital parameters of the TRAPPIST-1 planetary system exhibit a non-random behaviour, i.e., "the six inner planets form the longest known near-resonant chain of exoplanets, with the ratios of the orbital periods (P) $P_{\mathrm{c}}/P_{\mathrm{b}}$, $P_{\mathrm{d}}/P_{\mathrm{c}}$, $P_{\mathrm{e}}/P_{\mathrm{d}}$, $P_{\mathrm{f}}/P_{\mathrm{e}}$ and $P_{\mathrm{g}}/P_{\mathrm{f}}$ being close to the ratios of small integers, namely 8/5, 5/3, 3/2, 3/2 and 4/3, respectively", as noted in the recent *Nature* publication [1]. A property that is associated with an *orbital resonance*, or a mean-motion orbital resonance, in particular. Other examples of planetary systems where the *orbital periods* are in a specific resonance-like relationship include the exoplanetary systems Kepler-223 [3], Kepler-80 [4], GJ 876 [5] and HD 82943 [6]. If the orbital *periods* show this resonance phenomenon, then also the orbital *spacing* of a planetary system follows the same pattern – a direct consequence of Kepler's third law linking the orbital spacing (given as the semi-major axis, (a)) with the period of an planet orbiting a star, $P^2 \propto a^3$, leading to the relationships $a \propto P^{2/3}$ and $P \propto a^{3/2}$.

The orbital resonances can be analysed by examining the orbital spacings locally and separately, or by analysing the whole planetary system orbital spacing *in toto*. Foundational work on this second approach was conducted by J. Bohr and K. Olsen [9, 10] who showed that the orbital spacing of the planets of our solar system follows long-range order on a logarithmic scale, i.e., the logarithmic positions of the planets are correlated and follow a periodic pattern (a kind of "quantization") [9]. This long-range order of the orbital spacing was also detected in the exoplanetary system HD 10180 [10]. Stimulated by this work, I showed in 2013 that the orbital spacing of the exoplanetary system Kepler-62 exhibits a long-range order too and I predicted an additional planet (which has not been detected yet, however) based on this analysis [7].

The discovery of the TRAPPIST-1 planetary system [1] triggered the question of whether the orbital spacing of this system also follows a long-range order, and how the orbital structure of the planetary system can be described based on approach of orbital resonances. The aim of the present work was therefore to investigate these two asepcts in detail.

2 Materials and methods

2.1 Data

The parameter values of the TRAPPIST-1's exoplanets were obtained from Gillon et al. [1]. In the present work, two parameters were selected for analysis: the semi-major axis (a) and the radius (r) of each planet (see Table 1).

2.2 Analysis of the orbital long-range order

To analyse the TRAPPIST-1 system, the same approach as already employed for the previously published analysis of the Kepler-62 system [7] was used. In particular, the semi-major axis values a (given in units of 10^6 km) of each exoplanet were first divided by 10^6 km, then logarithmized ($\hat{a}_i = \ln(a_i/10^6\,\mathrm{km})$) and according to these values a multimodal probability distribution function (PDF) $p(\hat{a})$ was calculated by

$$p(\hat{a}) = \sum_{i=1}^{N} \alpha_i \, e^{-\beta}, \tag{1}$$

Planet	i	a [AU]	a [km]	r [$R_\oplus$]	r [km]	$\hat{a}$
b	1	0.01111 ± 0.00034	$1.6621\times 10^6 \pm 5.0864 \times 10^4$	1.086 ± 0.035	6926.508 ± 223.23	0.5081
c	2	0.01521 ± 0.00047	$2.2754 \times 10^6 \pm 7.0312 \times 10^4$	1.056 ± 0.035	6735.168 ± 223.23	0.8222
d	3	$0.02144^{+0.00066}_{-0.00063}$	$3.2074 \times 10^6\ ^{+9.8736\times 10^4}_{-9.4248\times 10^4}$	0.772 ± 0.03	4923.816 ± 191.34	1.1655
e	4	$0.02817^{+0.00083}_{-0.00087}$	$4.2142 \times 10^6\ ^{+1.2417\times 10^4}_{-1.3015\times 10^4}$	0.918 ± 0.039	5855.004 ± 248.742	1.4385
f	5	0.0371 ± 0.0011	$5.5502 \times 10^6 \pm 1.6456 \times 10^5$	1.045 ± 0.038	6665.01 ± 242.364	1.7138
g	6	0.0451 ± 0.0014	$6.7470 \times 10^6 \pm 2.0944 \times 10^5$	1.127 ± 0.041	7188.006 ± 261.498	1.9091
h	7	$0.063^{+0.027}_{-0.013}$	$9.4248 \times 10^6\ ^{+4.0392\times 10^6}_{-1.9448\times 10^6}$	0.755 ± 0.034	4815.39 ± 216.852	2.2433

Table 1: TRAPPIST-1 system parameters according to [1]. i: planet number counting outwardly from the star TRAPPIST-1, a: semi-major axis, r: radius of the planet, $\hat{a}_i = \ln(a_i/10^6\ \text{km})$, a and r are given in two different units ([AU], [km]) and ([$R_\oplus$], [km]), respectively.

with $N = 7$ (i.e., the maximum number of planets of the TRAPPIST-1 system) and β given as

$$\beta = \frac{j - \hat{a}_i}{w_p / 2\sqrt{2\ln(2)}}, \qquad (2)$$

for $j = 1, 1.01, 1.02, \ldots, 3$, with w_p the width (i.e., the full-width-at-half-maximum) of each Gaussian peak of the PDF, and α_i a scale factor. This approach was first introduced by Bohr and Olsen [9]. The scale factor α in equation (1) defines the magnitude of each peak of the PDF and was assigned to the radius of the specific planet ($\alpha_i = r_i$). With this the size of the planets is incorporated to determine the PDF, i.e., larger planets then contribute more to the overall multimodal PDF than smaller planets. The width of each peak w_p was set to such a parameter value that is was ensured that an optimum compromise between a too strong overlap of the Gaussian peaks on the one side and to small peaks on the other was realized. This was ensured with $w_p = 0.15$. The final multimodal PDF, $\rho(\hat{a})$, then represents a sum of Gaussian peaks located at the logarithmized planets' semi-major axis values ($\hat{a}$) and weighted by the individual radius value of the planet (α_i).

To quantify the correlation structure of $\rho(\hat{a})$, the autocorrelation function (ACF) of $\rho(\hat{a})$ was determined according to equations (3) and (4) given in [7]. The ACF properties correspond to the type and grade of the order (short- or long-range) of the input sequence. Finally, the frequency-dependent power spectral density (PSD) of the multimodal PDF $\rho(\hat{a})$ was determined by the periodogram method.

At present, the exact semi-major axis value of the exoplanet TRAPPIST-1h is known only with large uncertainity ($a = 0.063\ ^{+0.027}_{-0.013}$ AU). In an additional analysis, it was tested which a value in the range [0.05, 0.09] AU will maximize the long-range order of the orbital spacing. The maximum was determined by fitting an exponential function to the orbital spacing values while changing the a value for the planet 1h in the range given. The goodness-of-fit was then determined by the coefficient of determination (R^2) and the root-mean-square error (RMSE). The a value that maximized the R^2 and minimized the RMSE was chosen as the one to most likely representing the true value for this exoplanet.

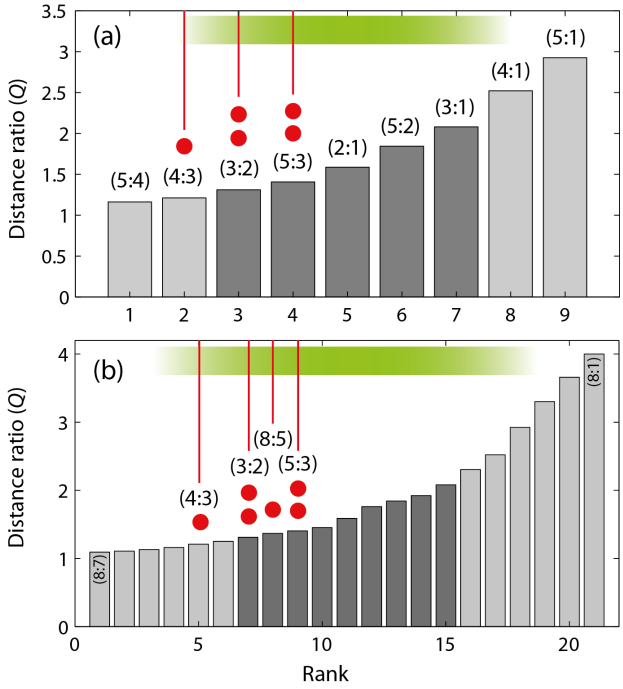

Fig. 1: Distance ratios Q with respect to the rank (given according to the period ratios q). The red dots and vertical lines mark the positions of the exoplanet's orbits according to the distance ratios. (a) Range of distance ratios as used by Aschwanden and McFadden [8]. (b) Range of distance ratios as used in the present study. The green bar marks the interval where it is most likely to find the distances ratios based on empirical data (according to [8]).

2.3 Analysis of harmonic orbital resonances

The methodology based on the recently published *harmonic orbit resonance model* by Aschwanden and McFadden [8] was employed for this analysis. The harmonic orbit resonance model states that the planetary system is best viewed as a self-organisation system where the orbital parameters evolve to attractor states in the sense of harmonical relations (the harmonic orbit resonance). Attracttor states of the orbits are realised when harmonical relations are reached, ensuring stability of the planetary system. The basic idea is that the distance ratios (Q) of semi-major axis values a are (i) not

Harmonic ratio ($H_{i+1} : H_i$)	Distance ratio (Q)	Period ratio (q)	Rank (#)
(8:7)	1.0931	1.1429	1
(8:5)	1.3680	1.6000	8
(8:3)	1.9230	2.6667	14
(8:1)	4.0000	8.0000	21
(7:6)	1.1082	1.1667	2
(7:5)	1.2515	1.4000	6
(7:4)	1.4522	1.7500	10
(7:3)	1.7592	2.3333	12
(7:2)	2.3052	3.5000	16
(7:1)	3.6593	7.0000	20
(6:5)	1.1292	1.2000	3
(6:1)	3.3019	6.0000	19
(5:4)	1.1604	1.2500	4
(5:3)	1.4057	1.6667	9
(5:2)	1.8420	2.5000	13
(5:1)	2.9240	5.0000	18
(4:3)	1.2114	1.3333	5
(4:1)	2.5198	4.0000	17
(3:2)	1.3104	1.5000	7
(3:1)	2.0801	3.0000	15
(2:1)	1.5874	2.0000	11

Table 2: Numerical values of the harmonic ratios, distance ratios and period ratios for all harmonic ratios in the interval (2 : 1) to (8 : 7). The rank of the harmonic ratios is given according to the period ratio values.

constant for a planetary system and (ii) show a quantization whereas only specific values are "allowed" according to

$$Q = \left(\frac{a_{i+1}}{a_i}\right) = \left(\frac{H_{i+1}}{H_i}\right)^{2/3}, \quad (1)$$

with H being harmonic numbers ($H = [1, 2, \ldots, M]$) that form harmonic ratios. Due to Kepler's third law, this equation leads automatically also to quantized orbital period ratios q:

$$q = \left(\frac{P_{i+1}}{P_i}\right) = \left(\frac{a_{i+1}}{a_i}\right)^{3/2} = Q^{3/2}. \quad (1)$$

For $M = 8$ (i.e., $H = [1, 2, \ldots, 8]$), the attractor states are realized by the harmonic ratios $Q = (H_{i+1}/H_i) = (8 : 7)$, $(8 : 5)$, $(8 : 3)$, $(8/1)$, $(7 : 6)$, $(7 : 5)$, $(7 : 3)$, $(7 : 2)$, $(7 : 1)$, $(6 : 5)$, $(6 : 1)$, $(5 : 4)$, $(5 : 3)$, $(5 : 2)$, $(5 : 1)$, $(4 : 3)$, $(4 : 1)$, $(3 : 2)$, $(3 : 1)$ and $(2 : 1)$. The associated numerical values of the distance and period ratios are given in Table 2. When sorted in ascending order of q, the attractor values of the distance ratios Q follow the function as shown in Figure 1. The most dominant ratios in a planetary system, according to Aschwanden and McFadden [8], are marked with a green bar.

3 Results

3.1 Orbital long-range order

As shown in Figure 2(c) the analysis of the semi-major axis values of TRAPPIST-1's planets b-h revealed an exponential function (or a quasi linear one when logarithmized values were used; Figure 2(d)). The parameter values for the exponential function $f(n) = \alpha \exp^{\beta n}$ were found to be (given as optimal value (95% confidence bound)): $\alpha = 4.086 \times 10^6$ $(3.85 \times 10^6, 4.321 \times 10^6)$, $\beta = 0.5936$ $(0.5398, 0.6475)$.

In an additional analysis, it was investigated if the fit with an exponential function related to the Titius-Bode law [12] in the form $f(n) = \alpha + \beta 2^n$ was better or worse at describing the data than the exponential function of type $f(n) = \alpha \exp^{\beta n}$ (with α and β free parameters), as also used by Naficy et al. [11] to describe the planetray orbit scaling. It was found (see Figures 4(a) and (b)) that the second exponential model fitted the data better than the first one (coefficient of determination (R^2: 0.9921 and 0.9944, respectively).

Figure 2(e) shows the calculated multimodal PDF. The ACF and the power spectrum are depicted in Figures 2(f) and 2(g), respectively. A clear peak of the spectrum of the multimodal PDF is evident with a center frequency of 3.47 $1/\hat{a}$, corresponding to a an orbital spacing regularity with a spacing of 0.288.

3.2 Prediction of the TRAPPIST-1h exoplanet position

Figure 3 depicts the results of the analysis investigating how the orbital position of the TRAPPIST-1h exoplanet has an effect on the long-range order. The "optimal" position (i.e., maximizing R^2 and minimizing RMSE) were found to be in the range $a = [0.060, 0.061$ AU].

3.3 Harmonic orbital resonances

The analysis with the *harmonic orbit resonance model* by Aschwanden and McFadden [8] revelaed that all exoplanets of the TRAPPIST-1 system occupy orbitals that are attractor states according to the harmonic orbital resonance model (see Figure 4(c)). The harmonic ratios describing the planetary system are found to be: $(H_{i+1}/H_i) = (4 : 3)$, $(3 : 2)$, $(8 : 5)$, and $(5 : 3)$. The ratios $(3 : 2)$, $(8 : 5)$, and $(5 : 3)$ are in the interval where the most dominant ratios are being expected according to Aschwanden and McFadden [8]. The ratios $(4 : 3)$ is at the border of this interval (see Figure 1).

4 Discussion and conclusion

The following conclusions can be drawn from the analysis conducted in the present study:

(i) The orbitals of the exoplanets of the TRAPPIST-1 planetary system exhibit a long-range order. This property is cleary visible in the linear periodicity of the multimodal PDF when lograithmizing the distances between the planets. The single peak in the power spectrum quantifies this characteristic.

(ii) The orbital postition of the TRAPPIST-1h exoplanet is most likely in the range of $a = [0.060, 0.061$ AU].

(iii) All exoplanets of the TRAPPIST-1 system occupy orbitals that are attractor states according to the harmonic orbital resonance model.

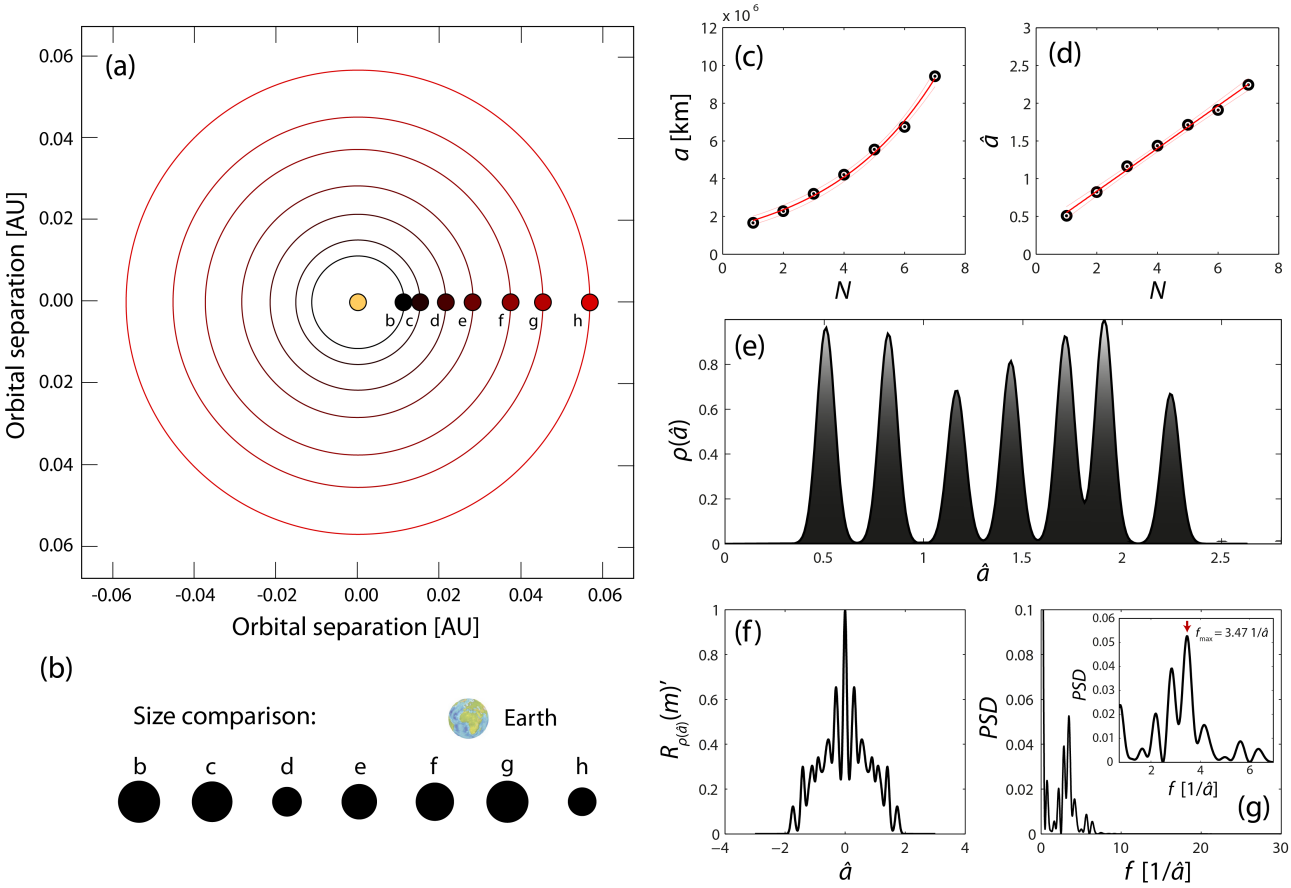

Fig. 2: (a) Diagram with the orbits of the exoplanets of TRAPPIST-1. (b) Comparison of the exoplanets' sizes with respect to the size of the Earth. (c, d) Semi-major axis values with respect to the rank (n), plotted in linear and logartihmic space, respectively. (e) Multimodal PDF of the seven exoplanets. (f) ACF and (f) power spectrum of the multimodal PDF

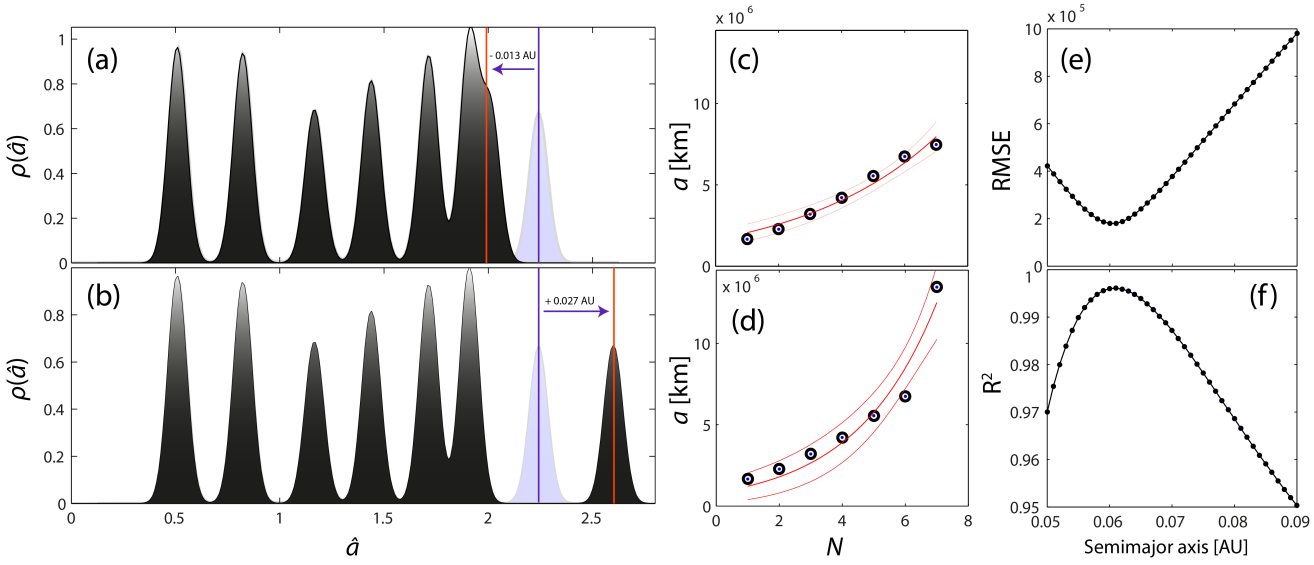

Fig. 3: (a, b) Multimodal PDFs $\rho(\hat{a})$ with different positions of the exoplanet TRAPPIST-1h. The corresponding scaling functions (a vs. rank (n)) are shown in (c) and (d), respectively. (e) R^2 vs. a. (f) RMSE vs. a.

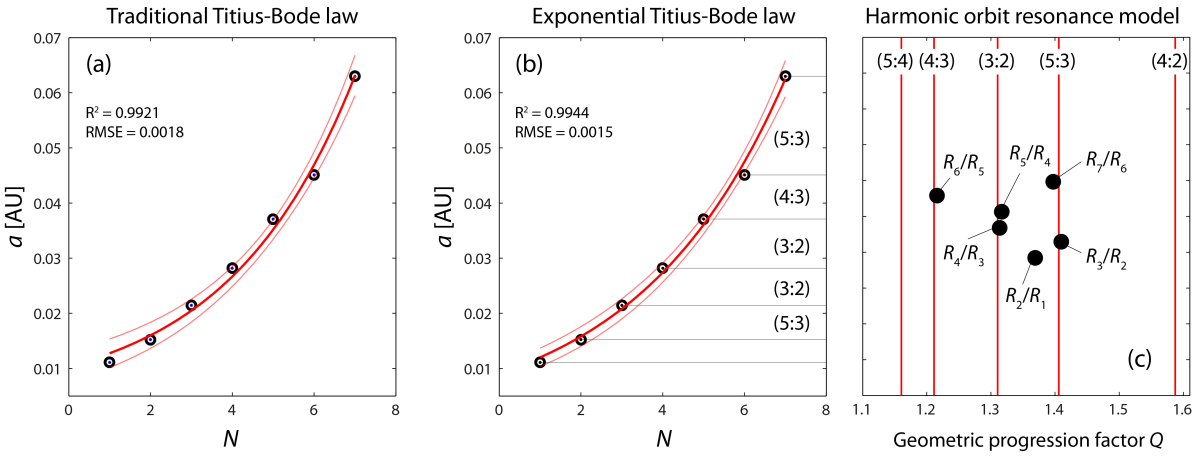

Fig. 4: Fitting of the semi-major axis values with two different types of exponential functions, i.e., (a) $f(n) = \alpha + \beta\, 2^n$ and (b) $f(n) = \alpha \exp^{\beta n}$. (c) Predicitons of the orbital positions according to the harmonic orbit resonance model, and the corresponding values of the TRAPPIST-1 exoplanetary system.

What is the physical mechanism causing this long-range order and the harmonic orbital resonances? A review of different approaches and models related to this question can be found in my previously published paper [7] as well as one recently published by Aschwanden and McFadden [8]. In my opinion, the most promising and interesting aproaches are those based on plasma physics [13–17], the concept of macroscopic quantization due to finite gravitational propagation speed [18], and the view that the solar system is a self-organising system with attractor states leading to harmonic orbit resonances [8].

In conclusion, the present analysis of the extrasolar planetary system TRAPPIST-1 reveals that the semi-major axis values of the planets follow (i) a long-range order and (ii) a quantization in accordance with the harmonic orbital resonance model. Furthermore, the analysis predicts that the exact position of the exoplanet TRAPPIST-1h is in the range of $a = [0.060, 0.061$ AU], slightly less then the determined mean semi-major axis value of 0.063 AU given by Gillon et al. [1].

References

1. Gillon M., Triaud A.H.M., Demory B.-O., Jehin E., Agol E., et al. Seven temperate terrestrial planets around the nearby ultracool dwarf star TRAPPIST-1. *Nature*, 2017, v. 542, 456–460.
2. Gillon M., Jehin E., Lederer S.M., Delrez L., et al. Temperate Earth-sized planets transiting a nearby ultracool dwarf star. *Nature*, 2016, v. 533, 221–224.
3. Mills S.M., Fabrycky D.C., Migaszewski C., Ford E.B., et al. A resonant chain of four transiting, sub-Neptune planets. *Nature*, 2016, v. 533, 509–512.
4. MacDonald M.G., Rogozzine D., Fabrycky D.C., Ford E.B., Holman M.J., et al. A dynamical analysis of the Kepler-80 system of five transiting planets. *The Astronomical Journal*, 2016, v. 152 (4), 105.
5. Man Hoi L. and Peale S.J. Dynamics and origin of the 2:1 orbital resonances of the GJ 876 planets. *The Astrophysical Journal*, 2002, v. 567 (1), 596–609.
6. Goździewski K. and Maciejewski A.J. Dynamical analysis of the orbital parameters of the HD 82943 planetary system. *The Astrophysical Journal*, 2001, v. 563 (1), L81.
7. Scholkmann F. A prediction of an additional planet of the extrasolar planetary system Kepler-62 based on the planetary distances' long-range order. *Progress in Physics*, 2013, v. 4, 85–89.
8. Aschwanden M.J. and McFadden L.A. Harmonic resonances of planet and moon orbits – From the Titius-Bode law to self-organizing systems *arXiv:1701.08181 [astro-ph.EP]*.
9. Bohr J. and Olsen K. Long-range order between the planets in the Solar system. *Monthly Notices of the Royal Astronomical Society*, 2010, v. 403, L59–L63.
10. Olsen K. and Bohr J. Pair-correlation analysis of HD 10180 reveals a possible planetary orbit at about 0.92 AU. 2010, arXiv: astro-ph.EP/1009.5507.
11. Naficy K., Ayubinia A. and Saeedi M. Exponential law as a more comp atible model to describe orbits of planetary systems. *Iranian Journal of Physics Research*, 2012, v. 12 (3), 25–31.
12. Jaki S. L. The early history of the Titius-Bode law. *American Journal of Physics*, 1972, v. 40 (7), 1014–1023
13. Wells D. R. Was the Titius-Bode series dictated by the minimum energy states of the generic solar plasma? *IEEE Transactions on Plasma Science*, 1990, v. 19 (1), 73–76.
14. Wells D. R. Titius-Bode and the helicity connection: a quantized field theory of protostar formation. *IEEE Transactions on Plasma Science*, 1989, v. 14 (6), 865–873.
15. Wells D. R. Quantization effects in the plasma universe. *IEEE Transactions on Plasma Science*, 1989, v. 17 (2), 270–281.
16. Wells D. R. Unification of gravitational, electrical, and strong forces by a virtual plasma theory. *IEEE Transactions on Plasma Science*, 1992, v. 20 (6), 939–943.
17. Livadiotis G., McComas D.J. Evidence of large-scale quantization in space plasmas. *Entropy*, 2013, v. 15, 1118–1134.
18. Giné J. On the origin of the gravitational quantization: The Titius–Bode law. *Chaos, Solitons & Fractals*, 2007, v. 32 (2), 362–369.

LETTERS TO PROGRESS IN PHYSICS

Introducing a Theory of Neutrosophic Evolution: Degrees of Evolution, Indeterminacy, and Involution

Florentin Smarandache
University of New Mexico, 705 Gurley Ave., Gallup, NM 87301, USA. E-mail: smarand@unm.edu

During the process of adaptation of a being (plant, animal, or human), to a new environment or conditions, the being partially evolves, partially devolves (degenerates), and partially is indeterminate i.e. neither evolving nor devolving, therefore unchanged (neutral), or the change is unclear, ambiguous, vague, as in neutrosophic logic. Thank to adaptation, one therefore has: evolution, involution, and indeterminacy (or neutrality), each one of these three neutrosophic components in some degree. The degrees of evolution/indeterminacy/involution are referred to both: the structure of the being (its body parts), and functionality of the being (functionality of each part, or inter-functionality of the parts among each other, or functionality of the being as a whole). We therefore introduce now for the first time the Neutrosophic Theory of Evolution, Involution, and Indeterminacy (or Neutrality).

1 Introduction

During the 2016–2017 winter, in December-January, I went to a cultural and scientific trip to Galápagos Archipelago, Ecuador, in the Pacific Ocean, and visited seven islands and islets: Mosquera, Isabela, Fernandina, Santiago, Sombrero Chino, Santa Cruz, and Rabida, in a cruise with Golondrina Ship. I had extensive discussions with our likeable guide, señor Milton Ulloa, about natural habitats and their transformations.

After seeing many animals and plants, that evolved differently from their ancestors that came from the continental land, I consulted, returning back to my University of New Mexico, various scientific literature about the life of animals and plants, their reproductions, and about multiple theories of evolutions. I used the online scientific databases that UNM Library has subscribed to, such as MathSciNet, Web of Science, EBSCO, Thomson Gale (Cengage), ProQuest, IEEE/IET Electronic Library, IEEE Xplore Digital Library etc., and DOAJ, Amazon Kindle, Google Play Books as well, doing searches for keywords related to origins of life, species, evolution, controversial ideas about evolution, adaptation and inadaptation, life curiosities, mutations, genetics, embryology, and so on.

My general conclusion was that each evolution theory had some degree of truth, some degree of indeterminacy, and some degree of untruth (as in neutrosophic logic), depending on the types of species, environment, timespan, and other hidden parameters that may exist.

And all these degrees are different from a species to another species, from an environment to another environment, from a timespan to another timespan, and in general from a parameter to another parameter.

By environment, one understands: geography, climate, prays and predators of that species, i.e. the whole ecosystem.

I have observed that the animals and plants (and even human beings) not only evolve, but also *devolve* (i.e. involve back, decline, atrophy, pass down, regress, degenerate). Some treats increase, other treats decrease, while others remains unchanged (neutrality).

One also sees: adaptation by physical or functional evolution of a body part, and physical or functional involution of another body part, while other body parts and functions remain unchanged. After evolution, a new process start, reevaluation, and so on.

In the society it looks that the most opportunistic (which is the fittest!) succeeds, not the smartest. And professional deformation signifies evolution (specialization in a narrow field), and involution (incapability of doing things in another field).

The paper is organized as follows: some information on taxonomy, species, a short list of theories of origin of life, another list of theories and ideas about evolution. Afterwards the main contribution of this paper, the *theory of neutrosophic evolution*, the dynamicity of species, several examples of evolution, involution, and indeterminacy (neutrality), neutrosophic selection, refined neutrosophic theory of evolution, and the paper ends with open questions on evolution/neutrality/involution.

2 Taxonomy

Let's recall several notions from classical biology.

The **taxonomy** is a classification, from a scientifically point of view, of the living things, and it classifies them into three categories: **species**, **genus**, and **family**.

3 Species

A **species** means a group of organisms, living in a specific area, sharing many characteristics, and able to reproduce with

each other.

In some cases, the distinction between a population subgroup to be a different species, or not, is unclear, as in the *Sorites Paradoxes* in the frame of *neutrosophy*: the frontier between <A> (where <A> can be a species, a genus, or a family), and <nonA> (which means that is not <A>) is vague, incomplete, ambiguous. Similarly, for the distinction between a series and its subseries.

4 Theories of origin of life

Louis Pasteur (1822–1895) developed in 1860 the theory of *precellular* (*prebiotic*) *evolution*, which says that life evolved from non-living chemical combinations that, over long time, arose spontaneously.

In the late 19th century a theory, called *abiogenesis*, promulgated that the living organisms originated from lifeless matter spontaneously, without any living parents' action.

Carl R. Woese (b. 1928) has proposed in 1970's that the *progenotes* were the very first living cells, but their biological specificity was small. The genes were considered probable (rather than identical) proteins.

John Burdon Sanderson Haldane (1872–1964) proposed in 1929 the *theory that the viruses were precursors to the living cells* [1].

John Bernal and A. G. Cairns-Smith stated in 1966 the *mineral theory*: that life evolved from inorganic crystals found in the clay, by natural selection [2].

According to the *little bags theory of evolution*, the life is considered as having evolved from organic chemicals that happened to get trapped in some tiny vesicles.

Eigen and Schuster, adepts of the *hypercycle theory*, asserted in 1977 that the precursors of single cells were these little bags, and their chemical reactions cycles were equivalent to the life's functionality [3].

Other theories about the origin of life have been proposed in the biology literature, such as: *primordial soup*, *dynamic state theory*, and *phenotype theory*, but they were later dismissed by experiments.

5 Theories and ideas about evolution

The theory of *fixism* says that species are fixed, they do not evolve or devolve, and therefore the today's species are identical to the past species.

Of course, the *creationism* is a fixism theory, from a religious point of view. Opposed to the fixism is the theory of *transformism*, antecedent to the evolutionary doctrine, in the pre-Darwinian period, which asserts that plants and animals are modified and transformed gradually from one species into another through many generations [22].

Jean Baptiste Pierre Antoine de Monet Lamarck (1749–1829), in 1801, ahead of Charles Darwin, is associated with the *theory of inheritance of acquired characteristics* (or *use-inheritance*), and even *of acquired habits*. Which is called *Lamarckism* or *Lamarckian Evolution*.

If an animal repeatedly stresses in the environment, its body part under stress will modify in order to overcome the environmental stress, and the modification will be transmitted to its offspring.

For example: the giraffe having a long neck in order to catch the tree leaves [4].

Herbert Spencer (1820–1903) used for the first time the term evolution in biology, showing that a population's gene pool changes from a generation to another generation, producing new species after a time [5].

Charles Darwin (1809–1882) introduced the natural selection, meaning that individuals that are more endowed with characteristics for reproduction and survival will prevail ("selection of the fittest"), while those less endowed would perish [6].

Darwin had also explained the structure similarities of leaving things in genera and families, due to the common descent of related species [7].

In his *gradualism* (or *phyletic gradualism*), Darwin said that species evolve slowly, rather than suddenly.

The adaptation of an organism means nervous response change, after being exposed to a permanent stimulus.

In the *modern gradualism*, from the genetic point of view, the beneficial genes of the individuals best adapted to the environment, will have a higher frequency into the population over a period of time, giving birth to a new species [8].

Herbert Spencer also coined the phrase survival of the fittest in 1864, that those individuals the best adapted to the environment are the most likely to survive and reproduce. Alfred Russel Wallace (1823–1913) coined in 1888 the terms *Darwinism* (individuals the most adapted to environment pass their characteristics to their offspring), and Darwinian fitness (the better adapted, the better surviving chance) [9].

One has upward evolution (*anagenesis*, coined by Alpheus Hyatt, 1838–1902, in 1889), as the progressive evolution of the species into another [10], and a *branching evolution* (*cladogenesis*, coined in 1953 by Sir Julian Sorell Huxley, 1887–1975), when the population diverges and new species evolve [11].

George John Romanes (1848–1894) coined the word *neo-Darwinism*, related to natural selection and the theory of genetics that explains the *synthetic theory of evolution*. What counts for the natural selection is the gene frequency in the population [12]. The Darwinism is put together with the paleontology, systematics, embryology, molecular biology, and genetics.

In the 19th century Gregor Johann Mendel (1822–1884) set the base of *genetics*, together with other scientists, among them Thomas Hunt Morgan (1866–1945).

The *Mendelism* is the study of heredity according to the chromosome theory: the living thing reproductive cells contain factors which transmit to their offspring particular characteristics [13].

August Weismann (1834-1914) in year 1892 enounced the germ plasm theory, saying that the offspring do not inherit the acquired characteristics of the parents [14].

Hugo de Vries (1848–1935) published a book in 1901 on *mutation theory*, considering that randomly genetic mutations may produce new forms of living things. Therefore, new species may occur suddenly [15].

Louis Antoine Marie Joseph Dollo (1857–1931) enunciated the *Dollo's principle* (*law* or *rule*) that evolution is irreversible, i.e. the lost functions and structures in species are not regained by future evolving species.

In the present, the *synergetic theory of evolution* considers that one has a natural or artificial multipolar selection, which occurs at all life levels, from the molecule to the ecosystem — not only at the population level.

But nowadays it has been discovered organisms that have re-evolved structured similar to those lost by their ancestors [16].

Life is... complicated!

The genetic assimilation (for *Baldwin Effect*, after James Mark Baldwin, 1861–1934) considered that an advantageous trait (or phenotype) may appear in several individuals of a population in response to the environmental cues, which would determine the gene responsible for the trait to spread through this population [17].

The British geneticist Sir Ronald A. Fisher (1890–1962) elaborated in 1930 the *evolutionary or directional determinism*, when a trait of individuals is preferred for the new generations (for example the largest grains to replant, chosen by farmers) [18].

The *theory of speciation* was associated with Ernst Mayr (b. 1904) and asserts that because of geographic isolation new species arise, that diverge genetically from the larger original population of sexually reproducing organisms. A subgroup becomes new species if its distinct characteristics allow it to survive and its genes do not mix with other species [19].

In the 20th century, Trofim Denisovitch Lysenko (1898–1976) revived the Lamarckism to the *Lysenkoism* school of genetics, proclaiming that the new characteristics acquired by parents will be passed on to the offspring [20].

Richard Goldschmidt (1878–1958) in 1940 has coined the terms of macroevolution, which means evolution from a long timespan (geological) perspective, and microevolution, which means evolution from a small timespan (a few generations) perspective with observable changes [1].

Sewall Wright (1889–1988), in the mid 20th century, developed the *founders effect of principle*, that in isolated places population arrived from the continent or from another island, becomes little by little distinct from its original place population. This is explained because the founders are few in number and therefore the genetic pool is smaller in diversity, whence their offspring are more similar in comparison to the offspring of the original place population.

The founders effect or principle is regarded as a particular case of the *genetic drift* (authored by the same biologist, Sewall Wright), which tells that the change in gene occurs by chance [21].

The mathematician John Maynard Smith has applied the game theory to animal behavior and in 1976 he stated the *evolutionary stable strategy* in a population. It means that, unless the environment changes, the best strategy will evolve, and persist for solving problems.

Other theories related to evolution such as: *punctuated equilibrium* (instantaneous evolution), *hopeful monsters*, and *saltation* (*quantum*) *speciation* (that new species suddenly occur; by Ernst Mayr) have been criticized by the majority of biologists.

6 Open research

By genetic engineering it is possible to make another combination of genes, within the same number of chromosomes. Thus, it is possible to mating a species with another closer species, but their offspring is sterile (the offspring cannot reproduce).

Despite the tremendous genetic engineering development in the last decades, there has not been possible to prove by experiments in the laboratory that: from an inorganic matter one can make organic matter that may reproduce and assimilate energy; nor was possible in the laboratory to transform a species into a new species that has a number of chromosomes different from the existent species.

7 Involution

According to several online dictionaries, **involution** means:

— Decay, retrogression or shrinkage in size; or return to a former state [Collins Dictionary of Medicine, Robert M. Youngson, 2005];

— Returning of an enlarged organ to normal size; or turning inward of the edges of a part; mental decline associated with advanced age (psychiatry) [Medical Dictionary for the Health Professions and Nursing, Farlex, 2012];

— Having rolled-up margins (for the plant organs) [Collins Dictionary of Biology, 3rd edition, W. G. Hale, V. A. Saunders, J. P. Margham, 2005];

— A retrograde change of the body or of an organ [Dorland's Medical Dictionary for Health Consumers, Saunders, an imprint of Elsevier, Inc., 2007];

— A progressive decline or degeneration of normal physiological functioning [The American Heritage, Houghton Mifflin Company, 2007].

8 Theory of Neutrosophic Evolution

During the process of adaptation of a being (plant, animal, or human) B, to a new environment η,

— B partially ***evolves***;

— B partially ***devolves*** (involves, regresses, degenerates);

— and B partially remains ***indeterminate*** which means *neutral* (unchanged), or ambigous — i.e. not sure if it is evolution or involution.

Any action has a reaction. We see, thank to adaptation: evolution, involution, and neutrality (indeterminacy), each one of these three *neutrosophic components* in some degree.

The degrees of evolution/indeterminacy/involution are referred to both: the **structure** of B (its body parts), and **functionality** of B (functionality of each part, or inter-functionality of the parts among each other, or functionality of B as a whole).

Adaptation to new environment conditions means **deadaptation** from the old environment conditions.

Evolution in one direction means involution in the opposite direction.

Loosing in one direction, one has to gain in another direction in order to survive (for equilibrium). And reciprocally.

A species, with respect to an environment, can be:

— in equilibrium, disequilibrium, or indetermination;

— stable, unstable, or indeterminate (ambiguous state);

— optimal, suboptimal, or indeterminate.

One therefore has a **Neutrosophic Theory of Evolution, Involution, and Indeterminacy** (neutrality, or fluctuation between Evolution and Involution). The evolution, the involution, and the indeterminate-evolution depend not only on natural selection, but also on many other factors such as: artificial selection, friends and enemies, bad luck or good luck, weather change, environment juncture etc.

9 Dynamicity of the species

If the species is in indeterminate (unclear, vague, ambiguous) state with respect to its environment, it tends to converge towards one extreme:

— either to equilibrium/stability/optimality, or to disequilibrium/instability/suboptimality with respect to an environment;

— therefore the species either rises up gradually or suddenly by mutation towards equilibrium/stability/optimality;

— or the species deeps down gradually or suddenly by mutation to disequilibrium/instability/suboptimality and perish.

The **attraction point** in this neutrosophic dynamic system is, of course, the state of equilibrium/stability/optimality. But even in this state, the species is not fixed, it may get, due to new conditions or accidents, to a degree of disequilibrium/instability/suboptimality, and from this new state again the struggle on the long way back of the species to its attraction point.

10 Several examples of evolution, involution, and indeterminacy (neutrality)

10.1 Cormorants example

Let's take the flightless cormorants (*Nannopterum harrisi*) in Galápagos Islands, their wings and tail have atrophied (hence **devolved**) due to their no need to fly (for they having no predators on the land), and because their permanent need to dive on near-shore bottom after fish, octopi, eels etc.

Their avian breastbone vanished (**involution**), since no flying muscles to support were needed.

But their neck got longer, their legs stronger, and their feet got huge webbed is order to catch fish underwater (**evolution**).

Yet, the flightless cormorants kept several of their ancestors' habits (functionality as a whole): make nests, hatch the eggs etc. (hence **neutrality**).

10.2 Cosmos example

The astronauts, in space, for extended period of time get accustomed to low or no gravity (**evolution**), but they lose bone density (**involution**). Yet other body parts do not change, or it has not been find out so far (**neutrality/indeterminacy**).

10.3 Example of evolution and involution

The whales **evolved** with respect to their teeth from pig-like teeth to cusped teeth. Afterwards, the whales **devolved** from cusped teeth back to conical teeth without cusps.

10.4 Penguin example

The Galápagos Penguin (Spheniscus mendiculus) evolved from the Humboldt Penguin by shrinking its size at 35 cm high (adaptation by involution) in order to be able to stay cool in the equatorial sun.

10.5 Frigate birds example

The Galápagos Frigate birds are birds that lost their ability to dive for food, since their feathers are not waterproof (**involution**), but they became masters of faster-and-maneuverable flying by stealing food from other birds, called kleptoparasite feeding (**evolution**).

10.6 Example of Darwin's finches

The 13 Galápagos species of Darwin's Finches manifest various degrees of evolution upon their beak, having different shapes and sizes for each species in order to gobble different types of foods (hence **evolution**):

— for cracking hard seeds, a thick beak (ground finch);

— for insects, flowers and cacti, a long and slim beak (another finch species).

Besides their beaks, the finches look similar, proving they came from a common ancestor (hence **neutrality**).

If one experiments, let's suppose one moves the thick-beak ground finches back to an environment with soft seeds, where it is not needed a thick beak, then the thick beak will atrophy and, in time, since it becomes hard for the finches to use the heavy beak, the thin-beak finches will prevail (hence **involution**).

10.7 El Niño example

Professor of ecology, ethology, and evolution Martin Wikelski, from the University of Illinois at Urbana-Champaign, has published in *Nature* a curious report, regarding data he and his team collected about marine iguanas since 1987. During the 1997–1998 El Niño, the marine algae died, and because the lack of food, on one of the Galápagos islands some marine iguanas shrank a quarter of their length and lost half of their weight (adaptation by **involution**).

After plentiful of food became available again, the marine iguanas grew back to their original length and weight (re-adaptation by **evolution**).

[J. Smith, J. Brown, The Incredible Shrinking Iguanas, in Ecuador & The Galápagos Islands, Moon Handbook, Avalon Travel, p. 325.]

10.8 Bat example

The bats are the only mammals capable of naturally flying, due to the fact that their forelimbs have developed into webbed wings (**evolution** by transformation). But navigating and foraging in the darkness, have caused their eyes' functionality to diminish (**involution**), yet the bats "see" with their ears (**evolution** by transformation) using the echolocation (or the bio sonar) in the following way: the bats emit sounds by mouth (one emitter), and their ears receive echoes (two receivers); the time delay (between emission and reception of the sound) and the relative intensity of the received sound give to the bats information about the distance, direction, size and type of animal in its environment.

10.9 Mole example

For the moles, mammals that live underground, their eyes and ears have degenerated and become minuscule since their functions are not much needed (hence adaptation by **involution**), yet their forelimbs became more powerful and their paws larger for better digging (adaptation by **evolution**).

11 Neutrosophic selection

Neutrosophic selection with respect to a population of a species means that over a specific timespan a percentage of its individuals evolve, another percentage of individuals devolve, and a third category of individuals do not change or their change is indeterminate (not knowing if it is evolution or involution). We may have a natural or artificial neutrosophic selection.

12 Refined Neutrosophic Theory of Evolution

Refined Neutrosophic Theory of Evolution is an extension of the neutrosophic theory of evolution, when the degrees of evolution/indeterminacy/involution are considered separately with respect to each body part, and with respect to each body part functionality, and with respect to the whole organism functionality.

13 Open questions on evolution/neutrality/involution

13.1. How to measure the degree of evolution, degree of involution, and degree of indeterminacy (neutrality) of a species in a given environment and a specific timespan?

13.2. How to compute the degree of similarity to ancestors, degree of dissimilarity to ancestors, and degree of indeterminate similarity-dissimilarity to ancestors?

13.3. Experimental Question. Let's suppose that a partial population of species S_1 moves from environment η_1 to a different environment η_2; after a while, a new species S_2 emerges by adaptation to η_2; then a partial population S_2 moves back from η_2 to η_1; will S_2 evolve back (actually devolve to S_1)?

13.4. Are all species needed by nature, or they arrived by accident?

14 Conclusion

We have introduced for the first time the concept of *Neutrosophic Theory of Evolution, Indeterminacy* (*or Neutrality*), *and Involution*.

For each being, during a long timespan, there is a process of partial evolution, partial indeterminacy or neutrality, and partial involution with respect to the being body parts and functionalities.

The function creates the organ. The lack of organ functioning, brings atrophy to the organ.

In order to survive, the being has to adapt. One has adaptation by evolution, or adaptation by involution — as many examples have been provided in this paper. The being partially evolves, partially devolves, and partially remains unchanged (fixed) or its process of evolution-involution is indeterminate. There are species partially adapted and partially struggling to adapt.

References

1. Barbieri M. The Semantic Theory of Evolution. Chur, Switzerland, 1985.
2. Cairns-Smith A.G. The Origin of Life and the Nature of Primitive Gene. *Journal of Theoretical Biology*, 1966, v. X, 53–88.
3. Eigen M. and Schuster P. The Hypercycle. A Principle of Natural Self-Organization. *Naturwissenschaften*, 1977, v. LXIV, 541–565.
4. Lamarck J.B. Zoological Philosophy. 1809.
5. Reader J. The Rise of Life. New York, 1988
6. Sober E. The Nature of Selection. Cambridge, MA, 1984.
7. Kohn D. The Darwinian Heritage. Princeton, NJ, 1985.

8. Eldredge N. Life Pulse: Episodes from the Story of the Fossil Record. New York, 1987.
9. Wallace A.R. Darwinism: An Exposition of the Theory of Natural Selection with Some of its Applications MacMillan, London, 1889.
10. Brown J. Biogeography. St. Louis, MO, 1983.
11. Delson E. Ancestors: The Hard Evidence. New York, 1985.
12. Bowler P. Evolution: The History of an Idea. Berkeley, California, 1984.
13. Olby R. The Origins of Mendelism. London-Chicago, 1985.
14. Weismann A. The Germ Plasm: A Theory of Heredity. London, 1893.
15. de Vries H. Mutationstheorie [Mutation Theory]. Leipzig. Veit und Co. 1901 & 1903.
16. Milner R. The Encyclopedia of Evolution: Humanity's Search for its Origins. New York, 1987.
17. Hitching F. The Neck of the Giraffe: Where Darwin Went Wrong. New Haven, Connecticut, 1987.
18. Eldredge N. Unfinished Synthesis. Oxfrd Univ. Press, Oxford, 1985.
19. Ereshefsky M. The Units of Evolution: Essays on the Nature of Species. Cambridge, Massachusetts, 1992.
20. Joravsky D. The Lysenko Affair. Cambridge, Massachusetts, 1970.
21. Magill F. Magill's Survey of Science: Life Science Series. Englewood Cliffs, NJ, 1991.
22. The Great Soviet Encyclopedia. 3rd Edition, The Gale Group, Inc., 2010.
23. Linfan Mao. Biological n-System with Global Stability. *International Conference on Applications of Mathematics in Topological Dynamics*, Section: "Physics, Biological and Chemical Systems", Kolkata, India, December 9–11, 2016.
24. Smarandache F. Galápagos sau Ținutul Broaștelor Țestoase Gigantice: Teoria Neutrosofică a Evoluției. Editura Agora, Sibiu, 2017.

On the Vacuum Induced Periodicities Inherent to Maxwell Equations

Fernando Ogiba
E-mail: fogiba@gmail.com

The hypothesis that the Planck's vacuum is inherent to all physical laws, given that it interact with massless elementary electrical charges, is examined exploring gauge invariance. It is then found that Compton's and de Broglie's periodicities, parameters of distinct vacuum induced fluctuations, are inherent to Maxwell equations.

Electromagnetic fields, in principle, are produced by electrical charges (and its movements), which are permanently actuated by the Planck's vacuum [1]. In this sense, it is expected that Maxwell's equations contain some (hidden) information about vacuum induced fluctuations.

The above hypothesis will be examined, firstly, considering the well-known redefinitions of the electromagnetic potentials that leaves the Maxwell equations unchanged, i.e.

$$\mathbf{A} \to \mathbf{A} + \nabla\chi, \quad \phi \to \phi - \partial_t\chi, \tag{1}$$

where χ is a scalar function (not as arbitrary as it may seem), together with the Lorenz condition (SI units)

$$c^{-2}\partial_t\phi + \nabla \cdot \mathbf{A} = 0, \tag{2}$$

which is not a condition (nor a gauge) but a physical law [2].

In order to preserve the local conservation law (2) under the redefinitions (1), χ must obey

$$\nabla^2\chi - c^{-2}\partial_{tt}\chi = 0, \tag{3}$$

as can be seen in the reference [3, p.$\dot{2}$39]. This wave equation (and the assumptions to get it) suggests that electrical charges – regardless of their ordinary translational motions – present *local* periodical space-time evolutions at the light speed c. It means that massless elementary electrical charges (MEECs), everywhere, incorporate the local space-time evolution of the incoming zero-point radiation (ZPR). Apart randomness, this interpretation agrees with the Schrödinger's *zitterbewegung* [4]; i.e., electrons describe random curvilinear paths (Compton's angular frequency) at the light speed.

Aiming to proof that the periodicity of the *local* Eq.(3) is indeed the Compton's one, the observed motion will be introduced through the simple (but rich in content) relation

$$\mathbf{A} = \left(\phi/c^2\right)\mathbf{v}, \tag{4}$$

which relates the potentials of a free charged particle moving with velocity $\mathbf{v}$, as can be verified from the corresponding current density $\mathbf{J} = \rho\mathbf{v}$, where ρ is charge density, together with

$$\nabla^2\mathbf{A} - c^{-2}\partial_{tt}\mathbf{A} = -\mu_o\mathbf{J}, \quad \nabla^2\phi - c^{-2}\partial_{tt}\phi = -\rho/\epsilon_o. \tag{5}$$

Following the same steps that led to Eq.(3), to preserve the form of Eq.(4) – relativistic energy-momentum relation (per unit charge) – under the redefinitions (1), χ must obey

$$\nabla\chi + c^{-2}\partial_t\chi = 0. \tag{6}$$

Assuming that the inferred periodicity of χ obeys the standard phase $\omega t - \mathbf{k} \cdot \mathbf{x}$, the Eq.(6) implies

$$-\mathbf{k} + (\omega/c^2)\mathbf{v} = 0, \tag{7}$$

from which we obtain the *improper* phase velocity

$$v_p = \omega/|\mathbf{k}| = c^2/v; \tag{8}$$

i.e., the phase velocity of the inherent de Broglie wave.

The above result implies that ω is the Compton's angular frequency ($\gamma m_o c^2/\hbar$), and $|\mathbf{k}|$ is the de Broglie wave number ($\gamma m_o v/\hbar$), where γ is the Lorentz factor [5].

Notice, the periodicity of the (co-moving) Eq.(3) is therefore $m_o c^2/\hbar$, as inferred in connection with *zitterbewegung*.

The improper nature of v_p and its close relation with inertia [6] are indicative of vibrations triggered by "imminent" violations of the radiation speed limit (ZPR absorbed-emitted by MEECs) when the ordinary motion takes place (quantum wave-packet), as suggested in the reference [5].

Keep the form of Eq.(4), considering the non-uniqueness of $\mathbf{A}$ and ϕ, is convenient for comparing $e\mathbf{A} = (e\phi/c^2)\mathbf{v}$, calculated in the domain d of the extended charge e producing the potentials, with the relativistic relation $\mathbf{p} = (E/c^2)\mathbf{v}$. It means admitting that $\mathbf{p} = [e\mathbf{A}]_d$ and $E = [e\phi]_d$. This, besides agreeing with the classical electron radius as well as with the canonical momentum of a charged particle in an external field, in the sense that $\mathbf{P} = e\mathbf{A}_{tot} = e\mathbf{A} + e\mathbf{A}_{ext} = m\mathbf{v} + e\mathbf{A}_{ext}$, implies that the mass E/c^2 is of electromagnetic origin [7].

References

1. de la Peña L., Cetto A. M., Hernandez A. V. The Emerging Quantum The Physics Behind Quantum Mechanics. Springer, 2015.
2. Jefimenko O. D. Presenting electromagnetic theory in accordance with the principle of causality. *European Journal of Physics*, 2004, v. 25, 287–296.
3. Jackson J. D. Classical Electrodynamics. 3rd ed., John Wiley and Sons Inc., 1999.
4. Dirac P. A. M. The Principles of Quantum Mechanics. 4ed. Oxford University Press, 1958.
5. Ogiba F. On the Quantum-relativistic Behavior of Moving Particles. *Progress in Physics*, 2016, v. 12, n. 4, 325–328.
6. Wignall J. W. G. De Broglie waves and the nature of mass. *Foundations of Physics*, 1985, v. 15, n. 2, 207–227.
7. Griffiths D.J. Electromagnetic Momentum. *American Journal of Physics*, 2012, v. 80, n. 7, 7–18.

Progress in Physics is an American scientific journal on advanced studies in physics, registered with the Library of Congress (DC, USA): ISSN 1555-5534 (print version) and ISSN 1555-5615 (online version). The journal is peer reviewed and listed in the abstracting and indexing coverage of: Mathematical Reviews of the AMS (USA), DOAJ of Lund University (Sweden), Scientific Commons of the University of St.Gallen (Switzerland), Open-J-Gate (India), Referential Journal of VINITI (Russia), etc. Progress in Physics is an open-access journal published and distributed in accordance with the Budapest Open Initiative: this means that the electronic copies of both full-size version of the journal and the individual papers published therein will always be acessed for reading, download, and copying for any user free of charge. The journal is issued quarterly (four volumes per year).

Electronic version of this journal: http://www.ptep-online.com

Postal address:
Department of Mathematics and Science, University of New Mexico,
705 Gurley Avenue, Gallup, NM 87301, USA